

**REMOVAL AND PHOTOCATALYSIS OF
4-NITROPHENOL USING
METALLOPHTHALOCYANINES**

**A thesis submitted in completion of the
requirements for the degree of**

MASTER OF SCIENCE

of

RHODES UNIVERSITY

by

ELOISE ANN MARAIS

November 2007

Dedicated to my late grandfather,

Lionel Fernie Baxter

(1922 - 2007),

whose epitaph reads:

"We make a living by what we get,
but we make a life by what we give"

Norman MacEwan

"The most exciting phrase to hear in science, the one that heralds the most discoveries, is not 'Eureka!' (I found it!), but:
'That's funny...'"

Isaac Asimov

(1920 – 1992)

Professor of Biochemistry and author of science fiction stories such as
I, Robot and the *Foundation* series.

ACKNOWLEDGEMENTS

There are a number of people who have assisted me in completing my Master's project at Rhodes University including friends, family, support staff and academic staff. The friendly demeanour and warmth that is characteristic of the Rhodes Chemistry Department allowed me to fit in with ease.

My Master's supervisor, **Prof Nyokong**, who accepted me despite my unsuccessful Master's year at UKZN, has rekindled my passion for Chemistry. Her guidance has helped me develop into an independent researcher. I am grateful for the opportunities I have had to develop as a researcher and network with other chemists at the SACI and SEANAC conferences I attended under her supervision.

I am also grateful to Dr Edith Antunes who assisted me in many ways, especially with the analysis of my samples on the LC/MS.

James Aitchison has encouraged me throughout my academic career. His support over the past two years has been immeasurable.

I have enjoyed having my family in close proximity to me during my Master's degree. The opportunity to participate in Matric dance preparations, birthdays, and weekend braai's has allowed me to forget about the pressures of Master's and recharge my batteries for the week ahead.

The friends I have met along the way, particularly Albert, Ben, Brent, Louise, Sunny and Tanya, have helped me survive many unsuccessful moments in the laboratory. The elaborate suppers, Friday pub lunches and intense *30 Seconds* games have been a welcome relief from stress.

The S22 group has made my time in the laboratory a truly cultural experience. I have met students from Nigeria, Turkey, Chile, China, Botswana and Zimbabwe. I have even had the

privilege of tasting mopani worms and genuine Turkish delight! I was made to feel welcome within the group from the day I arrived and there was always someone willing to assist me.

The support staff have been incredibly helpful during my Master's degree. Mrs Tarr and Ms Ah Yui have ensured that all administration has run smoothly, Mr Sonemann and Mr Fourie have been able to repair many temperamental instruments, and Mr Dondashe has been a reliable storeman.

The organisations I have to thank for providing financial support during my Master's degree include the National Research Foundation (NRF), the Department of Labour (DoL), the German Academic Exchange Service (DAAD) and Rhodes University.

ABSTRACT

Photodegradation of 4-nitrophenol (4-Np) in the presence of water-soluble zinc phthalocyanines and water-insoluble metallophthalocyanines is reported. The water-soluble phthalocyanines employed include zinc tetrasulphophthalocyanine (ZnPcS_4), zinc octacarboxyphthalocyanine ($\text{ZnPc}(\text{COOH})_8$) and a sulphonated ZnPc containing a mixture of differently sulphonated derivatives ($\text{ZnPcS}_{\text{mix}}$), while the water-insoluble phthalocyanines used include unsubstituted magnesium (MgPc), zinc (ZnPc) and chloroaluminium (ClAlPc) phthalocyanine complexes and the ring-substituted zinc tetranitro ($\text{ZnPc}(\text{NO}_2)_4$), zinc tetraamino ($\text{ZnPc}(\text{NH}_2)_4$), zinc hexadecafluoro (ZnPcF_{16}) and zinc hexadecachloro (ZnPcCl_{16}) phthalocyanines. The most effective water-soluble photocatalyst is $\text{ZnPcS}_{\text{mix}}$ in terms of the high quantum yield obtained for 4-Np degradation ($\Phi_{4\text{-Np}}$) as well as its photostability. While $\text{ZnPc}(\text{COOH})_8$ has the highest $\Phi_{4\text{-Np}}$ value relative to the other water-soluble complexes, it degrades readily during photocatalysis. The $\Phi_{4\text{-Np}}$ values were closely related to the singlet oxygen quantum yields Φ_{Δ} and hence aggregation. The rate constants for the reaction with 4-Np were $k_r = 0.67 \times 10^6 \text{ mol}^{-1} \text{ dm}^3 \text{ s}^{-1}$ for $\text{ZnPcS}_{\text{mix}}$ and $7.7 \times 10^6 \text{ mol}^{-1} \text{ dm}^3 \text{ s}^{-1}$ for $\text{ZnPc}(\text{COOH})_8$. ClAlPc is the most effective photocatalyst relative to the other heterogeneous photocatalysts for the phototransformation of 4-Np, with $89 \pm 8.4 \%$ degradation of 4-Np achieved after 100 min. The least effective catalysts were ZnPcCl_{16} and MgPc . The final products of the photocatalysis of 4-Np in the presence of the homogeneous photocatalysts include 4-nitrocatechol and hydroquinone, while degradation of 4-Np in the presence of the heterogeneous photocatalysts resulted in fumaric acid and 4-nitrocatechol.

ClAlPc was employed for the heterogeneous photocatalysis of the non-systemic insecticide, methyl paraoxon. Complete degradation of the pesticide was confirmed by the disappearance of the HPLC trace for methyl paraoxon after 100 min of irradiation with visible light.

The removal of 4-Np from an aqueous medium using commercially available Amberlite[®] IRA-900 modified with metal phthalocyanines was also investigated. The metallophthalocyanines immobilised onto the surface of Amberlite[®] IRA-900 include Fe (FePcS₄), Co (CoPcS₄) and Ni (NiPcS₄) tetrasulphophthalocyanines, and differently sulphonated phthalocyanine mixtures of Fe (FePcS_{mix}), Co (CoPcS_{mix}) and Ni (NiPcS_{mix}). Adsorption rates were fastest for the modified adsorbents at pH 9. Using the Langmuir-Hinshelwood kinetic model, the complexes showed the following order of 4-Np adsorption: CoPcS_{mix} > NiPcS₄ > NiPcS_{mix} > FePcS₄ > FePcS_{mix} > CoPcS₄. The adsorbents were regenerated using dilute HNO₃, with 76 % (7.6×10^{-5} mol) of 4-Np recovered within 150 min.

TABLE OF CONTENTS

Title Page	i
Dedication	ii
Quote	iii
Acknowledgements	iv
Abstract	vi
Table of Contents	viii
List of Abbreviations	xi
List of Symbols	xiii
List of Figures	xv
List of Schemes	xviii
List of Tables	xix

1. INTRODUCTION	1
1.1. Background on 4-Nitrophenol	1
1.2. Survey of Methods for the Removal and Degradation of 4-Nitrophenol	3
1.3. Phthalocyanines	8
1.3.1. Background on Phthalocyanines	8
1.3.2. General Synthesis of Phthalocyanines	10
1.3.3. Spectral Properties of Phthalocyanines	12
1.3.3.1. UV-visible Spectra	12
1.3.3.2. Infrared Spectra	14
1.3.4. Aggregation of Phthalocyanines	14
1.4. Phthalocyanines as Photocatalysts	16
1.4.1. Photocatalysis Mechanisms	17
1.4.2. Molecular Properties and Generation of Singlet Oxygen	20
1.4.3. Effect of Substituents and the Central Metal on Photocatalytic Activity	24

1.4.4.	Previous Photocatalytic Studies using MPcs as Photocatalysts	25
1.5.	Adsorption Studies	28
1.5.1.	Adsorption of 4-Np onto Bare Resin	28
1.5.2.	Adsorption of 4-Np onto Modified Resin	29
1.6.	Phthalocyanines Selected for Removal and Photocatalysis of 4-Np	29
1.7.	Summary of the Aims of the Study	31
2.	EXPERIMENTAL	32
2.1.	Materials	32
2.2.	Equipment	35
2.3.	Photocatalytic Calculations	37
2.4.	Immobilisation Studies	39
2.5.	Synthetic Methods	41
2.5.1.	Synthesis of Water-soluble Metallophthalocyanines	41
2.5.2.	Synthesis of Water-insoluble Metallophthalocyanines	44
2.6.	Immobilisation of Sulphonated Phthalocyanines	48
3.	RESULTS AND DISCUSSION	49
3.1.	Synthesis and Characterisation	50
3.1.1.	Synthesis of Water-soluble MPc Complexes	50
3.1.2.	Synthesis of Water-insoluble MPc Complexes	52
3.1.3.	Absorbance Spectra of MPc Complexes	55
3.1.3.1.	Water-soluble MPcs	55
3.1.3.2.	Water-insoluble MPcs	59
3.1.4.	HPLC Characterisation of MPcS ₄ and MPcS _{mix} Complexes	61

3.2. Homogeneous Photocatalysis of 4-Np using Water-soluble Zinc Pc Complexes	64
3.2.1. Catalyst Loading and $\Phi_{4\text{-Np}}$ Optimisation	64
3.2.2. Comparison of the Photocatalytic Activities of the Zinc Pc Sensitisers	67
3.2.3. Determination of Rate Constants for $\text{ZnPcS}_{\text{mix}}$ and $\text{ZnPc}(\text{COOH})_8$	71
3.2.4. Mechanism for the Photodegradation of 4-Np using Homogeneous Photosensitisers	73
3.3. Heterogeneous Photocatalysis of 4-Np using Suspended MPc Complexes	76
3.3.1. Identification of Degradation Products	77
3.3.2. Comparative Degradation of 4-Np	81
3.3.3. Mechanism for the Photodegradation of 4-Np using Water-insoluble MPcs	86
3.3.4. Practical Application of Water-insoluble MPcs	89
3.4. Adsorption of 4-Np onto Amberlite[®] IRA-900 Modified with MPcs	90
3.4.1. Optimisation of MPc Loading and pH of 4-Np Solution	96
3.4.2. Comparison of 4-Np Adsorption Rates on MPc-Modified Amberlite [®] IRA-900	98
3.4.3. Regeneration of the Modified Resin	100
3.4.4. Spectroscopic Study of the Interaction of 4-Np with MPcs	103
3.4.5. Langmuir-Hinshelwood Kinetic Model (LHKM)	104
4. CONCLUSION	106
5. REFERENCES	108

LIST OF ABBREVIATIONS

4-Cp	–	4-Chlorophenol
4-NC	–	4-Nitrocatechol
4-Np	–	4-Nitrophenol
ACE	–	Associated Chemical Enterprises
ACh	–	Acetylcholine
AChE	–	Acetylcholinesterase
ADMA	–	Tetrasodium α - α' -(anthracene-9,10-diyl) bis(methylmalonate)
aggr	–	aggregation
APCI	–	Atmospheric Pressure Chemical Ionization
BDH	–	British Drug House
BQ	–	1,4-Benzoquinone
DABCO	–	1,4-diazabicyclo[2.2.2]octane
DBU	–	1,8-diazabicyclo[5.4.0]undec-7-ene
deg	–	degradation
DMF	–	<i>N,N</i> -dimethylformamide
DMSO	–	Dimethyl sulfoxide
ESI-MS	–	Electrospray Ionisation – Mass Spectrometry
FA	–	Fumaric acid
FTIR	–	Fourier Transform Infrared
GCMS	–	Gas Chromatography Mass Spectrometry
HOMO	–	Highest Occupied Molecular Orbital
HPLC	–	High Performance Liquid Chromatography
HQ	–	Hydroquinone
IC	–	Internal conversion
IR	–	Infrared
ISC	–	Intersystem crossing
LCMS	–	Liquid Chromatography Mass Spectrometry
LHKM	–	Langmuir-Hinshelwood Kinetic Model
LUMO	–	Lowest Unoccupied Molecular Orbital
MeOH	–	Methanol
MPc	–	Metallated phthalocyanine
NIR	–	Near Infrared

ORL-RAT LD ₅₀	–	Lethal dosage of 50% of a population of rats after ingestion of a chemical
PAL	–	Positive Associates Limited
Pc	–	Phthalocyanine
[Pc(COOH) _n] _{poly}	–	A polymeric mixture of differently carboxylated phthalocyanine complexes
PCP	–	Pentachlorophenol
PcS ₄	–	Tetrasulphonated phthalocyanine
PcS _{mix}	–	Mixture of differently sulphonated phthalocyanine complexes
Pc(<i>t</i> -Bu) ₄	–	Tetratertiarybutyl phthalocyanine complex
PDT	–	Photodynamic Therapy
Ref	–	Reference
Sens	–	Photosensitiser
Sub	–	Substrate
THF	–	Tetrahydrofuran
UV	–	Ultraviolet
UV-vis	–	Ultraviolet-visible
VR	–	Vibrational relaxation

LIST OF SYMBOLS

$\Phi_{4\text{-Np}}$	–	4-Nitrophenol quantum yield
Φ_{Δ}	–	Singlet oxygen quantum yield
k_r	–	Rate constant for the reaction between singlet oxygen and 4-Np
k	–	Rate constant
π	–	Pi orbital
π^*	–	Pi antibonding orbital
Φ_T	–	Triplet state quantum yield
ε	–	Extinction coefficient/molar absorptivity
τ_T	–	Triplet state lifetime
$^1\Delta_g$	–	First excited state oxygen
$^1\Sigma_g^+$	–	Second excited state oxygen
$^3\Sigma_g^-$	–	Ground state oxygen
π_{2p}^*	–	2p pi antibonding orbital
k_p	–	Rate constant due to physical quenching of singlet oxygen
k_q	–	Rate constant due to chemical quenching of singlet oxygen
k_d	–	Rate constant for the decay of singlet oxygen in water
τ_{Δ}	–	Singlet oxygen lifetime
E_T	–	Energy of the excited triplet state
J	–	Total angular momentum quantum number
L	–	Orbital angular momentum quantum number
S	–	Spin quantum number
C_t	–	Concentration of 4-Np at time t
C_0	–	Concentration of 4-Np at time t = 0 min
V	–	Reaction volume
N_A	–	Avogadro's constant ($6.022 \times 10^{23} \text{ mol}^{-1}$)
I_{abs}	–	The overlap integral of the intensity of the light source for radiation and the light absorption of the sensitizer at 670 nm
S	–	Irradiation area
t	–	Time
Q_t	–	Amount of 4-Np adsorbed onto resin
V_L	–	Volume of the aqueous 4-Np solution
W	–	Mass of dry adsorbent

λ_{\max}	–	Maximum wavelength (nm)
ν_{\max}	–	Maximum wavenumber (cm^{-1})
$M^{\bullet+}$	–	Mass spectrum peak due to the molecular ion
K_{ad}	–	Adsorption coefficient
C_{sub}^0	–	Initial concentration of 4-Np
k_r	–	Rate constant for the adsorption of 4-Np
[]	–	Solution concentration in mol dm^{-3}
C_{4h}	}	Molecular point groups of peripherally-substituted tetrasulphonated Pcs
D_{2h}		
C_{2v}		
C_s		
$\mu\text{-oxo}$	–	Oxygen bridge formed between central metals of adjacent MPcs
S_0	–	Ground singlet state
S_1	–	First excited singlet state
T_1	–	First triplet state
P_x	–	P orbital oriented in the x plane
P_y	–	P orbital oriented in the y plane
h	–	Planck's constant ($6.626 \times 10^{-34} \text{ m}^2 \text{ kg s}^{-1}$)
ν	–	Frequency/wavenumber (cm^{-1})
A_Q	–	Absorbance of the Q band
m/z	–	Mass to charge ratio
pKa	–	Acid dissociation constant

LIST OF FIGURES

Figure 1.1.	Geometric structures of an (a) unmetallated porphyrin and an (b) unmetallated phthalocyanine.	9
Figure 1.2.	Electron delocalisation showing π conjugation within the phthalocyanine ring.	13
Figure 1.3.	The π - π^* transitions that give rise to the Q and B bands of phthalocyanines.	13
Figure 1.4.	Effect of dimerization of the molecular orbitals of D_{4h} phthalocyanines.	15
Figure 1.5.	Jablonski diagram depicting the likely energy transitions of photosensitisers.	18
Figure 1.6.	Potential energy curves for the three energy states of dioxygen.	21
Figure 1.7.	Electronic orientations of molecular oxygen in the outermost antibonding orbitals.	22
Figure 1.8.	Immobilisation of (a) sulphonated, and (b) carboxylated MPcs onto Amberlite [®] IRA-900.	25
Figure 1.9.	Molecular structures of selected Pcs for the photocatalysis and removal of 4-Np.	31
Figure 2.1.	Photochemical setup for the photocatalysis of 4-Np using homogeneous MPc catalysts.	36
Figure 2.2.	Photochemical setup for the photocatalysis of 4-Np using heterogeneous MPc catalysts.	36
Figure 2.3.	Schematic representation of the in-house LASER photolysis setup.	37
Figure 3.1.	Molecular structures of selected Pcs for the photocatalysis and removal of 4-Np.	50
Figure 3.2.	Structure of Triton X-100, a non-ionic surfactant.	55
Figure 3.3.	Spectral changes observed on addition of Triton X-100 to solutions of (a) $ZnPcS_{mix}$, (b) $ZnPcS_4$, and (c) $ZnPc(COOH)_8$.	56
Figure 3.4.	Spectral changes of (i) $Fe^{III}PcS_{mix}$ in 3:1 $CH_3CH:H_2O$ on addition of $NaBH_4$ resulting in (ii) $Fe^{II}PcS_{mix}$.	58
Figure 3.5.	Spectra obtained for the unsubstituted Pc complexes in DMSO. (a) $ClAlPc$, (b) $MgPc$, and (c) $ZnPc$.	60
Figure 3.6.	Spectra obtained for the substituted zinc Pc complexes in DMSO. (a) $ZnPc(NH_2)_4$, (b) $ZnPc(NO_2)_4$, (c) $ZnPcCl_{16}$, and (d) $ZnPcF_{16}$.	60
Figure 3.7.	Determination of λ_{max} values of the monomeric and dimeric species of $ZnPcF_{16}$ by sequential dilution in DMSO.	61
Figure 3.8.	HPLC traces of (a) $ZnPcS_{mix}$, (b) $CoPcS_{mix}$, (c) $FePcS_{mix}$, and (d) $NiPcS_{mix}$.	63

Figure 3.9.	Electronic absorption spectral changes observed during the photolysis of 1.0×10^{-4} mol dm ⁻³ 4-Np in the presence of 400 mg/L ZnPcS _{mix} .	65
Figure 3.10.	Plot of absorbance versus time to determine the initial rate of 4-Np degradation in the presence of ZnPcS _{mix} .	65
Figure 3.11.	Plot of Φ_{4-Np} versus concentration of ZnPcS _{mix} to determine the optimum concentration of ZnPcS _{mix} for the phototransformation of 4-Np.	66
Figure 3.12.	Plot of Φ_{4-Np} versus [4-Np] for its phototransformation in the presence of ZnPcS _{mix} .	66
Figure 3.13.	Plot of [4-Np] versus time for (a) ZnPcS _{mix} , (b) ZnPcS ₄ , and (c) ZnPc(COOH) ₈ .	68
Figure 3.14.	Spectral changes observed for (a) ZnPcS _{mix} , (b) ZnPcS ₄ , and (c) ZnPc(COOH) ₈ during the photocatalytic oxidation of 4-Np.	70
Figure 3.15.	Plot of $1/\Phi_{4-Np}$ versus $1/[4-Np]$ for the phototransformation of 4-Np in the presence of (a) ZnPcS _{mix} (400 mg/L) and (b) ZnPc(COOH) ₈ (200 mg/L).	72
Figure 3.16.	Effect of addition of NaN ₃ (an oxygen scavenger) on the rate of 4-Np degradation in the presence of ZnPcS _{mix} . (a) no NaN ₃ , (b) NaN ₃ added.	74
Figure 3.17.	Mass spectrum obtained for 4-nitrocatechol ($m/z = 155$ amu) fraction using ESI-MS (retention time = 1.75 min).	74
Figure 3.18.	HPLC traces of the reaction mixture after photocatalysis of 4-Np for 100 min using ZnPc(NH ₂) ₄ .	77
Figure 3.19.	Fragmentation patterns obtained for (a) FA ($m/z = 116$ amu), and (b) 4-NC ($m/z = 155$ amu) using ESI-MS.	78
Figure 3.20.	Average peak height versus loading of ZnPc to determine the effect of ZnPc on the phototransformation of 4-Np to FA.	80
Figure 3.21.	Plot of log (peak height) versus log (ZnPc loading) to determine the reaction order with respect to ZnPc.	81
Figure 3.22.	Triplet decay curve obtained for ZnPc in DMSO using ORIGIN Pro 6.0.	83
Figure 3.23.	Percentage degradation of 4-Np by selected Pc complexes.	84
Figure 3.24.	Comparison of the degree of formation of degradation products in the presence and absence of a singlet oxygen scavenger (DABCO), using ZnPc(NH ₂) ₄ .	86
Figure 3.25.	Electronic absorption spectral changes of ADMA during its visible light photolysis in the presence of ClAlPc.	88

Figure 3.26.	HPLC traces of methyl paraoxon solution (a) before photocatalysis, (b) after photocatalysis in the absence of ClAlPc, and (c) after photocatalysis in the presence of ClAlPc.	90
Figure 3.27.	Electronic spectral changes with time during the immobilisation of CoPcS _{mix} onto Amberlite [®] IRA-900 resin in a mixture of 1:1 CH ₃ CN:H ₂ O.	92
Figure 3.28.	Adsorption of 4-Np onto Amberlite [®] IRA-900 modified with ZnPcS _{mix} .	92
Figure 3.29.	Diffuse reflectance spectra of (a) FePcS, (b) NiPcS, and (c) CoPcS complexes after immobilisation onto Amberlite [®] IRA-900.	95
Figure 3.30.	Diffuse reflectance spectra of FePcS ₄ -Amb showing the effect of increasing the amount of immobilised FePcS ₄ .	96
Figure 3.31.	(a) Plot of initial adsorption rate versus FePcS ₄ loading to determine the optimum amount of FePcS ₄ immobilised onto Amberlite [®] IRA-900. (b) Plot of initial adsorption rate versus pH, for the adsorption of 4-Np onto FePcS ₄ -Amb.	98
Figure 3.32.	Plots of (a) initial rate of 4-Np adsorption and (b) Q_t (time = 30 min) for each MPc complex used to modify Amberlite [®] IRA-900.	99
Figure 3.33.	Diffuse reflectance spectral changes observed for FePcS ₄ -Amb (a) before adsorption of 4-Np, (b) after adsorption of 4-Np, and (c) following removal of 4-Np from (b) using dilute HNO ₃ .	101
Figure 3.34.	Electronic absorption spectra (a) of 4-Np in (i) acidic, and (ii) basic media, and (b) observed with time on immersion of FePcS ₄ -Amb containing 4-Np in HNO ₃ .	102
Figure 3.35.	Spectral changes of (a) CoPcS ₄ , and (b) FePcS ₄ on addition of 4-Np.	104

LIST OF SCHEMES

Scheme 1.1.	Electron delocalisation in the 4-nitrophenoxide ion.	1
Scheme 1.2.	Degradation pathway of nitrofen.	2
Scheme 1.3.	Degradation pathway of methyl paraoxon.	2
Scheme 1.4.	Inhibitory reaction between AChE and methyl paraoxon.	3
Scheme 1.5.	Synthetic routes for the preparation of metallated phthalocyanines.	11
Scheme 1.6.	Synthesis of a precursor for the formation of a tetrasubstituted phthalocyanine.	12
Scheme 1.7.	Type I reaction mechanism, where Sub represents 4-Np.	18
Scheme 1.8.	Type II reaction mechanism, where ISC is intersystem crossing.	18
Scheme 1.9.	Photobleaching of metallophthalocyanines by excited singlet oxygen.	23
Scheme 2.1.	Reaction mechanisms responsible for the consumption of $^1\text{O}_2$ during photocatalysis of 4-Np in the presence of a MPc.	38
Scheme 3.1.	Synthetic routes for the preparation of sulphonated phthalocyanines ($\text{M} = \text{Zn}^{2+}, \text{Fe}^{2+}, \text{Co}^{2+}, \text{or Ni}^{2+}$; $\text{R} = \text{SO}_3^- \text{Na}^+ \text{ or H}$).	51
Scheme 3.2.	Synthetic route for the preparation of water-soluble $\text{ZnPc}(\text{COOH})_8$.	52
Scheme 3.3.	Synthetic route for the preparation of 4-nitrophthalimide.	52
Scheme 3.4.	Synthetic route for the formation of $\text{ZnPc}(\text{NO}_2)_4$ and $\text{ZnPc}(\text{NH}_2)_4$.	53
Scheme 3.5.	Synthetic route for the formation of ZnPcF_{16} .	54
Scheme 3.6.	Synthetic steps for the preparation of ZnPcCl_{16} .	54
Scheme 3.7.	Proposed mechanisms for the phototransformation of 4-Np via the Type I reaction mechanism.	75
Scheme 3.8.	Transformation of 4-Np by singlet oxygen mechanism.	76
Scheme 3.9.	Proposed mechanism for the phototransformation of 4-Np to BQ and FA in the presence of water-insoluble MPc photocatalysts.	88
Scheme 3.10.	Proposed mechanism for the phototransformation of 4-Np to 4-NC in the presence of water-insoluble MPc photocatalysts.	89

LIST OF TABLES

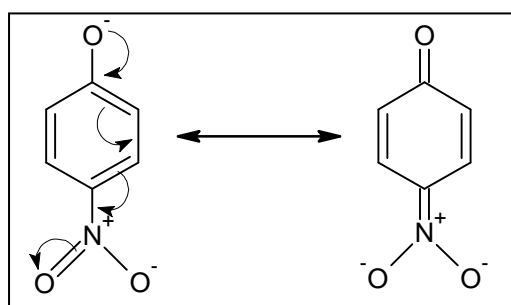
Table 1.1.	Toxicology, water solubility, LD ₅₀ and production values of mononitrophenol isomers.	2
Table 1.2.	Experimental conditions employed in previous studies for the photodegradation of 4-Np.	4
Table 1.3.	Results obtained for the photodegradation of 4-Np using experimental conditions listed in Table 1.2.	5
Table 1.4.	Resins used for the removal of phenolic complexes and dyes from aqueous media.	7
Table 1.5.	Photocatalysis of phenolic complexes in the presence of phthalocyanine complexes containing diamagnetic central metals.	27
Table 1.6.	Degradation products obtained for the phenolic complexes listed in Table 1.5.	28
Table 3.1.	λ_{\max} values and percentage aggregation of water-soluble MPcs in water at pH 7 (pH 8.2 for ZnPc(COOH) ₈).	57
Table 3.2.	λ_{\max} values obtained for the water-insoluble MPcs in DMSO.	61
Table 3.3.	Photosensitisation data for 4-Np transformation in the presence of the water-soluble photosensitisers under visible light irradiation.	68
Table 3.4.	Comparison of photosensitisation data obtained for the transformation of chlorophenols and the transformation of 4-Np in the presence of ZnPcS _{mix} .	70
Table 3.5.	Comparison of k_r and $(k_q + k_r)$ values obtained for selected photosensitisers.	73
Table 3.6.	Mass fragments obtained for fumaric acid and 4-nitrocatechol using ESI-MS.	79
Table 3.7.	Triplet lifetime and singlet oxygen quantum yield values obtained for the selected water-insoluble MPc complexes in DMSO, unless otherwise stated.	82
Table 3.8.	Effect of selected resins on the adsorption of 4-Np and immobilisation of ZnPcS _{mix} .	93
Table 3.9.	The LHKM parameters obtained for the adsorption of 4-Np onto MPc-Amb adsorbents.	105

1. INTRODUCTION

1.1. Background on 4-Nitrophenol

As a result of increased agricultural and industrial activity worldwide, the use of pesticides has increased,¹ which has led to an increase in the amount of phenols present in the environment, as many phenols are degradation products of various pesticides.²⁻⁴ Phenols are a threat to the environment and human health, due to their relatively high toxicity and persistence in aqueous media.⁵ Consequently there has been growth in research for the effective removal of phenols from our environment.

Nitrophenols are of interest in this study as they are listed as priority toxic pollutants by organisations such as the United States Environmental Protection Agency (USEPA).² Nitrophenols pose a threat to the environment as they are difficult to remove from groundwater due to their high stability and solubility in water, particularly 2- and 4-nitrophenol, which are both resonance stabilised (Scheme 1.1)^{5,6} Compounding this problem is their resistance to traditional methods of water purification,⁶ such as chemical oxidation, and microbial degradation.⁷



Scheme 1.1. Electron delocalisation in the 4-nitrophenoxide ion.⁵

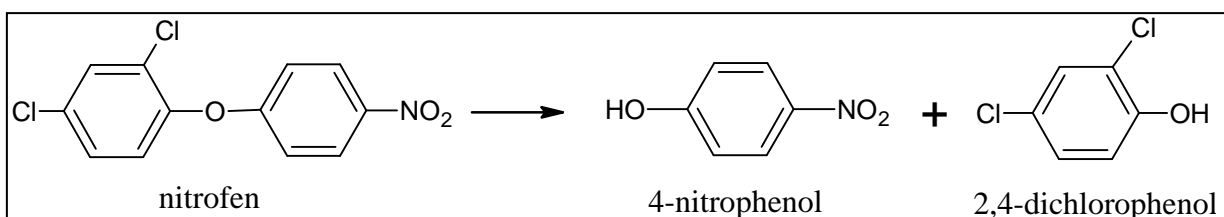
4-Nitrophenol (4-Np) was selected as it is produced in the highest quantities worldwide, has the highest toxicity and is more water-soluble than the other mononitrophenols (Table 1.1). 4-

Np is employed in the production of pharmaceutical drugs, pesticides, and dyes to darken leather. It is worth noting that the major use of 4-Np is in the production of pesticides, namely methyl- and ethyl- parathion. The influx of 4-Np into the environment is as a result of the degradation of pesticides such as nitrofen, methyl paraoxon, methyl parathion and ethyl parathion.^{2,3,8} Nitrofen, for example, is employed for weed control of rice, sugar, beets and cole crops;³ and methyl paraoxon is an organophosphorous pesticide that is used as a non-systemic insecticide.⁸ The pathway by which nitrofen and methyl paraoxon degrade has been proposed to occur via Scheme 1.2³ and Scheme 1.3,⁸ respectively.

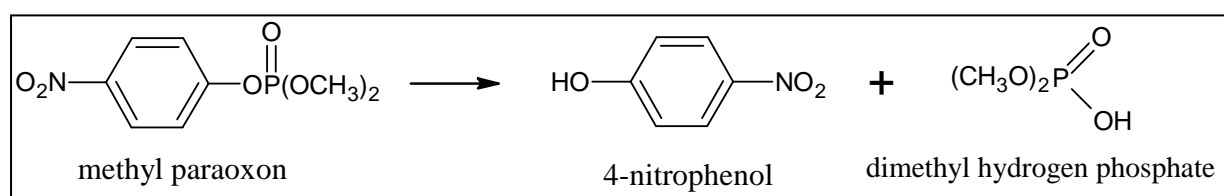
Table 1.1. Toxicology, water solubility, LD₅₀ and production values of mononitrophenol isomers (references in square brackets).

Compound	Toxicology [9]	Water solubility (g/L) [2]	ORL-RAT LD ₅₀ (mg kg ⁻¹) ^a [9]	Worldwide production (10 ⁶ kg) [2]
2-nitrophenol	Irritant	0.32 @ 38 °C	334	5 – 7
3-nitrophenol	Irritant	1.4 @ 25 °C	328	< 0.5
	Corrosive			
4-nitrophenol	Irritant	1.6 @ 25 °C	202	20
	Possible mutagen			

^alethal dosage for 50% of population (LD₅₀) of rats due to oral (ORL) ingestion

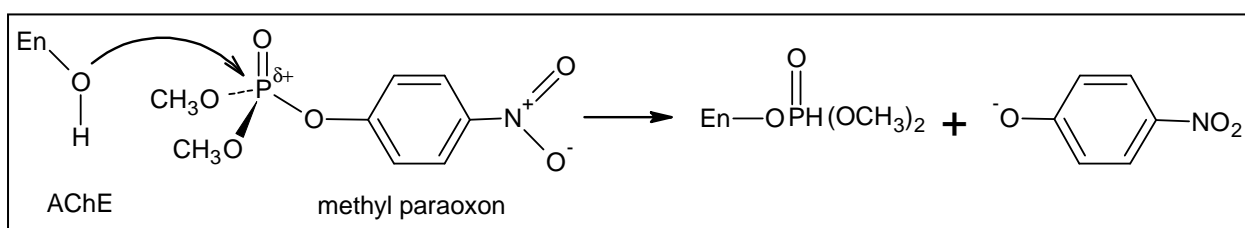


Scheme 1.2. Degradation pathway of nitrofen.³



Scheme 1.3. Degradation pathway of methyl paraoxon.⁸

Methyl paraoxon was selected as the pesticide for this study as it is known to have an inhibitory effect on acetylcholinesterase (AChE), a class of enzymes responsible for catalysing the hydrolysis of the neurotransmitter acetylcholine (ACh). Acetylcholine sends nerve impulses to muscles and organs within the body. The proposed chemical reaction between AChE and the pesticide (Scheme 1.4) leads to a build-up of ACh at the nerve synapses and neuro-muscular junction. The build-up of ACh within the body is hazardous as it leads to various neurotoxic effects with numerous symptoms, such as abdominal pain, diarrhoea, vomiting, bronchoconstriction, twitching and paralysis, amongst others.⁸



Scheme 1.4. Inhibitory reaction between AChE and methyl paraoxon, where En-OH is AChE.⁸

1.2. Survey of Methods for the Removal and Degradation of 4-Np

The experimental conditions and the corresponding results of a selection of photochemical studies that have been carried out for the photodegradation of 4-Np are listed in Tables 1.2 and 1.3, respectively. The predominant method that was employed for 4-Np degradation involves TiO_2 as a heterogeneous catalyst in a solution aerated with oxygen and irradiated with UV light. TiO_2 is a semiconductor oxide and has been found to be a relatively inefficient photosensitiser. The band gap for TiO_2 is 3.2 eV, which corresponds to near-UV light. A very small amount, approximately 4% of solar energy, is effective in this region, leading to its inefficacy as a photocatalyst for the oxidation of phenols in the presence of solar energy.¹⁰ Despite its inefficacies TiO_2 , as is evident from Table 1.2 and 1.3, has been used extensively for the photodegradation of 4-Np.¹¹⁻¹⁷

Table 1.2. Experimental conditions employed in previous studies for the photodegradation of 4-Np

Degradation system	Light source	4-Np concentration	Product analysis technique	Ref
Aerated TiO ₂	1500 W Xe lamp	0.072 mM (pH 5.5)	HPLC with UV-vis detector; Ion Chromatography, UV-vis Spectrophotometry	11
Aerated TiO ₂	125 W medium pressure Hg lamp	0.3 mM (unbuffered)	HPLC with UV-vis detector; Ion Chromatography	12
TiO ₂ impregnated with Cu(II)porphyrin or Cu(II) phthalocyanine	125 W medium pressure Hg lamp	20 mg/L (pH 4.0)	LCMS (APCI)	13
H ₂ O ₂	125 W Hg-Xe lamp	0.1 mM (unbuffered)	HPLC with UV detector	14
Excitation of NO ₂ ⁻ and NO ₃ ⁻ ions	6 low pressure Hg lamps	1 mM (unbuffered)	HPLC with UV detector; UV-vis Spectrophotometry	15
Aerated TiO ₂	365 nm UV light source	0.1 mM (pH 9)	GCMS, UV-vis Spectrophotometry	16
Aerated TiO ₂	450 W medium pressure Hg lamp	0.5 mM (pH 8.5)	HPLC with UV detector; hydrazine method (NO ₂ ⁻ , NO ₃ ⁻); phenate method (NH ₄ ⁺)	17

Table 1.3. Results obtained for the photodegradation of 4-Np using the experimental conditions listed in Table 1.2

Degradation system	Rate/degree of 4-Np degradation	Products detected	Ref
Aerated TiO ₂	$k = 1.5 \times 10^{-1} \text{ min}^{-1}$	4-aminophenol, hydroquinone, benzoquinone; NO ₂ ⁻ , NO ₃ ⁻ , NH ₄ ⁺ ions	11
Aerated TiO ₂	$k = 1.2 \times 10^{-2} \text{ min}^{-1}$	hydroquinone, 4-nitrocatechol; NO ₂ ⁻ , NO ₃ ⁻ , NH ₄ ⁺ ions	12
TiO ₂ impregnated with Cu(II)porphyrin or Cu(II) phthalocyanine	$\sim 3.8 \times 10^{-8} \text{ mol s}^{-1} \text{ L}^{-1}$	Dihydroxynitrobenzene isomers	13
H ₂ O ₂	40 % degradation after 10 min	hydroquinone, benzoquinone, 4-nitrocatechol	14
Excitation of NO ₂ ⁻ and NO ₃ ⁻ ions	$\Phi_{4\text{-Np}} = 0.05$	4-nitrocatechol, hydroquinone, benzoquinone, hydroxybenzoquinone, 4-nitrosophenol	15
Aerated TiO ₂	82 % degradation after 2.5 h ($k = 1.2 \times 10^{-2} \text{ min}^{-1}$)	hydroquinone, benzoquinone; NO ₂ ⁻ , NO ₃ ⁻ ions	16
Aerated TiO ₂	>99.9% degradation after 3 h	4-nitrocatechol, hydroquinone, benzoquinone, benzenetriol; NO ₂ ⁻ , NO ₃ ⁻ , NH ₄ ⁺ ions	17

Oxidation of 4-Np in the presence of either the Fenton reagent or H_2O_2 combined with UV light led to the phototransformation of 4-Np into 4-nitrocatechol, hydroquinone and benzoquinone.¹⁴ This method has its drawbacks as the oxidants employed, namely the Fenton reagent (a combination of H_2O_2 and an iron catalyst) and H_2O_2 are consumed in the degradation process.¹⁸ The regeneration of the catalyst, with regards to the Fenton reaction, has been achieved by electrochemical regeneration of the ferric ion.¹⁸ The drawback of using electrochemistry as a means of enhancing the degree of 4-Np degradation is the high cost associated with electrochemical instrumentation.

Photocatalysis is evidently the most frequently employed method for the degradation of 4-Np. The advantages that accompany photocatalysis have been identified by Ollis *et al.*:⁷

- (1) Complete oxidation of the substrate can be achieved within a few hours
- (2) The formation of polycyclised products is less likely to occur
- (3) Cheap, adaptable and highly active catalysts can be employed
- (4) Pollutants can be oxidised at low concentrations (e.g. parts per billion range).

Phthalocyanines (Pcs), which have been identified as effective photocatalysts for the degradation of phenolic complexes when irradiated with visible light, are employed in this study for the photodegradation of 4-Np. The drawbacks encountered when TiO_2 , H_2O_2 or the Fenton reagent are employed can be circumvented by making use of phthalocyanines. Prior to this work Pcs, as well as the isoelectronic porphyrins, have not been solely employed for the degradation of 4-Np. The structural properties of phthalocyanines, which contribute to their effectiveness as photocatalysts, are discussed in detail in Section 1.3.

The removal of phenols from aqueous solutions by adsorption onto the surface of polymeric resins has been explored extensively. Polymeric adsorbents, such as those listed in Table 1.4,

have replaced active carbon in the removal of aromatic compounds from wastewater. They are favoured alternatives to activated carbon as they are cheaper, have greater mechanical strength¹⁹ and are more varied in functionality, surface area and porosity.²⁰ Most commonly employed polymeric adsorbents include Amberlite XAD and NDA series.¹⁹⁻²⁵ Modification of polymeric resins using porphyrins to promote increased adsorption rates has only been reported for the adsorption of phenol and chlorophenols onto Amberlite XAD-2 and XAD-4 resins.²¹ The modification of a cationic resin, such as Amberlite[®] IRA-900, using phthalocyanine complexes has not been reported. Modified resins are under investigation as higher recoveries of the phenolic compounds are possible due to an increase in π - π interactions between the adsorbent and adsorbate.²¹ Metallophthalocyanines (MPcs) were employed in this study for the modification of Amberlite[®] IRA-900. MPcs have a more complex macroporous structure than porphyrins, resulting in the possibility of increased π - π interactions between phenols and the MPc modifiers.

Table 1.4. Resins used for the removal of phenolic complexes and dyes from aqueous media.

Resins used	Adsorbates	Modifiers	Ref
Amberlite XAD-2, Amberlite XAD-4	phenol, 2-, 4-, di-, tri- penta-chlorophenol	Protoporphyrin IX, tetrakis(<i>p</i> - carboxyphenyl)porphyrin	21
Amberlite XAD-4, Amberlite NDA-101, Amberlite D-301	phenol	none	20
Amberlite XAD-4, Lewatit EP63, Poly(EDMA), Sample 390	phenol	none	25
Amberlite NDA-103, Amberlite IRA-96C, Amberlite XAD-4	phenol	none	23
Amberlite XAD-4, ZCH-101	phenol, methylene blue, reactive orange X-GN	none	19
Amberlite IRA-420	phenol	none	22
Amberlite XAD-4, AmberliteXAD-7	phenol, 4-Np	none	24

The resins listed in Table 1.4 have different properties such as polarity, pore size, structure and functionality. There is however limited information available for most resins that have been employed in the studies referenced in Table 1.4. The Amberlite XAD series, Lewatit EP 63 and ZCH-101 are non-ionic, polymeric adsorbents.^{19-21,23-25} XAD-2, XAD-4, Lewatit EP 63 and ZCH-101 are polystyrene resins,^{19-21,23-25} whereas XAD-7 is a moderately polar, acrylic ester.²⁴

Ionic resins include:

- Amberlite D-301 – anion exchange resin²⁰
- Amberlite NDA-101 – aminated, cationic, moderately polar resin²⁰
- Amberlite NDA-103 – weak base, highly polar resin²³
- Amberlite IRA-96C – weak base, highly polar resin²³
- Amberlite IRA-420 – strong base, anion exchange resin²²

1.3. Phthalocyanines

In order to comprehend the effectiveness of MPCs as photocatalysts it is important to understand the structural features that contribute to their photocatalytic properties.

1.3.1. Background on Phthalocyanines

Phthalocyanine complexes were first synthesized in 1907, however, the correct structure of a phthalocyanine complex was only published in 1934, by Professor Linstead of the Imperial College. He coined the name “phthalocyanine” to account for its origin from phthalic anhydride (*phthalo*) and its similarity in colour to *cyanine* dyes. Phthalocyanine complexes were originally used as dyes and pigments, due to their intense colours. Today their use extends as far as nanotechnology, photodynamic therapy (PDT), electrophotography, flash fusion and the security

industry, as well as their inclusion in ink jet printers and washing powders. All phthalocyanines used in these processes have been structurally manipulated for optimum performance.²⁶

Structurally, phthalocyanines are planar, macrocyclic, aromatic compounds that are isoelectronic with porphyrins (Figure 1.1). They consist of four isoindole subunits linked together by N atoms. Phthalocyanines possess high thermal stability due to closure of the ring by the interlinking N atoms.²⁷ An extended π conjugated system, due to the peripheral benzene rings, contributes to the stability of phthalocyanines.²⁸ The structural features of phthalocyanines are advantageous as they provide a canvas for further manipulation of their structure, such as addition of a metal in the centre of the ring, addition of substituents to the peripheral benzene rings or extension of π conjugation through the addition of phenyl rings to the peripheral benzene rings.

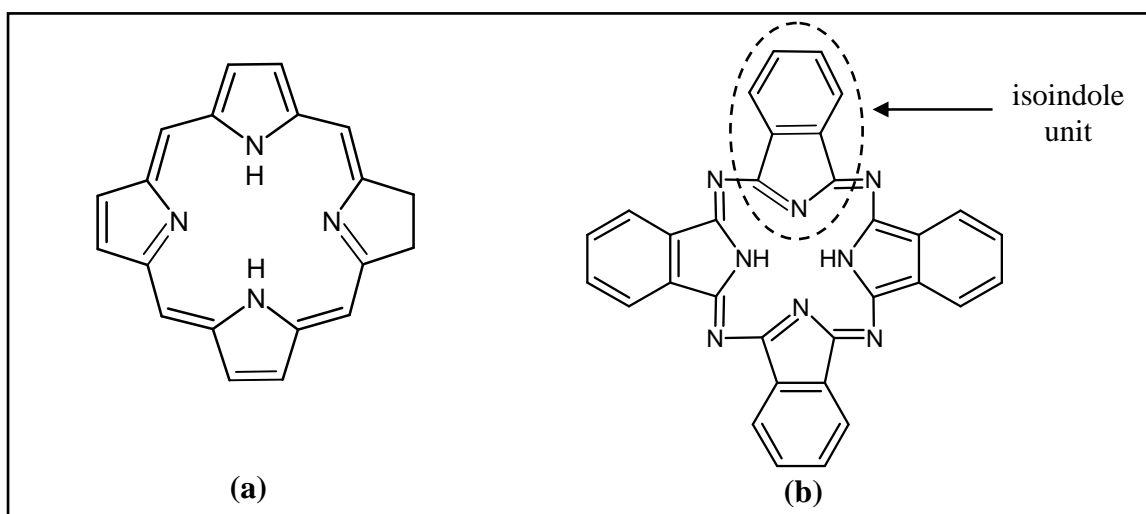


Figure 1.1. Geometric structures of an (a) unmetallated porphyrin and an (b) unmetallated phthalocyanine.²⁸

The centre of the phthalocyanine dianion (Pc^{2-}) is capable of hosting a number of elements, namely group 1 and group 2 metals, transition metals, lanthanides, actinides, and main group metals and metalloids. The diagonal distance of two N atoms within the centre of the ring is approximately 396 pm. Metals that are capable of insertion into the centre of the ring, without

affecting the planarity of the complex, lift the symmetry of the phthalocyanine from D_{2h} of H_2Pc (unmetallated phthalocyanine) to D_{4h} for MPcs (metallated phthalocyanines).²⁹

Peripheral substitution on the Pc ring and axial ligation at the metal centre are advantageous as they can result in reduced aggregation of the complex and improved solubility in a wider variety of solvents. Solvation and aggregation are affected as the distance between adjacent planar macrocycle rings carrying the π electrons is increased.²⁸ Section 1.3.4 provides a detailed explanation of aggregation and its influence on the photocatalytic properties of phthalocyanines. Peripheral and axial substituents are also capable of increasing Φ_T (triplet quantum yield – defined in Section 1.4) values through increased intersystem crossing from S_1 to T_1 , which is as a result of enhanced spin-orbit coupling due, in turn, to the “heavy-atom” effect.^{30,31} A detailed explanation of spin-orbit coupling is provided in Section 1.4.1.

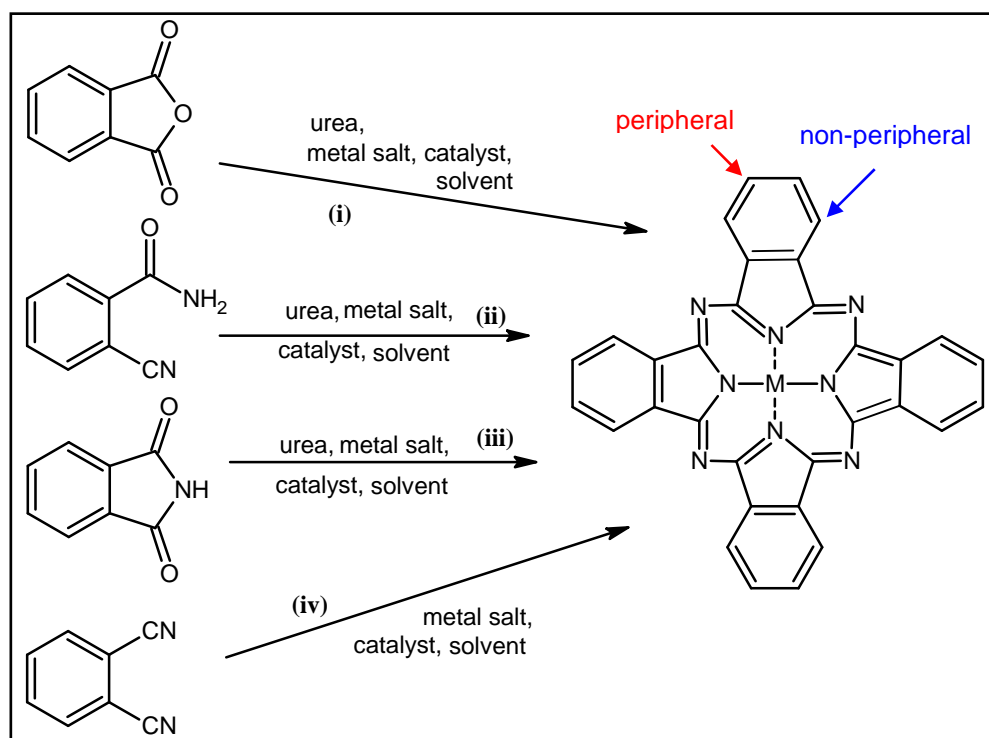
1.3.2. General Synthesis of Phthalocyanines

Unsubstituted phthalocyanines may be synthesized by heating a mixture containing a metal salt (or metal) and (i) phthalic anhydride, (ii) *o*-cyanobenzamide, (iii) phthalimide or (iv) phthalonitrile (as examples) in the presence of various reagents (Scheme 1.5).^{26,32}

The catalyst employed in most synthetic routes is ammonium molybdate. Urea is used as a source of N atoms for bridging the isoindole groups. The reactions usually occur in one synthetic route through complex reaction mechanisms. The reaction intermediates have only been isolated in a few synthetic processes.²⁷

The phthalic anhydride route (i) is employed for large-scale production of phthalocyanines, as it requires relatively inexpensive starting materials. Higher purity products are obtained using

phthalonitrile as the starting material. The phthalonitrile route (iv) is generally employed for the synthesis of phthalocyanines necessary for high-technology applications, such as flash fusion and PDT.²⁶ Synthesis of phthalocyanines is also achieved through microwave irradiation. This method is advantageous as it affords fast reaction rates and does not require the use of expensive and environmentally hazardous solvents.^{33,34}

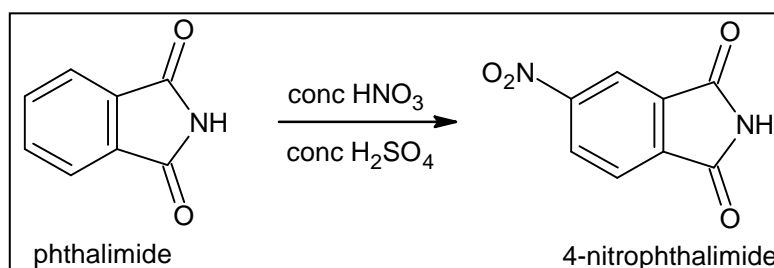


Scheme 1.5. Synthetic routes for the preparation of metallated phthalocyanines.^{26,32}

Substituted phthalocyanines, i.e. tetra- and octa- substituted phthalocyanines, are prepared by substitution of a preformed Pc ring (i.e. H₂Pc) or by condensation of a substituted precursor (eg. phthalimide or phthalonitrile) (Scheme 1.6). Substituted precursors are preferred over the preformed Pc ring as harsh conditions are necessary for the insertion of a metal into the centre of the Pc ring. The formation of tetrasubstituted phthalocyanines at the peripheral position (Scheme 1.5) leads to the formation of mixtures of constitutional isomers with the following symmetry: (C_{4h}) 2,9,16,23-, (D_{2h}) 2,10,16,24-, (C_{2v}) 2,9,17,24-, and (C_s) 2,9,16,24- tetrasubstituted Pcs. The ratio in which the constitutional isomers of peripherally tetrasubstituted phthalocyanines is

obtained has been determined experimentally to be 1:1:2:4 for C_{4h} , D_{2h} , C_{2v} and C_s , respectively.³⁵ The phthalimide and phthalonitrile precursors can be purchased, however their synthesis is relatively straightforward, requiring inexpensive starting materials and leading to high yields of the substituted derivative (Scheme 1.6). Octasubstituted phthalocyanines can be substituted at the eight peripheral (2,3,9,10,16,17,23,24-octasubstituted Pc) or eight non-peripheral (1,4,8,11,15,18,22,25-octasubstituted Pc) positions (Scheme 1.5). Isomerically pure products result with the use of disubstituted precursors, hence the purification of octasubstituted Pc complexes is considerably easier than purification of tetrasubstituted Pc complexes.

The synthesis of hexadecasubstituted Pc complexes can be achieved using the substituted H_2Pc complex or a tetrasubstituted precursor without the formation of isomeric mixtures.



Scheme 1.6. Synthesis of a precursor for the formation of a tetrasubstituted phthalocyanine.³⁶

1.3.3. Spectral Properties of Phthalocyanines

1.3.3.1. UV-visible Spectra

The 18 π system of the inner most 16-membered ring governs the spectral properties of Pcs (Figure 1.2).²⁸ The purity and intense colour of Pc complexes can be attributed to the isolated band that appears at the red end of the visible spectrum near 670 nm for metallated Pcs without ring substituents. This band, termed the Q band, has molar absorptivity (ϵ) values that exceed 10^5

$\text{dm}^3 \text{mol}^{-1} \text{cm}^{-1}$, which is a desirable feature of photosensitiser complexes (Section 1.4.2). A second, broader and less intense band appears in the blue region and is termed the B or Soret band. The four-orbital model that has been proposed for phthalocyanines shows that the Q band arises as a result of the energy transition from the highest occupied molecular orbital (HOMO – a_{1u}) to the lowest unoccupied molecular orbital (LUMO – e_g) (Figure 1.3). Two B bands, B_1 and B_2 , are often observed for Pcs. The B_1 and B_2 bands arise as a result of transitions from a_{2u} to e_g and b_{2u} to e_g , respectively (Figure 1.3). Other absorption bands, which appear in the UV region, include the N, L and C bands. Hence, the bands that can be observed for phthalocyanines, in increasing order of energy, include the Q, B_1 , B_2 , N, L and C bands.²⁹

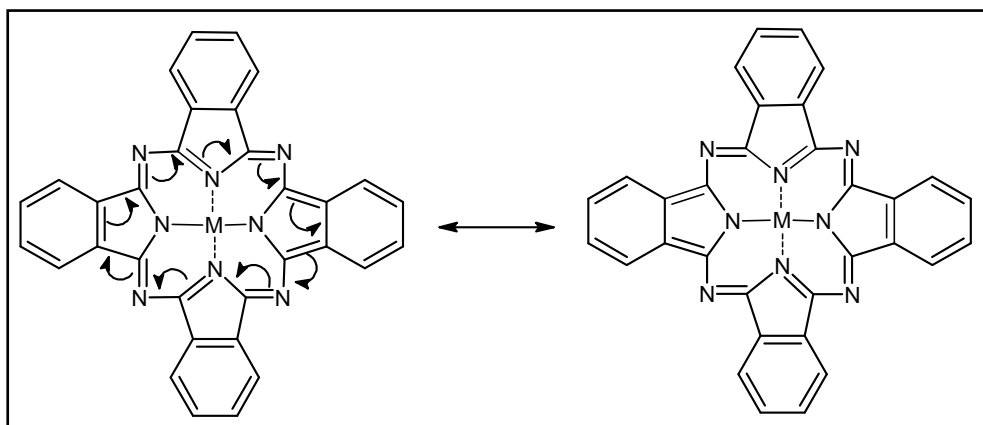


Figure 1.2. Electron delocalisation showing π conjugation within the phthalocyanine ring.

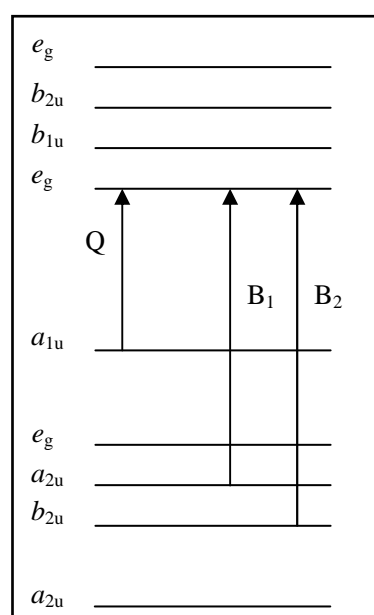


Figure 1.3. The π – π^* transitions that give rise to the Q and B bands of phthalocyanines.²⁹

The position of the Q band in the spectrum depends on the central metal, peripheral and non-peripheral substituents, axial ligands, the solvent in which the phthalocyanine is dissolved, aggregation, and the extent of π conjugation. The Q band can be either blue-shifted (termed a hypsochromic shift) or red-shifted (a bathochromic or hyperchromic shift) as a result of changes in the structure of the phthalocyanine. A change in the shape of the Q band occurs when the symmetry of the complex is altered.²⁸

1.3.3.2. Infrared Spectra

Metallated phthalocyanine complexes possess relatively similar infrared (IR) spectra. The shift in characteristic MPc bands is about 50 cm^{-1} as the central metal is replaced by another. Typical phthalocyanine skeletal vibrations occur between $400\text{--}1100\text{ cm}^{-1}$. Other bands that appear outside this region for the phthalocyanine ring include the C-H stretching vibration at about 3030 cm^{-1} , and the C-C benzene ring stretching vibrations at 1610 and 1475 cm^{-1} . Metal sensitive bands appear at about 1490 and 1410 cm^{-1} .³⁷

Complete metallation of the complex is confirmed by the absence of strong bands at about 715 and 1000 cm^{-1} , which are due to the metal-free phthalocyanine complex.³⁸

1.3.4. Aggregation of Phthalocyanines

The formation of phthalocyanine aggregates is of significance in this study as aggregation has an adverse effect on the photophysical behaviour of phthalocyanines, reducing their ability to act efficiently as photosensitisers.⁷ Aggregates do not always form chemical bonds, but are generally loosely associated species.²⁸ Phthalocyanine aggregates are commonly formed in one of four ways:²⁹

- Direct linkages between two or more phthalocyanine rings
- Covalent bonds between adjacent metals, known as μ -oxo links (e.g. Fe or Si)
- Two rings share one central metal, referred to as sandwich-type complexes (e.g. SnPc_2 or LuPc_2)
- Weak interactions between peripheral substituents on two adjacent Pc rings.

Dimerization (aggregation between two adjacent Pc complexes) between symmetrical phthalocyanines is depicted by a hypsochromic shift in the Q band (to approximately 620 nm), band broadening, or splitting of the Q band. Spectral effects will depend on the proximity of the adjacent rings, the position of the overlap, the tilt angle of the rings and the bulkiness of the peripheral substituents. On a molecular level, there is a split in the LUMO to form two further degenerate states. This phenomenon occurs for phthalocyanines with a D_{4h} symmetry, where two rings lie parallel (Figure 1.4). The degenerate states that undergo a bathochromic shift are denoted B^- and Q^- , and those that undergo a hypsochromic shift are denoted B^+ and Q^+ .²⁹

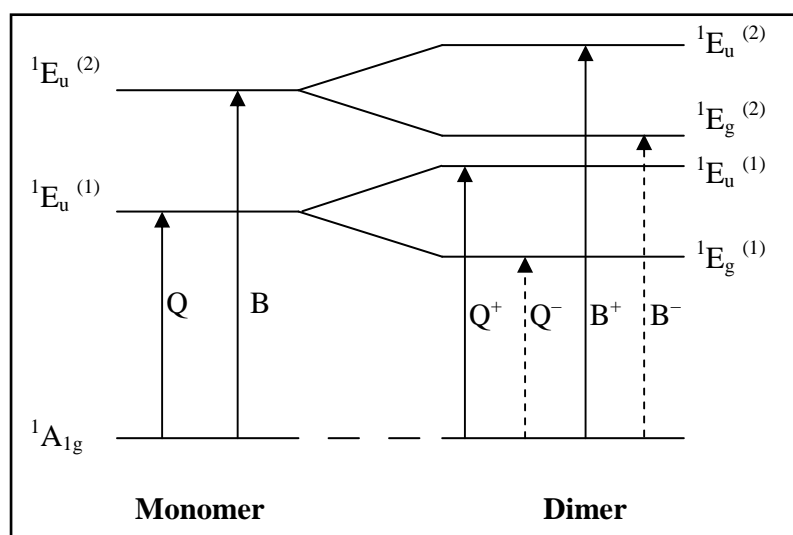


Figure 1.4. Effect of dimerization on the molecular orbitals of D_{4h} phthalocyanines

(----- forbidden transitions, ——— allowed transitions).²⁹

The addition of an organic solvent or a surface acting agent (surfactant), such as Triton X-100, can lead to the dissociation of aggregates. The ability of the solvent (or surfactant) to monomerise the aggregate depends on the polarity of the solvent (or surfactant). Solvents with a relatively low polarity will cause the monomer-dimer equilibrium to favour the formation of the monomeric species. Dilution of the phthalocyanine will also lead to the formation of the monomeric species. Sequential dilution of the phthalocyanine complex, followed by spectrophotometric analysis of the solution, is an experimental tool used to confirm aggregation of the complex and determine the wavelength of the monomeric and dimeric species in a specific solvent.²⁸

1.4. Phthalocyanines as Photocatalysts

Quantum yields (Φ) are used to quantify the efficiency of a photochemical or photophysical process (Eq. (1)). The process it defines is one that begins with the absorption of a photon and ends with either the disappearance of the molecule or its deactivation to a non-reactive state. Two quantities are required to determine quantum yields, namely the change in concentration of the reactant (or product) and the number of photons absorbed by the reactant (or product).^{39,40}

$$\Phi = \frac{\text{No. of molecules/unit volume/unit time undergoing a specific process}}{\text{No. of photons (quanta)/unit volume/unit time absorbed by the system}} \quad (1)$$

Triplet quantum yields (Φ_T) can be defined as a measure of the amount of photosensitisers that undergo the transition from the first excited singlet state to the first triplet state ($S_1 \rightarrow T_1$).

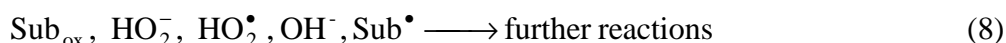
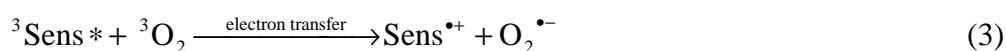
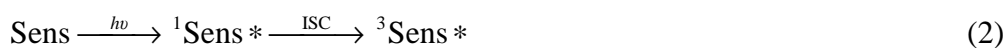
The lifetime of a complex is defined as the amount of time required to reduce the number of molecules which populate an excited state to $1/e$ (i.e. 3.68×10^{-1}) of its original value. The

deactivation of the excited state is generally a first or pseudo-first order process. Deactivation can occur by means of a chemical reaction and/or physical deactivation.³⁹ The triplet lifetime of a molecule (τ_T) is therefore the amount of time required for the molecules populating the excited triplet state to reduce their population to $1/e$ of their original value due to relaxation from the excited triplet state to the ground singlet state ($T_1 \rightarrow S_0$).

1.4.1. Photocatalysis Mechanisms

There are two broad mechanistic pathways (Type I and Type II reaction mechanisms) by which photosensitisers, such as phthalocyanines, in the presence of light and singlet oxygen, can cause the oxidation of a substrate.⁴⁰⁻⁴³ The Type I reaction mechanism (Eqs. (2)–(8)) involves the formation of a radical species ($\text{Sens}^{\bullet+}$) which is capable of reacting with ground state oxygen to generate a superoxide radical anion ($\text{O}_2^{\bullet-}$). The superoxide species is unstable and reactive, which results in the generation of hydroxyl radicals. The overall reaction is a photochemically initiated autoxidation (Scheme 1.7).

Similarly, the Type II reaction mechanism (Eqs. (9)–(11)) is initiated photochemically, where excitation of the photosensitiser is induced by irradiation with visible light, yielding the excited singlet state photosensitiser ($^1\text{Sens}^*$). Intersystem crossing follows, resulting in the formation of an excited triplet state sensitiser ($^3\text{Sens}^*$). Energy transfer from $^3\text{Sens}^*$ to ground state oxygen ($^3\text{O}_2$, $^3\Sigma_g^-$) results in active singlet oxygen ($^1\text{O}_2$, $^1\Delta_g$), which is capable of oxidising the substrate (Sub). The energy transfers that occur in Scheme 1.8 are illustrated in the Jablonski diagram in Figure 1.5.



Scheme 1.7. Type I reaction mechanism, where Sub represents 4-Np.⁴¹



Scheme 1.8. Type II reaction mechanism, where ISC is intersystem crossing.⁴¹

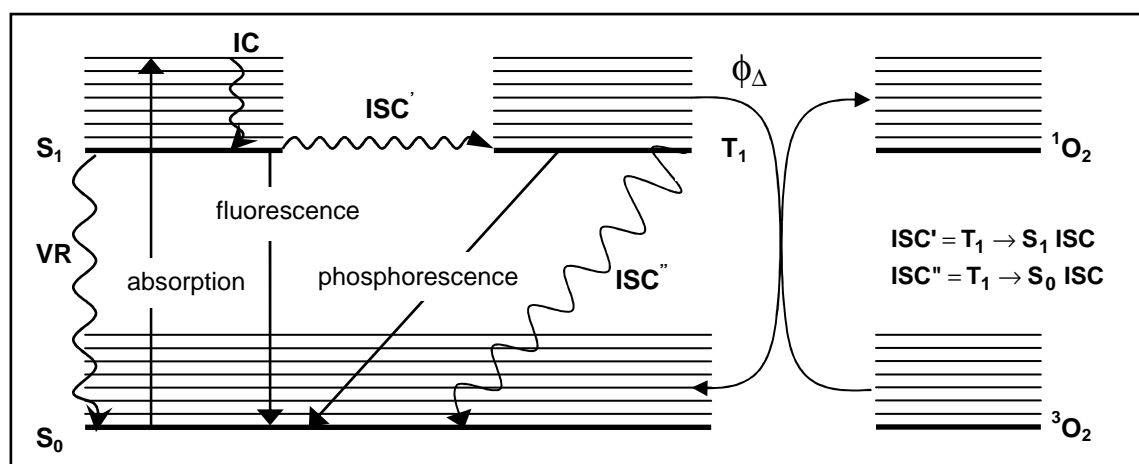


Figure 1.5. Jablonski diagram depicting the likely energy transitions of photosensitisers.⁴⁰⁻⁴³ (IC = internal conversion, ISC = intersystem crossing, VR = vibrational relaxation).

Reports show that the dominant process in the photo-oxidation of environmental substrates is the route via $^1\text{O}_2$. Side reactions may occur via the Type I reaction mechanism.⁴²

Ordinarily singlet-triplet transitions are spin-forbidden, as the transition involves a change in the relative orientation of the spins of the outermost electrons in a complex, such as the transition from an anti-parallel pair of electrons (singlet) to a parallel pair of electrons (triplet). Coupling of the spin and orbital angular momenta, known as spin-orbit coupling, relaxes the spin selection rule.^{40,43,44} An interaction between the electron spin and the magnetic field generated by the orbital motion of the electron occurs, which blurs the distinction between states of different multiplicities. In the case of spin-orbit coupling, the spin quantum number (S) and the orbital angular momentum quantum number (L) are no longer independent, and as a result a new quantum number (J), that incorporates both S and L to define the energy of states, is employed.⁴⁵

The major contribution in determining the energy of orbitals of light atoms (including 3d and 4f elements) is the relative orientation of the spins of electrons, followed by the relative orientation of their orbital angular momenta. For heavier atoms (4d, 5d and 5f elements) the relative orientation of the spin as well as the orbital angular momenta of electrons are both important for energy determination.⁴⁴ In general, spin-forbidden transitions are weaker than spin-allowed transitions. However, the intensity of spin-forbidden transitions increases as the atomic number of the atom in the complex increases, and as a result this phenomenon is referred to as the “heavy-atom” effect.^{43,44} The “heavy-atom” effect can be quantified by comparing the intersystem crossing rates for ClAlPcS₄, (chloroaluminium tetrasulphonated Pc) ClGaPcS₄ (chlorogallium tetrasulphonated Pc) and ClInPcS₄ (chloroindium tetrasulphonated Pc), which are 5.9×10^7 , 1.8×10^8 and $2.4 \times 10^9 \text{ s}^{-1}$, respectively.⁴⁶ An increase in atomic number results in increased contribution of the orbital angular momentum, resulting in enhanced spin-orbit coupling. Consequently the rate of intersystem crossing from the excited singlet state to the first

triplet state and relaxation from the latter to the ground singlet state are affected. The amount of singlet oxygen produced by transfer of energy from an excited triplet state photosensitiser to triplet state oxygen will also be affected, i.e. singlet oxygen quantum yield (Φ_{Δ} - Eq. (12)), by spin-orbit coupling.³⁰

$$\Phi_{\Delta} = \frac{\text{number of } ^1\text{O}_2 \text{ molecules formed/unit volume/unit time}}{\text{number of quanta absorbed/unit volume/unit time}} \quad (12)$$

1.4.2. Molecular Properties and Generation of Singlet Oxygen

The degradation of phenols has been achieved by their oxidation in the presence of excited singlet oxygen ($^1\text{O}_2$). $^1\text{O}_2$ is ~1 V more oxidizing than oxygen in its triplet (ground) state ($^3\text{O}_2$) and as a result is more electrophilic than $^3\text{O}_2$ and therefore capable of reacting readily with unsaturated carbon-carbon bonds. The oxidation of phenols occurs due to electron transfer from the electron-rich phenol to electrophilic singlet oxygen. The final degradation products are generally *p*-benzoquinones which form due to dehydration of hydroperoxide intermediates.³⁰

The ground state of oxygen is called a triplet state because, on exposure to a magnetic field, the spins of the electrons can align in one of three ways:⁴⁷

- 1) Both spins align up (oxygen deflects downwards in a magnetic field),
- 2) Both spins align down (oxygen deflects upwards in a magnetic field),
- 3) Spins are anti-parallel (oxygen passes unperturbed through the magnetic field).

Dioxygen has two singlet excited states above the triplet state, denoted as $^1\Delta_g$ and $^1\Sigma_g^+$. The first singlet state, $^1\Delta_g$, possesses an energy equivalent to 94 kJ/mol (22.5 kcal/mol), while $^1\Sigma_g^+$

is higher in energy (132 kJ/mol or 31.5 kcal/mol) (Figure 1.6). The differences between the energy states is evident from the orientation of the electrons in the π -antibonding orbitals (π_{2p}^*) – illustrated in Figure 1.7.³⁰ Differences in stability between $^1\Delta_g$ and $^1\Sigma_g^+$ states can be confirmed by comparing their radiative lifetimes, which are $10^{-6} - 10^{-3}$ s and $10^{-11} - 10^{-9}$ s in solution, respectively.³⁰ Singlet oxygen lifetimes are lower in aqueous media compared with organic media, due to the dissipation of its energy as heat. The energy dissipation is due to similarities in energy between the first excited-state oxygen ($^1\Delta_g$) and the oxygen-hydrogen stretching of water.⁴⁷

The first singlet state of oxygen is relatively long-lived as the transition from $^1\Delta_g$ state to $^3\Sigma_g^-$ state is spin-forbidden. However, the second singlet state is short-lived due to the spin-allowed transition from $^1\Sigma_g^+$ state to $^1\Delta_g$ state. The state of dioxygen that will be of significance in this study is the first singlet state ($^1\Delta_g$),³⁰ therefore, from this point on, any mention of the excited singlet state of oxygen refers to its first excited singlet state as opposed to its second excited singlet state.

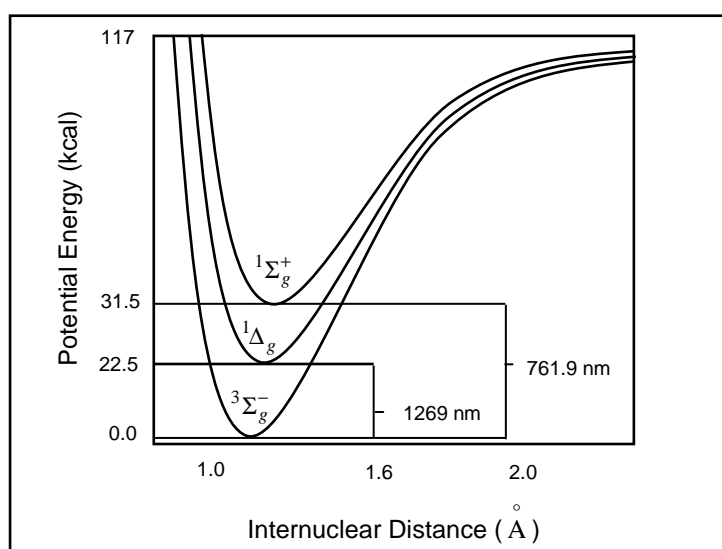


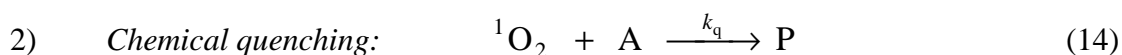
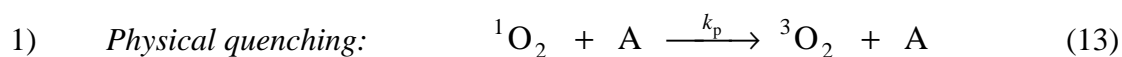
Figure 1.6. Potential energy curves for the three energy states of dioxygen.³⁰

State	Orbital Assignment	
$1\Sigma_g^+$	\uparrow_π	\downarrow_π
$1\Delta_g$	$\uparrow\downarrow_\pi$	π
$3\Sigma_g^-$	\uparrow_π	\uparrow_π

Figure 1.7. Electronic orientations of molecular oxygen in the outermost antibonding orbitals.³⁰

It is evident from Figure 1.7 that the electrons in the outermost antibonding orbitals of ground state oxygen comply with Hund's rule, as the outermost electrons of the lowest energy state have different magnetic quantum numbers and the same spin quantum number. The Pauli exclusion principle is also obeyed, as the electrons, which are not spin paired, are distributed in separate orbitals (i.e. P_x and P_y antibonding orbitals). The interaction of ground state oxygen with an excited triplet state photosensitiser leads to an inversion of the spin of one of these electrons. The quantum numbers of the two electrons are now unique, which allows them to pair up in the same antibonding orbital leading to destabilisation of dioxygen.⁴⁷

Once in its excited state dioxygen can be deactivated via physical quenching (Eq. (13)) or chemical quenching (Eq. (14)):

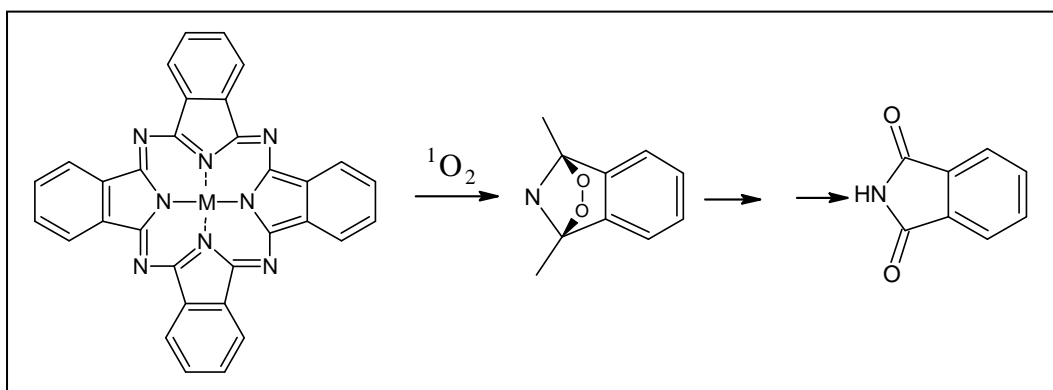


Chemical quenching differs from physical quenching, as oxygen consumption and the formation of products results from chemical quenching of singlet oxygen. The ability of destabilised excited singlet oxygen to undergo chemical quenching allows for the oxidation of substrates, such as phenolic complexes, that are unaffected by oxygen in its triplet (ground) state.³⁰

As previously mentioned, excited triplet state photosensitisers are required to convert $^3\text{O}_2 (^3\Sigma_g^-)$ to $^1\text{O}_2 (^1\Delta_g)$ through a radiationless transition.⁴⁷ Therefore, in order to produce $^1\text{O}_2$ the following are necessary: light of an appropriate wavelength to convert the photosensitiser to its triplet excited state; oxygen; and a photosensitiser capable of absorbing and using the available energy to excite oxygen to its singlet state. Effective photosensitisers should possess the following characteristics:³⁰

- 1) High absorption coefficient (ϵ) in the spectral region of the light source
- 2) Excited triplet state energy equal to or higher than that of $^1\text{O}_2$ (i.e. $E_T \geq 94 \text{ kJ/mol}$)
- 3) High triplet quantum yields ($\Phi_T > 0.4$) and long triplet lifetimes ($\tau_T > 1 \mu\text{s}$)
- 4) Resistance to photobleaching

As mentioned above the photostability of MPCs is important for the photocatalysis of phenols, as photobleaching leads to reduced photocatalytic activity.³⁰ Photobleaching of the MPCs can occur during irradiation of the complex with visible light. It has been proposed that an interaction between the HOMO of the phthalocyanine and the LUMO of excited singlet oxygen occurs, resulting in the formation of the corresponding phthalimide complex due to a chemical reaction between energy-rich singlet oxygen and the photosensitiser (Scheme 1.9).^{48,49}



Scheme 1.9. Photobleaching of metallophthalocyanines by excited singlet oxygen.^{48,49}

1.4.3. Effect of Substituents and the Central Metal on Photocatalytic Activity

Non-transition metal ions, such as Al(III), Zn(II) and Si(IV), in the centre of the Pc ring result in long triplet lifetimes (τ_T) and relatively high quantum yields for singlet oxygen formation (Φ_Δ), as they possess closed p and d shells.^{31,50,51} Conversely the presence of paramagnetic metal ions results in short triplet lifetimes, for example, zinc tetrasulphonated Pc (ZnPcS₄) has a long triplet lifetime ($\tau_T = 245 \mu\text{s}$), whereas copper tetrasulphonated Pc (CuPcS₄) has a τ_T of $0.06 \mu\text{s}$.³⁰ Paramagnetic metal ions are, however, capable of enhancing intersystem crossing, which leads to relatively large Φ_T values,⁵² as orbiting electrons generate a magnetic moment proportional to that of the angular momentum, which results in enhanced spin-orbit coupling.⁵³

The photocatalytic efficiency of Pcs can be optimised not only by manipulation of the metal centre, but also through the addition of substituents on the benzene ring of the isoindole units. The addition of substituents with large molecular weights can increase the overall molecular weight of the photosensitiser, and therefore enhance spin-orbit coupling due to the “heavy-atom” effect, resulting in improved Φ_T values.³⁰ The substituents also influence the photostability of phthalocyanines depending on their electron-withdrawing or electron-donating properties. Electron-donating substituents destabilise the HOMO, resulting in a reduction in the distance between the HOMO and the LUMO, which shifts the Q band to longer wavelengths. The opposite is true for electron-withdrawing groups. The resultant effect is greater photo-oxidative stability of the MPc complexes on addition of electron-withdrawing substituents.⁴⁹

The presence of axial substituents, which is possible for the diamagnetic metals Si(IV), Ge(III), Sn(IV) and Al(III), contributes to the photostability and the “heavy-atom” effect of the photosensitiser, and reduces aggregation. Consequently phthalocyanines containing axial substituents have relatively high Φ_Δ values.⁴⁸

MPcs can be employed in aqueous media as a result of the inclusion of peripheral sulpho (SO_3^-) or carboxyl (COO^-) groups, as these substituents are polar and can interact with polar water molecules.³¹ Anionic substituents also lead to relatively high τ_T and Φ_T values due to their poor ability to dissipate energy nonradiatively.⁵¹ Another advantage of Pcs with anionic substituents is that they are capable of immobilisation onto cationic resins, such as Amberlite® IRA-900, leading to improved photostability of the photosensitiser^{48,54} (Figure 1.8). The disadvantage of employing carboxylated MPcs is the possibility of increased aggregation between adjacent complexes due to hydrogen bonding.³¹

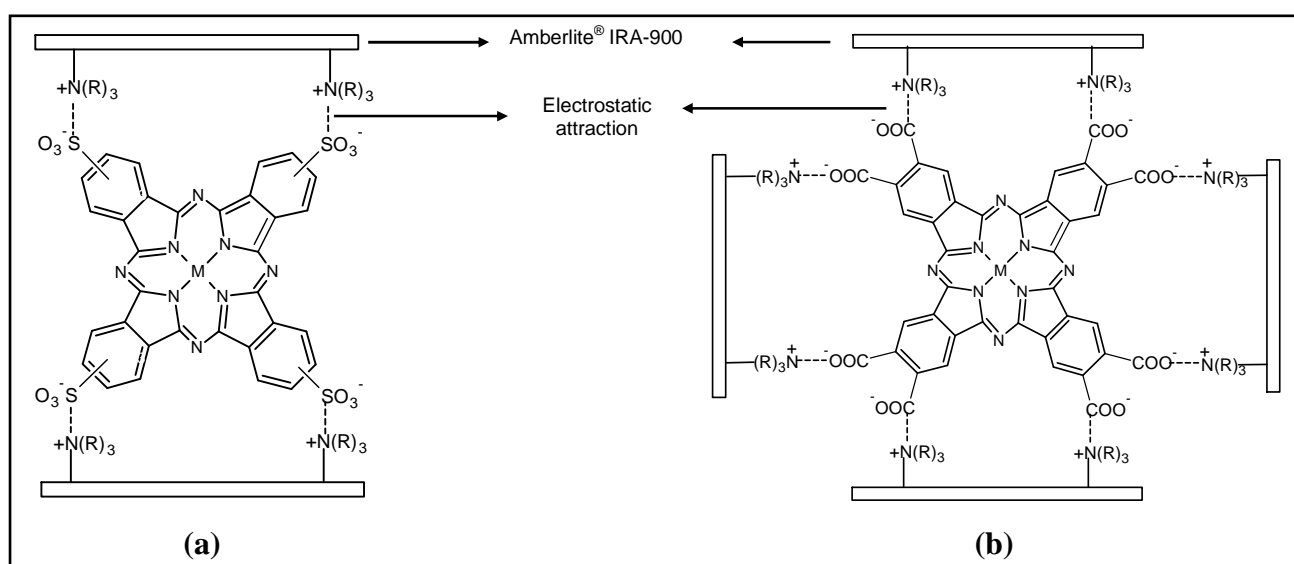


Figure 1.8. Immobilisation of (a) sulphonated, and (b) carboxylated MPcs onto Amberlite® IRA-900.⁵⁴

1.4.4. Previous Photocatalytic Studies using MPcs as Photocatalysts

Some Pcs that have been employed prior to this work for the photocatalytic degradation of phenolic complexes are listed in Table 1.5.^{42,54-59} In all cases the pH of the solution was buffered to ensure that the phenolic complexes were present as the corresponding phenolate ion. Previous reports have proven that the rate of degradation of phenols is highest in the presence of the

unprotonated phenolic complex as the phenolate ion is more reactive towards singlet oxygen than the neutral phenolic species.⁵⁵ All experiments, except those involving polynuclear Pcs and $\text{Zn}\{\text{Pc}(t\text{-Bu})_4\}$, were carried out in aqueous solution. Photocatalysis in the presence of the polynuclear Pcs was carried out in a mixture of water and ethanol,⁵⁹ whereas a mixture of acetonitrile and aqueous sodium hydroxide was employed for photocatalysis in the presence of $\text{Zn}\{\text{Pc}(t\text{-Bu})_4\}$.⁵⁸ The predominant degradation products obtained for the phenolic compounds used in Table 1.5 are listed in Table 1.6. It was not possible to quantitatively compare photocatalytic efficiencies of all MPcs listed, as different experimental conditions were used in most cases.

A comparison can be drawn between degradation rates obtained for the degradation of phenol in the presence of polynuclear Pcs and tetrasulphonated Pcs, as the rate of oxygen consumption was measured in both studies. In the presence of $[\text{ZnPc}(\text{COOH})_n]_{\text{poly}}$ and $[\text{AlPc}(\text{COOH})_n]_{\text{poly}}$ the rates of degradation are 98.0 and 31.0 mol O_2 /min/mol photosensitiser, respectively.⁵⁹ However, in the presence of AlPcS_4 the degradation rate was considerably higher (164 mol O_2 /min/mol photosensitiser). Degradation rates of phenol in the presence of GaPcS_4 and ZnPcS_4 were lower than that obtained for AlPcS_4 (18.8 and 92.0 mol O_2 /min/mol photosensitiser, respectively).⁴²

The trends in the photocatalytic activities of the Pcs are described in Table 1.5 where possible. It is evident from the trends in the degradation of pentachlorophenol (PCP) that Zn(II) as a central metal results in more efficient degradation of PCP in the presence of a heterogeneous catalyst.⁵⁴ However, Al(III) appears to be more effective in a homogeneous system.⁵⁶

Table 1.5. Photocatalysis of phenolic complexes in the presence of phthalocyanine complexes containing diamagnetic central metals.

Phthalocyanines used	Phase of catalyst	Substrate	Efficiency	Ref
ZnPcS ₄ , AlPcS ₄ , ZnPcS _{mix} , AlPcS _{mix} , ZnPc(COOH) ₈ , AlPc(COOH) ₈	Homogeneous	4-chlorophenol	ZnPcS _{mix} > AlPcS _{mix} > ZnPc(COOH) ₈ > AlPcS ₄ > AlPc(COOH) ₈ ≈ ZnPcS ₄	55
AlPcS _{mix} , AlPcS ₄ , ZnPcS _{mix} , SiPcS _{mix} , SnPcS _{mix}	Homogeneous	trichlorophenol	AlPcS _{mix} > ZnPcS _{mix} > AlPcS ₄ > SiPcS _{mix} > SnPcS _{mix}	56
AlPcS _{mix} , AlPcS ₄ , ZnPcS _{mix} , SiPcS _{mix} , SnPcS _{mix}	Homogeneous	pentachlorophenol	AlPcS _{mix} > AlPcS ₄ > SiPcS _{mix} > ZnPcS _{mix} > SnPcS _{mix}	56
AlPc(COOH) ₈ , ZnPc(COOH) ₈ , AlPcS ₄ , ZnPcS ₄ , AlPcS _{mix} , ZnPcS _{mix} , GePcS _{mix} , SiPcS _{mix} , SnPcS _{mix}	Heterogeneous	pentachlorophenol	ZnPc(COOH) ₈ > SiPcS _{mix} > SnPcS _{mix} > ZnPcS _{mix} > GePcS _{mix} > ZnPcS ₄ > AlPcS _{mix} > AlPc(COOH) ₈ > AlPcS ₄	54
AlPc(COOH) ₈ , ZnPc(COOH) ₈ , AlPcS ₄ , ZnPcS ₄ , AlPcS _{mix} , ZnPcS _{mix} , GePcS _{mix} , SiPcS _{mix} , SnPcS _{mix}	Heterogeneous	4-, di-, tri-chlorophenol	—	54
AlPcS ₄ , ZnPcS ₄ , GaPcS ₄	Homogeneous	phenol	AlPcS ₄ > GaPcS ₄ > ZnPcS ₄	42
AlPc	Heterogeneous	phenol, 4-nitrophenol 4-, di-, tri-chlorophenol	—	57
Zn{Pc(<i>t</i> -Bu) ₄ }	Homogeneous	phenol, 2-, 3-, 4-, tri-chlorophenol	—	58
[CoPc(COOH) _n] _{poly} , ZnPc(COOH) ₄ , AlOHPc(COOH) ₄ , [ZnPc(COOH) _n] _{poly} , [AlPc(COOH) _n] _{poly}	Homogeneous	phenol	[ZnPc(COOH) _n] _{poly} >> [AlPc(COOH) _n] _{poly} > AlOHPc(COOH) ₄ > ZnPc(COOH) ₄	59

Table 1.6. Degradation products obtained for the phenolic complexes listed in Table 1.5.

Substrate	Degradation products	Ref
phenol	1,4-benzoquinone	42
2-chlorophenol	2-chloro-1,4-hydroquinone	58
3-chlorophenol	2-chloro-1,4-hydroquinone	58
4-chlorophenol	1,4-benzoquinone	54,55,58
dichlorophenol	2-chloro-1,4-benzoquinone	54
trichlorophenol	2,5-dichloro-1,4-benzoquinone	54,56
pentachlorophenol	2,3,5,6-tetrachloro-1,4-benzoquinone	54,56

The lack of similarities in trends in Table 1.5 implies that the photocatalysis of phenols in the presence of Pcs is relatively complex. As previously mentioned, there are many factors that influence the photocatalytic ability of phthalocyanines such as aggregation, photostability, the magnetic nature of the central metal, and the nature and size of the peripheral and axial substituents. As a result, no clear correlation can be found between either one of these factors and the photocatalytic activity of the Pc complexes.

1.5. Adsorption Studies

1.5.1. Adsorption of 4-Np onto Bare Resin

The removal of 4-Np from wastewater has been reported in Table 1.4 using Amberlite XAD-7 as the adsorbent.²⁴ Amberlite XAD-7 is a non-ionic, highly porous resin that has a structural backbone composed of a carboxylic ester. A 97 % regeneration efficiency was obtained for the recovery of 4-Np from the surface of the resin, where ethanol was used as the regenerant. The non-ionic resin and highly polar adsorbate interact via van der Waals forces.²⁴

1.5.2. Adsorption of 4-Np onto Modified Resin

There are no reported studies on the modification of the surface of the adsorbent for adsorption of 4-Np from wastewater. The only reported study on the modification of the surface of an adsorbent is listed in Table 1.4, Section 1.2. In this study Amberlite XAD-2 and XAD-4 resins were modified with porphyrin complexes for the adsorption of phenol and chlorophenols.²¹ Higher recoveries were achieved for these modified adsorbents than underivatized adsorbents. The increase in recovery yields is due to increased opportunity for π - π interactions between the adsorbent and adsorbate. More than 90 % recovery was achieved for all adsorbates used in this study.²¹ Pcs are employed in this study as they have a more complex macrostructure than porphyrins, and should therefore allow a greater opportunity for π - π interactions than porphyrins.

Amberlite[®] IRA-900 was used as the adsorbent in this study. There are two main reasons for employing Amberlite[®] IRA-900 for the removal of 4-Np from solution:

- Amberlite[®] IRA-900 has benzyltrialkylammonium functionality, which allows for electrostatic interaction between the ammonium groups on the adsorbent and negatively-charged substituents attached to the phthalocyanine ring (Figure 1.8).⁵⁴
- Amberlite[®] IRA-900 has a large surface area for improved adsorption of 4-Np, due to its moderately high porosity and macroporous network.⁵⁴

1.6. Phthalocyanines Selected for Removal and Photocatalysis of 4-Np

The phthalocyanines that were selected for the photocatalytic transformation of 4-Np can be divided into two categories:

- 1) Homogeneous photocatalysts
- 2) Heterogeneous photocatalysts

The phthalocyanines that were selected for the homogeneous photocatalysis of 4-Np include zinc tetrasulphophthalocyanine (ZnPcS_4), zinc octacarboxyphthalocyanine ($\text{ZnPc}(\text{COOH})_8$) and a sulphonated ZnPc containing a mixture of differently sulphonated derivatives ($\text{ZnPcS}_{\text{mix}}$) (Figure 1.9). All homogeneous photocatalysts possess anionic substituents to ensure water-solubility and relatively high τ_T and Φ_T (and hence Φ_A) values.^{31,51}

The phthalocyanines that were selected for heterogeneous photocatalysis of 4-Np include magnesium phthalocyanine (MgPc), zinc phthalocyanine (ZnPc), chloroaluminium phthalocyanine (ClAlPc), zinc tetranitrophthalocyanine ($\text{ZnPc}(\text{NO}_2)_4$), zinc tetraaminophthalocyanine ($\text{ZnPc}(\text{NH}_2)_4$), zinc hexadecafluorophthalocyanine (ZnPcF_{16}) and zinc hexadecachlorophthalocyanine (ZnPcCl_{16}) (Figure 1.9). All photosensitisers selected host a central diamagnetic metal necessary for high triplet lifetimes.^{30,31,50,51} The axial ligand on ClAlPc will have an influence on the degree of aggregation of the MPc.⁴⁸ The inclusion of peripheral substituents on the ZnPc photosensitisers should lead to enhanced spin-orbit coupling, resulting in large Φ_T values.³⁰ The attachment of electron-withdrawing substituents (i.e. nitro, fluoro and chloro groups) on the phthalocyanine ring should aid in photostability of these MPcs on exposure to visible light.⁴⁹

The phthalocyanines that were selected for the modification of the Amberlite[®] IRA-900 resin for the removal of 4-Np from wastewater include iron, cobalt and nickel tetrasulphophthalocyanine (FePcS_4 , CoPcS_4 and NiPcS_4 , respectively) as well as the corresponding sulphonated MPcs containing a mixture of differently sulphonated derivatives, namely $\text{FePcS}_{\text{mix}}$, $\text{CoPcS}_{\text{mix}}$ and $\text{NiPcS}_{\text{mix}}$. Co and Fe, which are optically inactive, were selected as CoPc and FePc derivatives readily undergo axial ligation. NiPc derivatives were selected for comparative purposes.

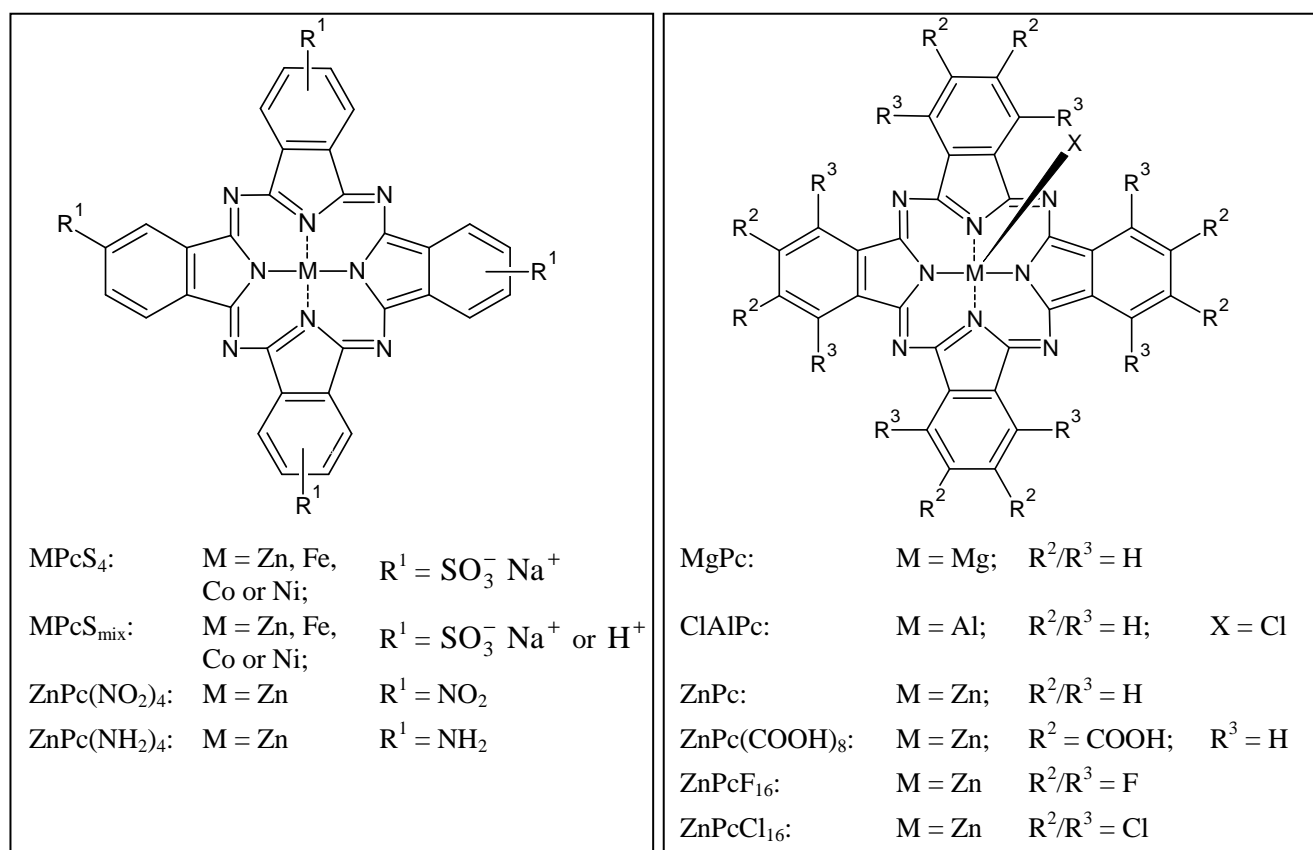


Figure 1.9. Molecular structures of selected Pcs for the photocatalysis and removal of 4-Np.

1.7. Summary of the Aims of the Study

Hence, the principle aims of this study include:

- (i) Synthesis and characterisation of complexes detailed in Figure 1.9,
- (ii) Employ selected complexes for the homo- and hetero-geneous photocatalysis of 4-Np, ideally resulting in the formation of compounds that are considerably less toxic than 4-Np.
- (iii) Photodegradation of methyl paraoxon using the photocatalyst that was most successful in degrading 4-Np, in order to eliminate one of the influx sources of 4-Np into our environment, and
- (iv) Removal of 4-Np from wastewater using Amberlite[®] IRA-900 modified with selected MPc complexes, where removal efficiencies should exceed 90% for the system to be effective.

2. EXPERIMENTAL

2.1. Materials

Materials purchased from British Drug House (BDH) Chemicals include:

- zinc acetate dihydrate ($\text{Zn}(\text{OOCCH}_3)_2 \cdot 2\text{H}_2\text{O}$),
- 4-nitrophenol (4-Np),
- sodium nitrite (NaNO_2)
- methanol (MeOH) and acetonitrile HiperSolTM.

Chemicals purchased from Sigma-Aldrich include:

- urea,
- phthalimide,
- phthalonitrile,
- nitrobenzene,
- chloronaphthalene,
- tetrafluorophthalonitrile,
- tetrachlorophthalic anhydride,
- 4-sulphophthalic acid,
- cobalt phthalocyanine (CoPc), iron phthalocyanine (FePc), nickel phthalocyanine (NiPc),
- *t*-octyl phenoxy-polyethoxyethanol (Triton X-100),
- benzene-1,2,4,5-tetracarboxylic dianhydride (pyromellitic dianhydride),
- 1,4-diazabicyclo[2.2.2]octane (DABCO),
- 4-nitrocatechol (4-NC),
- Amberlite[®] IRA-900,
- sodium azide (NaN_3), and

- acetonitrile

ZnPc, ClAlPc and MgPc were either synthesized using established methods^{26,60} or purchased from Sigma-Aldrich.

Hydroquinone was obtained from May & Baker Ltd.

Potassium dihydrogen orthophosphate ($\text{KH}_2(\text{PO}_4)_3$) was purchased from ACE (Associated Chemical Enterprises) Chemical Co. and used as received.

PAL (Positive Associates Limited) were suppliers of dipotassium phosphate ($\text{K}_2\text{H}(\text{PO}_4)_3$) and aluminium chloride (AlCl_3).

Saarchem were suppliers of the following solvents and reagents:

- acids, including 55% HNO_3 , 98% H_2SO_4 and 32% HCl ,
- zinc chloride (ZnCl_2),
- ammonium molybdate ($\text{Mo}_7\text{H}_{24}\text{N}_6\text{O}_{24}$),
- ammonium chloride (NH_4Cl), sodium chloride (NaCl),
- sodium sulfide nonahydrate ($\text{Na}_2\text{S} \cdot 9\text{H}_2\text{O}$),
- magnesium chloride (MgCl_2),
- silver nitrate (AgNO_3),
- sodium hydroxide pellets (NaOH),
- dimethyl sulfoxide (DMSO),
- *N,N*-dimethylformamide (DMF),
- tetrahydrofuran (THF), and
- petroleum ether, toluene, chloroform, acetone, and methanol.

Chemicals purchased from Merck include:

- potassium bromide (KBr),
- silica gel 60 (0.040 – 0.063 mm), and
- 1-octanol.

Chemicals that were purchased from Fluka include 1,8-diazabicyclo[5.4.0]undec-7-ene (DBU) and tetrasodium α - α' -(anthracene-9,10-diyl) bis(methylmalonate) (ADMA).

The PESTANAL[®] analytical standard, namely methyl paraoxon, was obtained from Riedel de-Haën and used as received.

Deionised water was employed for the purification of the selected photocatalysts. The deioniser that is used to generate deionised water consists of a mixed-bed resin obtained from Permutit Co. Ltd, Birmingham, New Jersey.

All kinetic reactions were performed in Millipore water. The system for preparing Millipore water is a Milli-Q Water System obtained from Millipore Corp., Bedford, Massachusetts. Fuming sulphuric acid (30% SO_3) was a gift from a chemical company based in KwaZulu-Natal.

In order to prepare the buffer solutions two separate solutions of 0.1 M $\text{K}_2\text{H}(\text{PO}_4)_3$ and 0.1 M $\text{KH}_2(\text{PO}_4)_3$ were prepared. The pH of the 0.1 M $\text{K}_2\text{H}(\text{PO}_4)_3$ solution was monitored as the 0.1 M $\text{KH}_2(\text{PO}_4)_3$ solution was added dropwise until the desired pH was obtained. Any necessary adjustments were made using 0.1 M NaOH solution.

2.2. Equipment

Characterisation of the selected Pcs was achieved through the use of UV-vis spectrometry (Cary 500 UV-vis/NIR spectrophotometer) and infrared (IR) spectrometry (Perkin-Elmer spectrum 2000 FTIR spectrometer). KBr pellets were used for the IR analysis of the selected MPcs.

The photochemical setup that was employed for the photocatalysis of 4-Np consisted of a light source (300 W/120 V General Electric Quartz line lamp), a 600 nm glass cut-off filter (Schott), a water filter and the reaction vessel. A 1 cm pathlength UV-vis spectrophotometric cell, fitted with a tight-fitting stopper, was used as the reaction vessel for the first study (i.e. homogeneous photocatalysis) (Figure 2.1), whereas the reaction vessel that was employed for the second study (i.e. heterogeneous photocatalysis) (Figure 2.2) consists of a reaction vessel surrounded by a water jacket. The reaction vessel in Figure 2.2 has three ports – for sampling, introducing the substrate and photocatalyst, and bubbling oxygen through the reaction medium. The 600 nm glass cut-off filter and water filter were used to filter off ultraviolet light and far infrared radiation, respectively, so that only the phthalocyanine Q band is irradiated, avoiding direct photodegradation of 4-Np by UV light. The intensity of the light reaching the vessel holding the sample was measured using a power meter (Lasermate/A) and was found to be 4.1×10^{16} photons $\text{s}^{-1} \text{cm}^{-2}$ for the setups in Figures 2.1 and 2.2. The pH of the buffer solutions was measured using a WTW pH 330/SET-1 pH meter.

Agilent 1100 series High Performance Liquid Chromatography (HPLC) connected to a variable wavelength UV-vis detector set at 210 nm, 230 nm or 400 nm was used to partly characterise the MPcS_{mix} complexes, monitor the degradation of 4-Np, determine the degradation products of 4-Np by spiking solutions with known standards, and separate the degradation products for further analysis. The HPLC system was fitted with an analytical Prodigy 5 μm ODS (150 x 4.6 mm)

column and a mobile phase of 70:30 methanol:water was used for the partial characterisation of the MPcS_{mix} complexes. A semi-preparative LUNA 10μ ODS C18 (250 x 10 mm) HPLC column with a mobile phase of 85:15 water:acetonitrile was used for the determination and separation of the degradation products obtained as a result of the degradation of 4-Np in the presence of heterogeneous photocatalysts. Different mobile phases were employed as better separation was achieved for the degradation products and characterisation of the MPcS_{mix} complexes using an acetonitrile-water mixture and a methanol-water mixture, respectively.

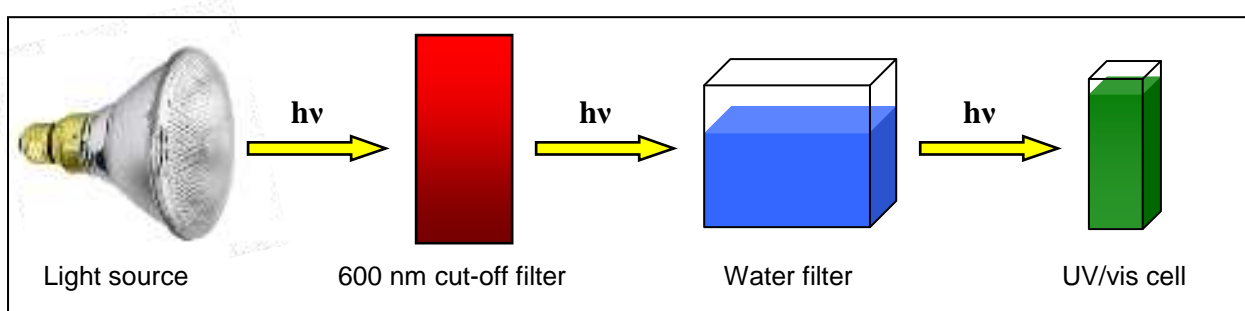


Figure 2.1. Photochemical setup for the photocatalysis of 4-Np using homogeneous MPc catalysts.

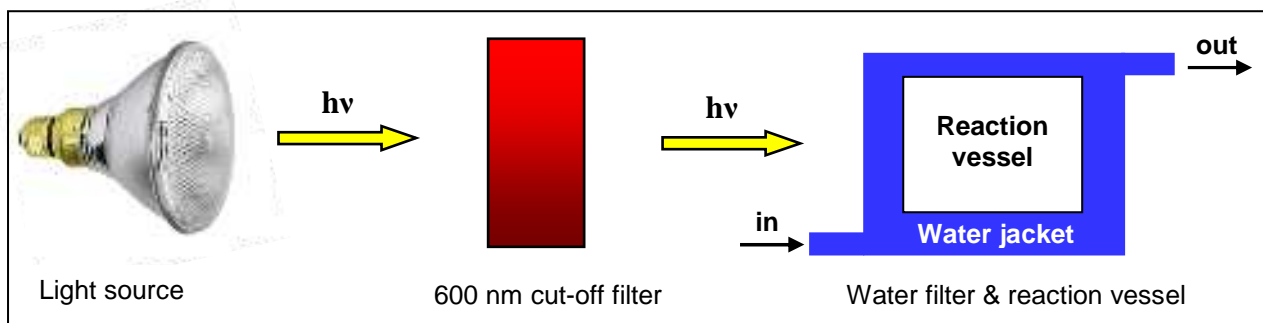


Figure 2.2. Photochemical setup for the photocatalysis of 4-Np using heterogeneous MPc catalysts.

Liquid Chromatography coupled with Mass Spectroscopy (LC/MS) was used to identify ionisable degradation products of 4-Np. Determination of degradation products in the presence of homogeneous photocatalysts was achieved using a Finnigan LCQ-MS, with Electrospray Ionisation (ESI), coupled with an analytical Prodigy 5μ ODS (150 x 4.6 mm) column using a mobile phase of 85:15 acetonitrile:water. The degradation products obtained for the degradation

of 4-Np in the presence of heterogeneous photocatalysts were determined by direct injection using ESI-MS, of the fractions obtained using semi-preparative HPLC.

Triplet lifetimes (τ_T) for the heterogeneous catalysts were obtained using an Nd-YAG laser providing 400 mJ, 90 ns of laser light at 10 Hz, pumping a Lambda-Physik FL 3002 dye laser. Pyridin 1 dye is employed. A 300 W xenon arc lamp (Thermo Oriel) provides the analysing light. Kinetic curves are averaged over 256 laser pulses using a Tektronix TDS 360 digital oscilloscope (Figure 2.3). The τ_T values are obtained by fitting an exponential curve to the kinetic data using ORIGIN Pro 6.0.

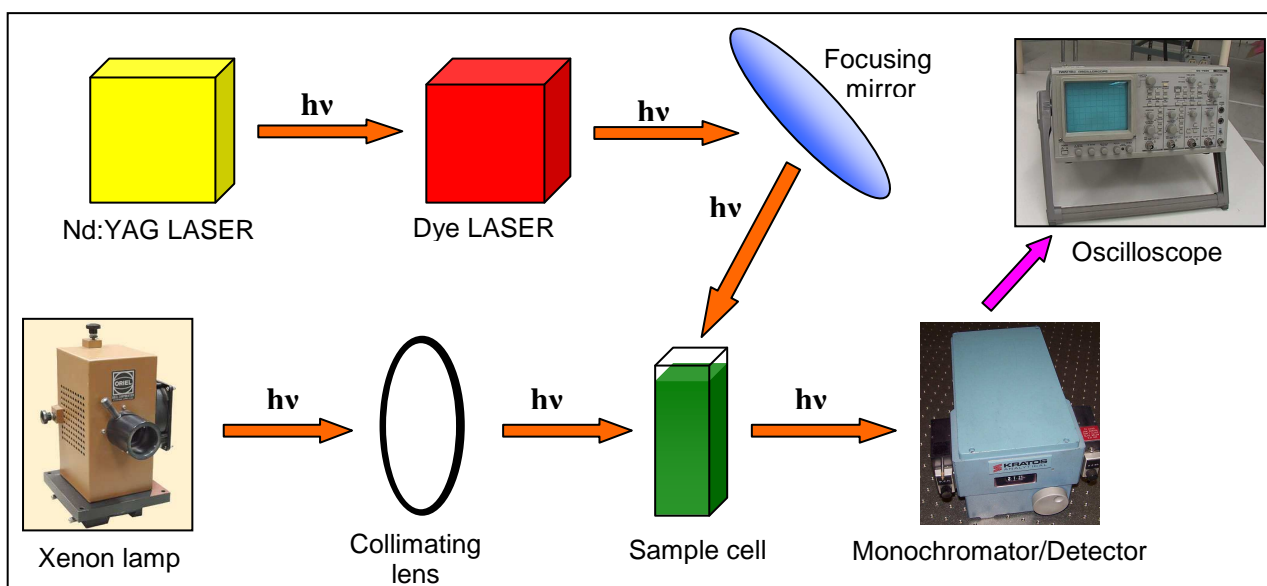


Figure 2.3. Schematic representation of the in-house LASER photolysis setup.

2.3. Photocatalytic Calculations

Quantum yields for the photodegradation of 4-Np (Φ_{4-Np} – Eq. (15)) were calculated using Eq. (16):

$$\Phi_{4-Np} = \frac{\text{Amount of 4 - Np produced/unit volume/unit time}}{\text{No. of quanta of light consumed/unit volume/unit time absorbed}} \quad (15)$$

$$\Phi_{4\text{-Np}} = -\frac{(C_t - C_0) V N_A}{I_{abs} S t} \quad (16)$$

where V is the reaction volume (4.5 cm^3), t is the irradiation time, N_A is Avogadro's constant ($6.022 \times 10^{23} \text{ mol}^{-1}$), and S is the irradiation area (1 cm^2). C_0 and C_t are 4-Np concentrations before and after irradiation, respectively. The extinction coefficient (ϵ) of 4-Np, determined to be $1.8 \times 10^4 \text{ dm}^3 \text{ mol}^{-1} \text{ cm}^{-1}$ at 400 nm (pH = 9), was used to calculate the concentration of 4-Np at time t . I_{abs} (the intensity of absorbed light) from Eq. (16) is the overlap integral of light intensity of the source of radiation and the light absorption of the sensitizer at 670 nm.⁶¹

The rate constants that are of interest in this study are those involved in the Type II reaction mechanism (Section 1.4.1) for the photodegradation of 4-Np. k_d , k_q and k_r are the rate constants for the decay of $^1\text{O}_2$ in water, "physical" quenching of $^1\text{O}_2$ by the substrate (4-Np) and formation of oxidation products, respectively. These are represented by Scheme 2.1 (Eq. (17)-(19)).



Scheme 2.1. Reaction mechanisms responsible for the consumption of $^1\text{O}_2$ during photocatalysis of 4-Np in the presence of a MPc

Eq. (17) to (19) can be used to derive Eq. (20):^{55,56}

$$\Phi_{4\text{-Np}} = \Phi_{\Delta} \frac{k_r [4\text{-Np}]}{k_d + (k_q + k_r) [4\text{-Np}]} \quad (20)$$

Where Φ_{Δ} is the singlet oxygen quantum yield (defined in Section 1.4.1).

Eq. (20) can then be rearranged to give Eq. (21):

$$\frac{1}{\Phi_{4-\text{Np}}} = \frac{1}{\Phi_{\Delta}} \left(\frac{k_q + k_r}{k_r} + \frac{k_d}{k_r[4 - \text{Np}]} \right) \quad (21)$$

k_d , the singlet oxygen decay rate constant in water, can be calculated using Eq. (22):

$$k_d = \frac{1}{\tau_{\Delta}} \quad (22)$$

where τ_{Δ} , the lifetime of singlet oxygen, is 3.09×10^{-6} s (in H_2O and at 1 atm),⁶² therefore k_d is $3.24 \times 10^5 \text{ s}^{-1}$.

The rate constants of k_r and $(k_q + k_r)$ can be determined by plotting a graph of $1/\Phi_{4-\text{Np}}$ versus $1/[4-\text{Np}]$ using Eq. (21). The literature values of Φ_{Δ} for $\text{ZnPcS}_{\text{mix}}$, ZnPcS_4 and $\text{ZnPc}(\text{COOH})_8$ in pH 10 buffer are 0.48, < 0.01 and 0.52, respectively,^{54,55} and were employed to calculate the rate constants k_r and $(k_q + k_r)$.

2.4. Immobilisation Studies

Optimisation studies were carried out using varying loadings of FePcS_4 on Amberlite® IRA-900, while the concentration of 4-Np was kept constant at $1.0 \times 10^{-4} \text{ mol dm}^{-3}$. The optimum loading of FePcS_4 was determined by comparing the rates of 4-Np adsorption onto the modified surface of the adsorbent. On establishing the optimum FePcS_4 loading, MPc-Amb resins were prepared at this loading for the rest of the MPc complexes, and the rate of adsorption of 4-Np was compared for all modified adsorbents, using the mass balance relationship in Eq. (23):^{19,23}

$$Q_t = V_L \frac{(C_0 - C_t)}{W} \quad (23)$$

where Q_t is the amount of 4-Np adsorbed onto the resin (mmol g^{-1}) after time t , C_0 and C_t are the initial and final (after a known time) concentrations of 4-Np (mmol L^{-1}), respectively, V_L is the volume of aqueous solution (L) and W is the mass of dry adsorbent (g). V_L , C_0 and W were maintained at 5×10^{-3} L, $1.0 \times 10^{-4} \text{ mol dm}^{-3}$ and 0.010 g, respectively, for all analyses.

The $1.0 \times 10^{-4} \text{ mol dm}^{-3}$ 4-Np solution was prepared in pH 9 buffer, as 4-Np is very soluble at this pH (solubility = 1.73 mol L^{-1} , calculated using Advanced Chemistry Development (ACD/Labs) Software V8.14 for Solaris) and the predominant species in solution is the phenolate ion of 4-Np. The time “ t ” at which Q_t was determined was 30 min for all analyses. Adsorption rates were monitored spectroscopically, by observing the decrease in 4-Np absorption.

Regeneration of the modified adsorbent, following adsorption of 4-Np on MPC-Amb was carried out using the optimum loading of FePcS₄ (as an example) on the macroreticular resin. A 5 mL solution of $1.0 \times 10^{-4} \text{ mol dm}^{-3}$ 4-Np was added to a known amount of FePcS₄-Amb and left to stir overnight in order to reach equilibrium. The adsorption process was monitored spectroscopically to determine the concentration of 4-Np adsorbed onto the FePcS₄-Amb, by recording the decrease in the intensity of the absorption of the 4-Np solution. Adsorption was carried out until there were no spectral changes for the 4-Np solution, then the resin was removed from the solution and washed with deionised water. Following this, $1 \times 10^{-3} \text{ mol dm}^{-3}$ nitric acid solution (5 mL) was used to remove 4-Np from the surface of the resin to regenerate the adsorbent and recycle the FePcS₄-Amb. The FePcS₄-Amb adsorbent was washed three times with deionised water after removal of 4-Np with HNO₃. The rate of adsorption of a fresh solution of $1.0 \times 10^{-4} \text{ mol dm}^{-3}$ 4-Np after regeneration of the FePcS₄-Amb adsorbent was then calculated.

2.5. Synthetic Methods

2.5.1. Synthesis of Water-soluble Metallophthalocyanines

Synthesis of Monosodium Salt of 4-Sulphophthalic Acid:⁶³ (**1**)

A mixture of 30% 4-sulphophthalic acid (12.3 g, 15 mmol) and NaOH pellets (0.60 g, 15 mmol) was stirred for 24 hours, yielding a pink crystalline product. The product (**1**) was filtered, washed with water and air dried. **Yield:** 3.7 g (92%). **IR** [KBr ($\nu_{\max}/\text{cm}^{-1}$): 3440, 3065, 2655 & 2536 (O-H), 1745 & 1705 (C=O), 1595, 1574, 1496 & 1437 (C-C), 1396, 1375, 1280, 1242 & 1175 (C-O or O-H), 1070 (S=O), 832, 794 & 720 (C-H).

Synthesis of MPcS₄ Complexes:⁶⁴ (Scheme 3.1a)

Some of the MPcS₄ complexes could be purchased, however they were synthesized in this work to gain skills in synthetic methods. Following literature methods,⁶⁴ a mixture of the monosodium salt of 4-sulphophthalic acid (**1**) (1.1g, 4.0 mmol), ammonium chloride (0.12 g, 2.2 mmol), excess urea (1.4 g, 24 mmol), ammonium molybdate (0.017 g, 0.015 mmol), and a metal salt (1.0 mmol) (zinc(II) sulphate, iron(II) chloride, cobalt(II) sulphate, or nickel(II) acetate were used for the synthesis of ZnPcS₄, FePcS₄, CoPcS₄ or NiPcS₄, respectively) were finely ground. The ground solid was added to nitrobenzene (8 mL) at 180-200 °C in a three-necked round bottom flask fitted with a thermometer and condenser over a period of 1 hour. The mixture was stirred and maintained at 200 °C for 7 hours. The nitrobenzene was removed from the resulting dark solid by Soxhlet extracting with methanol (250 mL). The solid product was then purified by dissolving it in 25 mL HCl (1.0 M) saturated with NaCl and boiling the solution for 10 min. The solution was cooled to room temperature, filtered, dissolved in 20 mL NaOH (0.1 M), heated to

80 °C, and filtered to remove insoluble impurities. NaCl (10 g) was added to the filtrate to precipitate the solid product. The slurry was heated, while stirring, to 80 °C and maintained at this temperature until ammonia evolution ceased. The reprecipitation process using NaCl was repeated twice. The product was filtered and washed with 80% ethanol until the filtrate was chloride-free (tested using AgNO₃). The product was then refluxed for 4 hours in absolute ethanol (40 mL), after which it was cooled to room temperature, filtered, then dried in an oven at 110 °C overnight.

ZnPcS₄: **Yield:** 0.41 g (42%). **IR** [KBr ($\nu_{\max}/\text{cm}^{-1}$)]: 3412 (O-H), 1628, 1560 & 1517 (C=C), 1399 (C-N), 1320, 1187, 1140 & 1104 (C-H), 1028 (S=O), 907, 827, 743, 693 & 639 (C-H), 591 (C-C). **UV-Vis** [water, pH 7, λ_{\max}/nm (log ϵ)]: 677 (4.54), 633 (5.05), 342 (4.94).

FePcS₄: **Yield:** 0.44 g (45%). **IR** [KBr ($\nu_{\max}/\text{cm}^{-1}$)]: 3411 (O-H), 1640 & 1560 (C=C), 1441 & 1401m (C-N), 1189, 1143, 1106 & 1058 (C-H), 1028 (S=O), 927, 830, 746, 696 & 643 (C-H), 593 & 559 (C-C). **UV-Vis** [water, pH 7, λ_{\max}/nm (log ϵ)]: 665 (3.62), 630 (4.31), 327 (5.22).

CoPcS₄: **Yield:** 0.78 g (80%). **IR** [KBr ($\nu_{\max}/\text{cm}^{-1}$)]: 1643 (C=C), 1457 & 1399 (C-N), 1185, 1145, 1109 & 1056 (C-H), 1028 (S=O), 829, 749, 698 & 636 (C-H), 595 (C-C). **UV-Vis** [water, pH 7, λ_{\max}/nm (log ϵ)]: 657 (5.12), 628 (4.98), 315 (5.25).

NiPcS₄: **Yield:** 0.72 g (74%). **IR** [KBr ($\nu_{\max}/\text{cm}^{-1}$)]: 3420 (O-H), 1630 & 1526 (C=C), 1457 & 1401 (C-N), 1326, 1187, 1145, 1110 & 1058 (C-H), 1028 (S=O), 934, 830, 750, 698 & 638 (C-H), 595 (C-C). **UV-Vis** [water, pH 7, λ_{\max}/nm (log ϵ)]: 660 (4.46), 623 (4.62), 332 (4.56), 287 (4.71), 270 (4.74), 248 (4.70), 207 (4.88).

Synthesis of MPcS_{mix} Complexes:⁶⁵ (Scheme 3.1b)

The synthesis of MPcS_{mix} complexes is a relatively straightforward procedure. The method described follows the procedure reported by Ambroz *et al.*⁶⁵ The unsubstituted metallated phthalocyanine (c.a. 2.0 mmol) (i.e. ZnPc, FePc, CoPc or NiPc for ZnPcS_{mix}, FePcS_{mix}, CoPcS_{mix} or NiPcS_{mix}, respectively) was stirred and heated to 100 °C. Fuming sulphuric acid (5 mL consisting of 30% SO₃) was added dropwise to the MPc. The mixture was stirred rapidly and maintained at 100 °C for 25 min. Quenching of the sulphonation reaction was achieved by pouring the mixture onto about 100 g crushed ice and adjusting the pH to between 7.0 – 7.5 using NaOH (1.0 M). The neutral solution was evaporated to dryness, and the resulting crude solid was Soxhlet extracted using methanol (250 mL) overnight. On rotary evaporating the solvent a sulphonated phthalocyanine mixture was obtained.

ZnPcS_{mix}: IR [KBr (v_{max}/cm⁻¹): 3223 (O–H), 1735, 1624 & 1566 (C=C), 1394 (C–N), 1228, 1166 & 1087 (C–H), 1026 (S=O), 985, 895, 741 & 721 (C–H). UV-Vis [water, pH 7, λ_{max}/nm]: 673, 633, 335.

FePcS_{mix}: IR [KBr (v_{max}/cm⁻¹): 3206 (O–H), 1730, 1636 & 1570 (C=C), 1401 (C–N), 1368 & 1185 (C–H), 1038 (S=O), 860, 743 & 714 (C–H). UV-Vis [water, pH 7, λ_{max}/nm]: 663, 638, 338.

CoPcS_{mix}: IR [KBr (v_{max}/cm⁻¹): 1756, 1625 & 1560 (C=C), 1396 (C–N), 1167 & 1109 (C–H), 1028 (S=O), 994, 919, 746 & 694 (C–H). UV-Vis [water, pH 7, λ_{max}/nm]: 660, 595, 320.

NiPcS_{mix}: **IR** [KBr ($\nu_{\max}/\text{cm}^{-1}$): 3244 (O–H), 1726, 1629 & 1559 (C=C), 1399 (C–N), 1143, & 1089 (C–H), 1030 (S=O), 983, 899, 740 & 702 (C–H). **UV-Vis** [water, pH 7, λ_{\max}/nm]: 665, 610, 335, 325, 285, 270.

Synthesis of Zinc Octacarboxyphthalocyanine (ZnPc(COOH)₈):⁶⁶ (Scheme 3.2)

A mixture of pyromellitic dianhydride (benzene-1,2,4,5-tetracarboxylic dianhydride) (**2**) (1.9 g, 8.5 mmol), excess urea (9.6 g, 0.16 mol), DBU (0.079 g, 0.52 mmol) and zinc acetate (3.1 g, 17 mmol) were placed in a 100 mL two-necked round bottom flask fitted with a reflux condenser and a thermometer. The mixture was heated to 250 °C under reflux and maintained at this temperature until the reaction mixture fused. The fused product was then washed with deionised water, acetone and HCl (6 M). The tetra-amide product (**3**) was dried, then refluxed in 5 mL H₂SO₄ (20%) for 3 days to yield ZnPc(COOH)₈. The resulting product was washed with 100 mL portions of H₂SO₄ (5%), 50 mL portions of deionised water and acetone, and recovered using centrifugation. After drying in air the product was purified by multiple chromatography on an alumina column using a NaOH solution (2%) as the eluent. The green product was reprecipitated after each separation using HCl (20%). The pure product was finally filtered and dried at 110 °C for 4 hours. **Yield:** 0.22 g (11%). **IR** [KBr ($\nu_{\max}/\text{cm}^{-1}$): 3393 (O–H), 3187 (C–H), 1698 (C=O), 1638, 1622, 1560 & 1446 (C–C), 1403 (C–N), 1304, 1246 & 1193 (C–O and/or O–H), 1076, 1059, 1017, 975, 905 & 725 (C–H). **UV-Vis** [water, pH 10, λ_{\max}/nm (log ϵ): 685 (5.26), 653 (5.21), 358 (4.96).

2.5.2. Synthesis of Water-insoluble Metallophthalocyanines

ZnPc, ClAlPc and MgPc were either purchased from Aldrich or synthesized according to established procedures.^{26,60}

Synthesis of 4-Nitrophthalimide:³⁶ (**5**) (Scheme 3.3)

4-Nitrophthalimide, which was synthesized according to reported procedures,³⁶ was used for the synthesis of $\text{ZnPc}(\text{NO}_2)_4$ and $\text{ZnPc}(\text{NH}_2)_4$. After slowly adding 55% HNO_3 (20 mL) to 98% H_2SO_4 (100 mL), the mixture was left to cool to 15 °C in an ice bath. Phthalimide (**4**) (21 g, 0.14 mol) was added in portions to the $\text{H}_2\text{SO}_4/\text{HNO}_3$ mixture while stirring and maintaining the temperature between 10 and 15 °C. The temperature was then increased to 35 °C and stirred at this temperature for 1 hour. After cooling the mixture to 0 °C the clear pale yellow slurry was poured slowly over crushed ice (c.a. 1 kg), while stirring the ice mixture vigorously. The resulting suspension was filtered, washed thoroughly with cold water and dried at 110 °C for 4 hours to yield **5**. **Yield:** 19 g (71%). **IR** [KBr ($\nu_{\text{max}}/\text{cm}^{-1}$)]: 3430 (N–H), 1778, 1717 (CO–NH–CO), 1538 (NO_2 asym), 1342 (NO_2 sym).

Synthesis of Zinc Tetranitrophthalocyanine ($\text{ZnPc}(\text{NO}_2)_4$):^{67,68} (Scheme 3.4)

The synthesis of $\text{ZnPc}(\text{NO}_2)_4$ is based upon the methods developed by Achar *et al*⁶⁷ and Metz *et al*.⁶⁸ The synthetic method employed in this study for the synthesis of $\text{ZnPc}(\text{NO}_2)_4$ involved the use of **5**. Zinc chloride (1.8 g, 13 mmol), 4-nitrophthalimide (**5**) (9.6 g, 50 mmol), ammonium molybdate (0.23 g, 0.20 mmol), ammonium chloride (1.3 g, 25 mmol) and excess urea (15 g, 250 mmol) were finely ground and slowly added to a 250 mL round-bottom flask containing 14 mL nitrobenzene between 160-180 °C. The mixture was refluxed between 180-190 °C for 5 hours. The product was washed with methanol and air-dried. The remaining nitrobenzene was removed by Soxhlet extracting the complex in methanol (250 mL). Purification of the crude product was achieved over a number of steps. Firstly, the product was washed with 125 mL HCl solution (1.0 M) saturated with NaCl, boiled for 5 min, cooled to room temperature and centrifuged to obtain the solid product. The next step involved washing the solid with 125 mL NaOH (1.0 M)

containing 50 g NaCl, heating the solution to 90 °C, and stirring the solution for 1 hour while maintaining the solution temperature at 90 °C. After separating the solid by centrifugation, the product was treated with HCl (1.0 M), centrifuged, then treated with NaOH (1.0 M) and centrifuged. The acid/base purification cycle was repeated twice, after which the product (ZnPc(NO₂)₄) was neutralised using deionised water, centrifuged and dried at 110 °C. **Yield:** 3.7 g (39%). **IR** [KBr ($\nu_{\text{max}}/\text{cm}^{-1}$): 3080 (C-H), 1517 (NO₂ asym), 1331 (NO₂ sym), 1132, 1082, 1048, 927, 846 & 754 (C-H). **UV-Vis** [DMSO, $\lambda_{\text{max}}/\text{nm}$ (log ϵ): 678 (4.88), 643 (4.66), 352 (4.79).

Synthesis of Zinc Tetraaminophthalocyanine (ZnPc(NH₂)₄):⁶⁷ (Scheme 3.4)

ZnPc(NO₂)₄ (1.5 g, 2.0 mmol) was finely ground and added to 40 mL deionised water. Sodium sulphide nonahydrate (Na₂S.9H₂O) (7.0 g, 29 mmol) was added to the slurry, which was then left to stir at 50 °C for 5 hours. The reaction mixture was centrifuged to obtain the solid product, which was then treated with 120 mL HCl (1.0 M). The solid was recovered using centrifugation, added to 80 mL NaOH (1.0 M) and stirred for 1 hour. The product (ZnPc(NH₂)₄) was neutralised with several washes of deionised water and dried in an oven at 110 °C for 4 hours. **Yield:** 1.2 g (94%). **IR** [KBr ($\nu_{\text{max}}/\text{cm}^{-1}$): 3337 (NH₂ asym), 3178 (NH₂ sym) 1607 (NH₂ def), 1400 (C-C), 1334, 1299 & 1250 (C-N), 1126, 1087, 1049, 935, 864, 825, 742 & 729 (C-H). **UV-Vis** [DMSO, $\lambda_{\text{max}}/\text{nm}$ (log ϵ): 713 (4.75), 647 (4.40), 357 (4.75).

Synthesis of Zinc Hexadecafluorophthalocyanine (ZnPcF₁₆):^{69,70} (Scheme 3.5)

The synthesis of ZnPcF₁₆ was achieved using the reported procedures.^{69,70} Dried, anhydrous zinc acetate (0.092 g, 0.50 mmol) and tetrafluorophthalonitrile (**6**) (0.52 g, 2.6 mmol) were added to 8 mL chloronaphthalene. The mixture was refluxed for 24 hours. The crude compound was

purified using a short column of silica gel, with acetone as the eluent. The purified compound (ZnPcF₁₆) was then dried under vacuum. **Yield:** 0.37 g (85%) **IR** [KBr ($\nu_{\max}/\text{cm}^{-1}$): 2589, 1641, 1617 & 1517 (C=C), 1484 & 1447 (C-N), 1312 & 1260 (C-C), 1142 (aryl-F), 1068, 956, 928, 834, 746, 653 (C-H), 596 (C-C). **UV-Vis** [THF, λ_{\max}/nm (log ϵ): 670 (5.17), 640 (4.70), 608 (4.51), 350 (4.69), 316 (4.61).

Synthesis of Zinc Hexadecachlorophthalocyanine (ZnPcCl₁₆):^{69,71,72} (Scheme 3.6)

ZnPcCl₁₆ was prepared by combining urea (6.0g, 100 mmol), tetrachlorophthalic anhydride (**7**) (9.7 g, 34 mmol), zinc chloride (1.1 g, 8.0 mmol) and ammonium molybdate (0.047 g, 0.040 mmol). The mixture was finely ground and added to 25 mL nitrobenzene. The mixture was heated to between 180 and 190 °C and maintained within this range for 4-5 hours. The reaction mixture was cooled and filtered. The nitrobenzene was removed from the product by Soxhlet extraction with methanol (250 mL) overnight. The product was then washed by boiling it in aqueous HCl (1.0%), followed by washing with boiling aqueous NaOH (1.0%). The acid/base washing cycle was repeated twice, after which the product was neutralised using deionised water. Further purification was achieved by washing the product with acetone and ether. The solid product (ZnPcCl₁₆) was obtained by filtration and oven-dried for 4 hours at 110 °C. **Yield:** 1.9 g (21%). **IR** [KBr ($\nu_{\max}/\text{cm}^{-1}$): 1609 & 1557 (C=C), 1462 (C-N), 1387, 1314, 1298 & 1272 (C-C), 1136 (aryl-Cl), 1098, 935, 768, 746 & 668 (C-H). **UV-Vis** [DMF, λ_{\max}/nm (log ϵ): 687 (4.38), 648 (4.39), 340 (4.22). [1-methyl-2-pyrrolidinone, λ_{\max}/nm (log ϵ): 696 (4.54), 654 (4.41), 386 (4.28), 344 (4.32).

2.6. Immobilisation of Sulphonated Phthalocyanines

The sulphonated MPc complexes (i.e. MPcS_4 and MPcS_{mix}), which are negatively charged, were selected for immobilisation onto Amberlite[®] IRA-900. Immobilisation was achieved using the reported literature procedure.⁷³ A 0.01 g sample of the resin was weighed and added to a 40 mL solution of the sulphonated MPc dissolved in water:acetonitrile (1:1). Changes in absorbance values before and after immobilisation were monitored using a Cary 500 UV-vis/NIR spectrophotometer in order to calculate the number of moles of MPc that immobilize onto the surface of the resin. The MPc loadings are represented as “mol MPc/g Amb” for the tetrasulphonated complexes, and as “g MPc/g Amb” for the MPcS_{mix} complexes. After 48 hours of gentle stirring the modified resin was isolated by filtration and washed with 40 mL water:acetonitrile (3:1) solution, followed by large quantities of deionised water. No MPcs were detected in the filtrate. Finally, the resin was air-dried at room temperature and then oven-dried at 65 °C overnight. Diffused reflectance spectra were obtained for the solid MPc-Amb resins using a Cary 500 UV-vis/NIR spectrophotometer to confirm immobilisation of the selected MPcs onto Amberlite[®] IRA-900.

3. RESULTS AND DISCUSSION

The results presented and discussed in these sections have been published in or submitted to peer-reviewed journals. The details of these articles are listed below and are not referenced within the text:

- 1) E. Marais, R. Klein, E. Antunes, T. Nyokong, *Photocatalysis of 4-nitrophenol using zinc phthalocyanines*, J. Mol. Catal. A: Chem. **261** (2006) 36.
- 2) E. Marais, T. Nyokong, *Adsorption of 4-nitrophenol onto Amberlite[®] IRA-900 modified with metallophthalocyanines*, J. Hazard. Mater. (2007) *In press, Corrected Proof*.
- 3) E. Marais, E. Antunes, T. Nyokong, *Photocatalytic transformation of 4-nitrophenol in aqueous media using suspended water-insoluble metallophthalocyanine complexes*, J. Mol. Catal. A: Chem. *Submitted*.

The results obtained in this study are presented in three sections:

- 1) Synthesis and characterisation of photocatalysts.
- 2) Homogeneous photocatalysis of 4-Np using water-soluble zinc Pc complexes.
- 3) Heterogeneous photocatalysis of 4-Np using suspended MPc complexes.
- 4) Adsorption of 4-Np onto Amberlite[®] IRA-900 modified with MPcs.

3.1. Synthesis and Characterisation

The structures of the complexes that were selected for the heterogeneous and homogeneous photocatalysis of 4-Np as well as the modification of Amberlite® IRA-900 are presented in Figure 3.1 below.

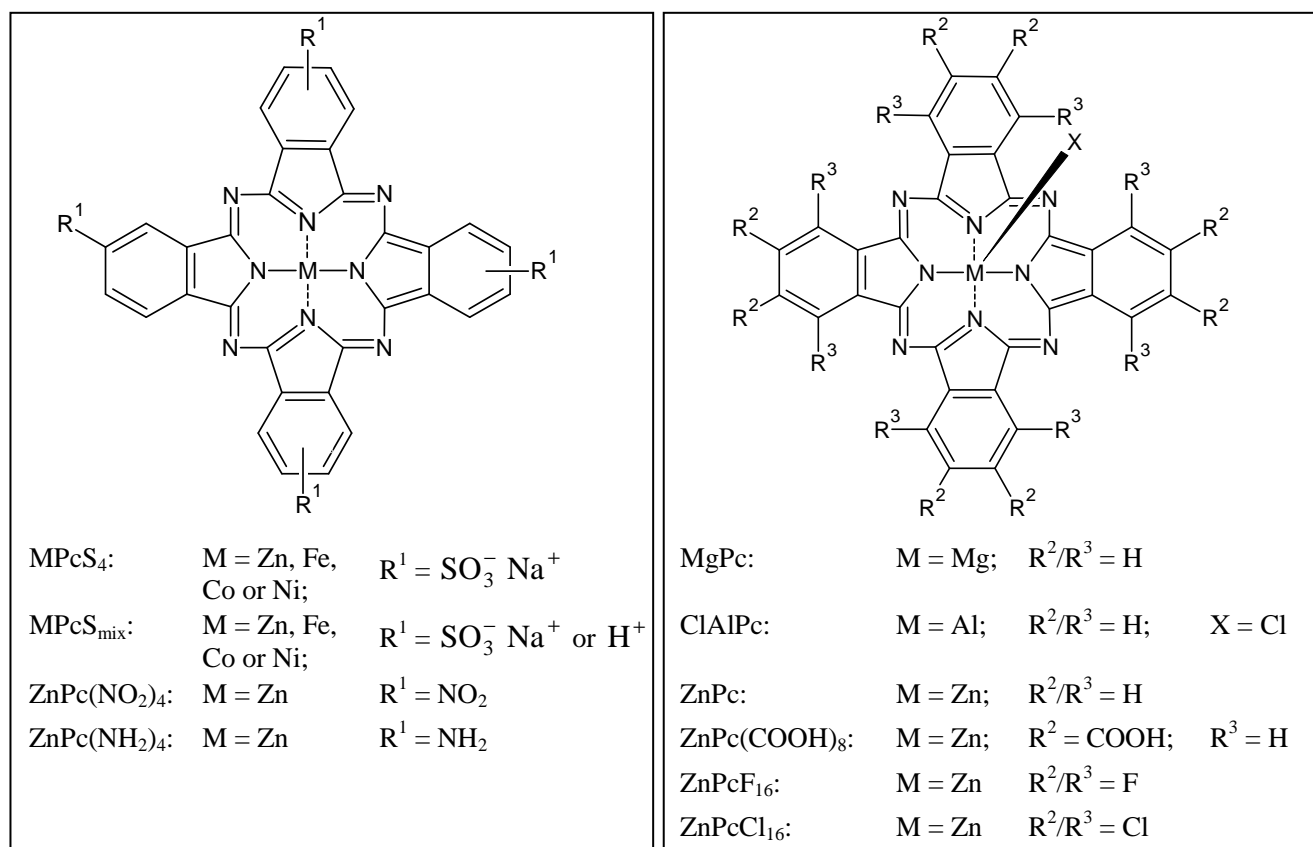
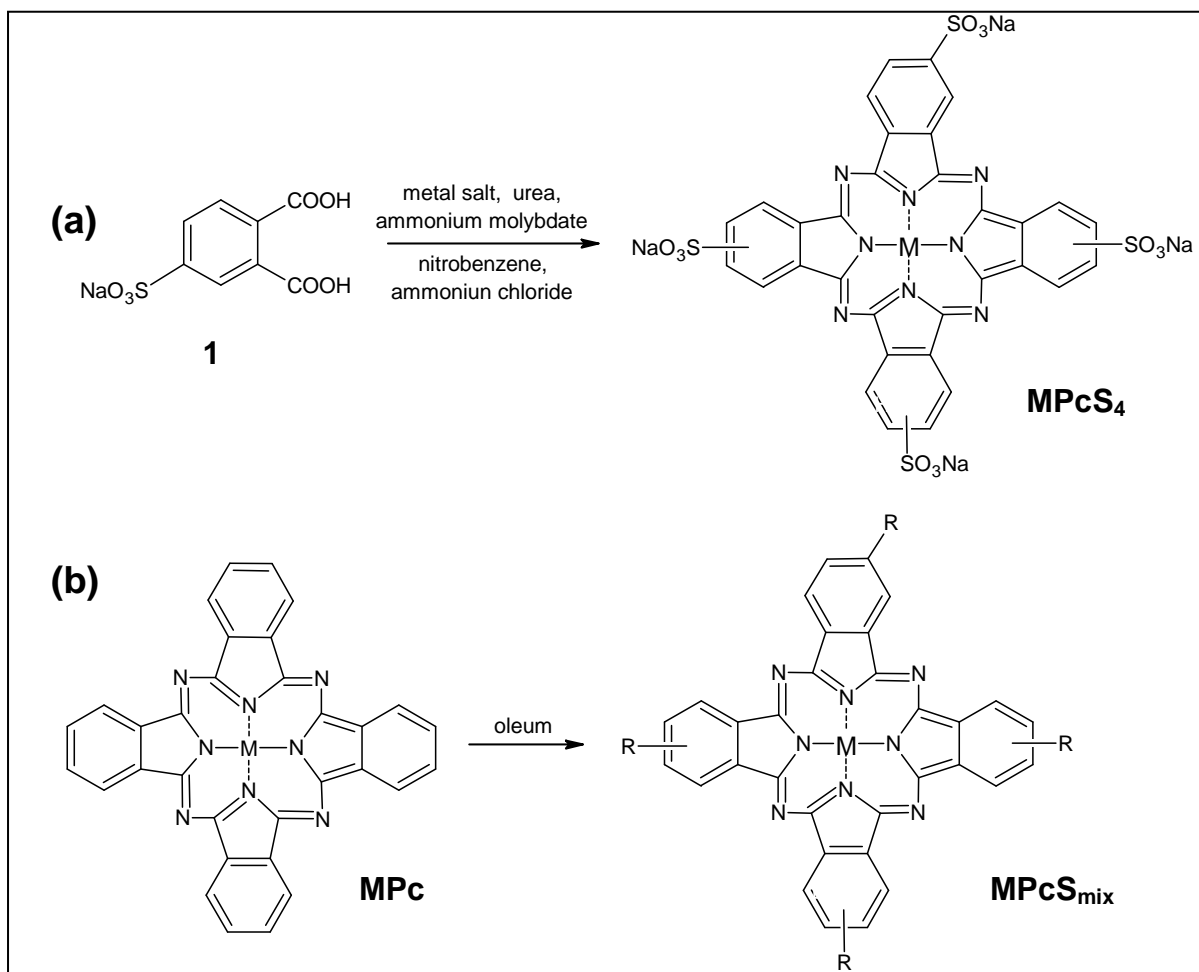


Figure 3.1. Molecular structures of selected Pcs for the photocatalysis and removal of 4-Np.

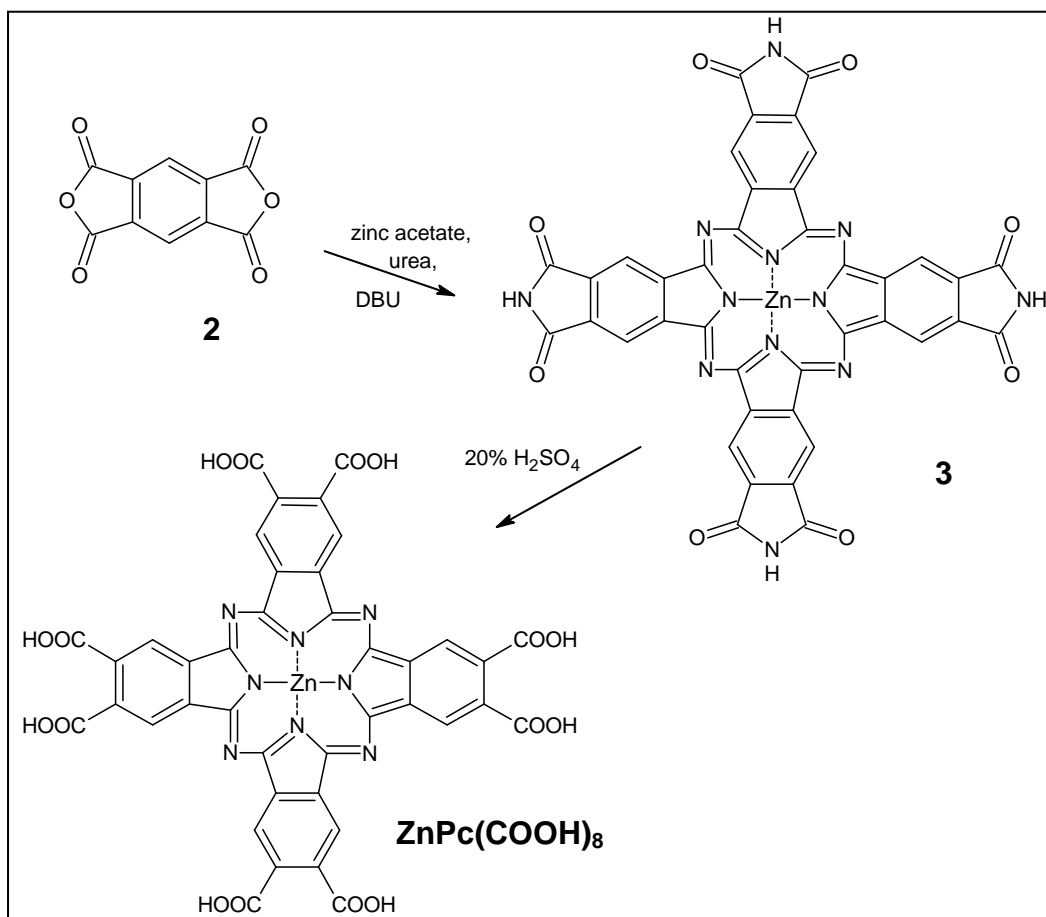
3.1.1. Synthesis of Water-soluble MPc Complexes

MPcS₄ and MPcS_{mix} complexes were synthesized according to the reported procedures (Scheme 3.1).^{64,65} MPcS₄ complexes are synthesized in relatively high yields, as evidenced by the values reported in the Experimental section. The characteristic S=O vibrations are observed within the 1030-1040 cm⁻¹ IR range for the MPcS₄ and MPcS_{mix} complexes. MPcS₄ and MPcS_{mix} complexes are soluble in water and alcohol-water mixtures.



Scheme 3.1. Synthetic routes for the preparation of sulphonated phthalocyanines.^{64,65} ($M = \text{Zn}^{2+}$, Fe^{2+} , Co^{2+} , or Ni^{2+} ; $R = \text{SO}_3^- \text{Na}^+$ or H).

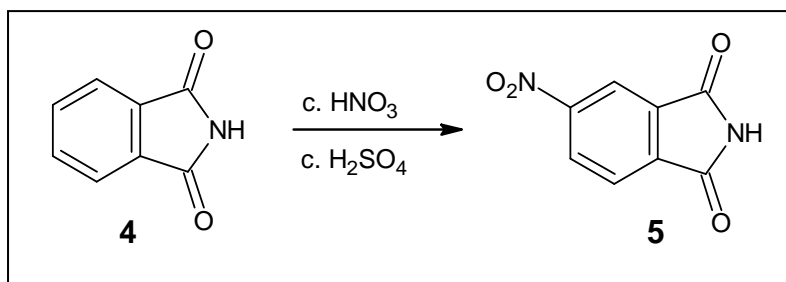
The synthesis of $\text{ZnPc}(\text{COOH})_8$ (Scheme 3.2) resulted in a low synthetic yield, which is characteristic of octacarboxyphthalocyanine complexes.⁶⁶ The O-H, C=O and C-O bands were obtained at 3393, 1698 and 1193 cm^{-1} , respectively, in the IR spectrum for $\text{ZnPc}(\text{COOH})_8$. $\text{ZnPc}(\text{COOH})_8$ is soluble in water at high pH values as deprotonation of the carboxyl group occurs in basic media, which results in a charged, water-soluble species.



Scheme 3.2. Synthetic route for the preparation of water-soluble $\text{ZnPc}(\text{COOH})_8$.⁶⁶

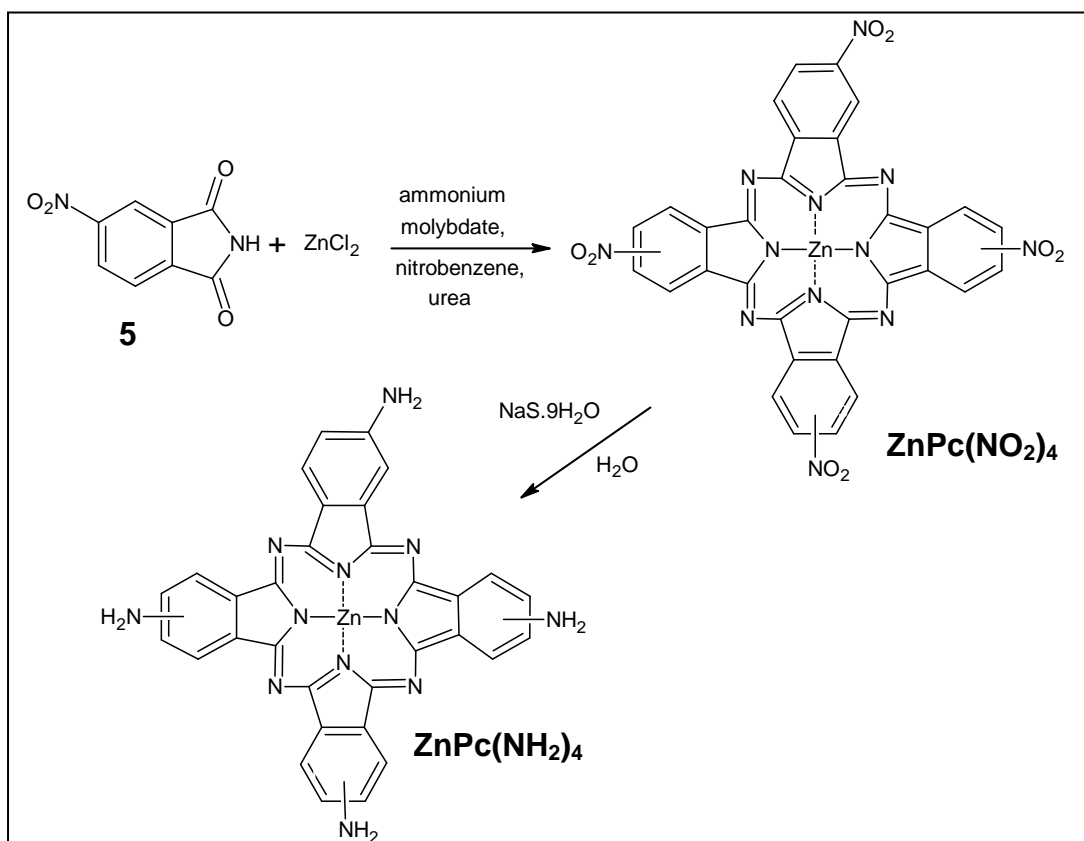
3.1.2. Synthesis of Water-insoluble MPc Complexes

Substitution of phthalimide (**4**) was achieved using concentrated HNO_3 as the reagent and concentrated H_2SO_4 as the acid catalyst (Scheme 3.3). The synthetic yield was relatively high (71%), which is consistent with literature values.³⁶



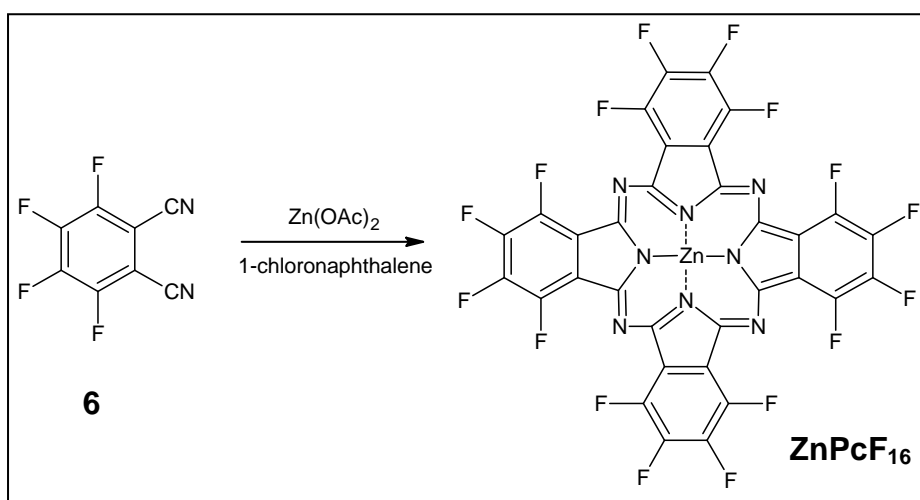
Scheme 3.3. Synthetic route for the preparation of 4-nitrophthalimide.³⁶

The synthesis of $\text{ZnPc}(\text{NO}_2)_4$ was achieved using 4-nitrophthalimide (**5**) as the phthalocyanine building block (Scheme 3.4). The reported methods on which the synthesis of $\text{ZnPc}(\text{NO}_2)_4$ is based make use of 4-nitrophthalic acid⁶⁷, 4-nitrophthalonitrile or 4-nitrophthalic anhydride⁶⁸ as the starting reagent. Attempts were made to synthesize $\text{ZnPc}(\text{NO}_2)_4$ with the reagents used in literature, however the desired product was not obtained, as a result 4-nitrophthalimide was used. The bands for the $-\text{NO}_2$ symmetric and asymmetric stretches were obtained at 1331 and 1517 cm^{-1} , respectively, in the IR spectrum of $\text{ZnPc}(\text{NO}_2)_4$. The reduction of the NO_2 groups on $\text{ZnPc}(\text{NO}_2)_4$ in order to form $\text{ZnPc}(\text{NH}_2)_4$ was achieved using $\text{NaS}\cdot 9\text{H}_2\text{O}$.⁶⁷ The disappearance of the $-\text{NO}_2$ bands at 1331 and 1517 cm^{-1} confirmed reduction of the nitro groups. Characteristic bands for $-\text{NH}_2$ asymmetric and symmetric stretching vibrations were observed at 3337 and 3178 cm^{-1} , respectively.

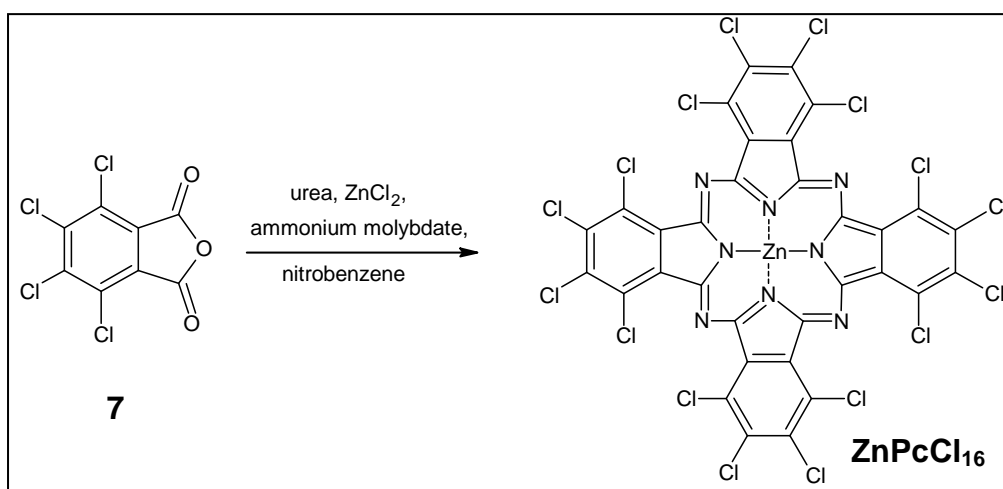


Scheme 3.4. Synthetic route for the formation of $\text{ZnPc}(\text{NO}_2)_4$ and $\text{ZnPc}(\text{NH}_2)_4$.^{67,68}

The synthesis and purification of ZnPcF_{16} was relatively straightforward (Scheme 3.5) and resulted in high synthetic yields of the desired product.^{69,70} The hexadecachlorinated species (ZnPcCl_{16}) required numerous purification steps before obtaining a product of reasonable purity (Scheme 3.6).^{69,71,72} The synthetic yield was also considerably lower than that obtained for ZnPcF_{16} , which is consistent with literature values. The IR spectra for both species showed aryl-halogen stretching bands at 1142 cm^{-1} for ZnPcF_{16} and 1136 cm^{-1} for ZnPcCl_{16} . Both complexes are soluble in DMF. ZnPcF_{16} is soluble DMSO, whereas ZnPcCl_{16} is sparingly soluble in DMSO. Fluorination of ZnPc renders it soluble in most common organic solvents (e.g. acetone, THF).



Scheme 3.5. Synthetic route for the formation of ZnPcF_{16} .^{69,70}



Scheme 3.6. Synthetic steps for the preparation of ZnPcCl_{16} .^{69,71,72}

3.1.3. Absorbance Spectra of MPc Complexes

3.1.3.1. Water-soluble MPcs

The formation of aggregates in MPcS complexes is characterized by band broadening in the visible region of the spectrum and the presence of a low energy band near 630 nm due to sandwich-type dimer formation.⁷³ At the concentration employed for photocatalysis in this work all photosensitisers were aggregated. Disaggregation was achieved using the non-ionic surfactant Triton X-100 (Figure 3.2), except for ZnPc(COOH)₈, where DMSO was employed as a disaggregating agent, as complete disaggregation was not achieved using Triton X-100. The percentage aggregation values of the water-soluble species were determined using Eq. (24):⁷⁴

$$\% \text{ Aggregation} = \left(\frac{A_Q(\text{Triton X-100}) - A_Q(\text{solvent})}{A_Q(\text{Triton X-100})} \right) \times 100\% \quad (24)$$

where A_Q is the maximum absorbance of the Q-band in the solvent ($A_Q(\text{solvent})$) and on addition of Triton X-100 to the solution ($A_Q(\text{Triton X-100})$). For ZnPc(COOH)₈ DMSO replaces Triton X-100 in Eq. (24).

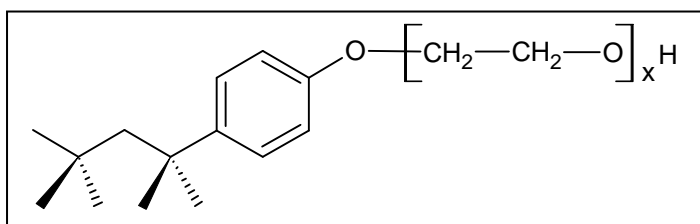


Figure 3.2. Structure of Triton X-100, a non-ionic surfactant.

Figure 3.3 shows that adequate monomerization was obtained for ZnPcS₄, ZnPcS_{mix}, but not for ZnPc(COOH)₈ on addition of Triton X-100.

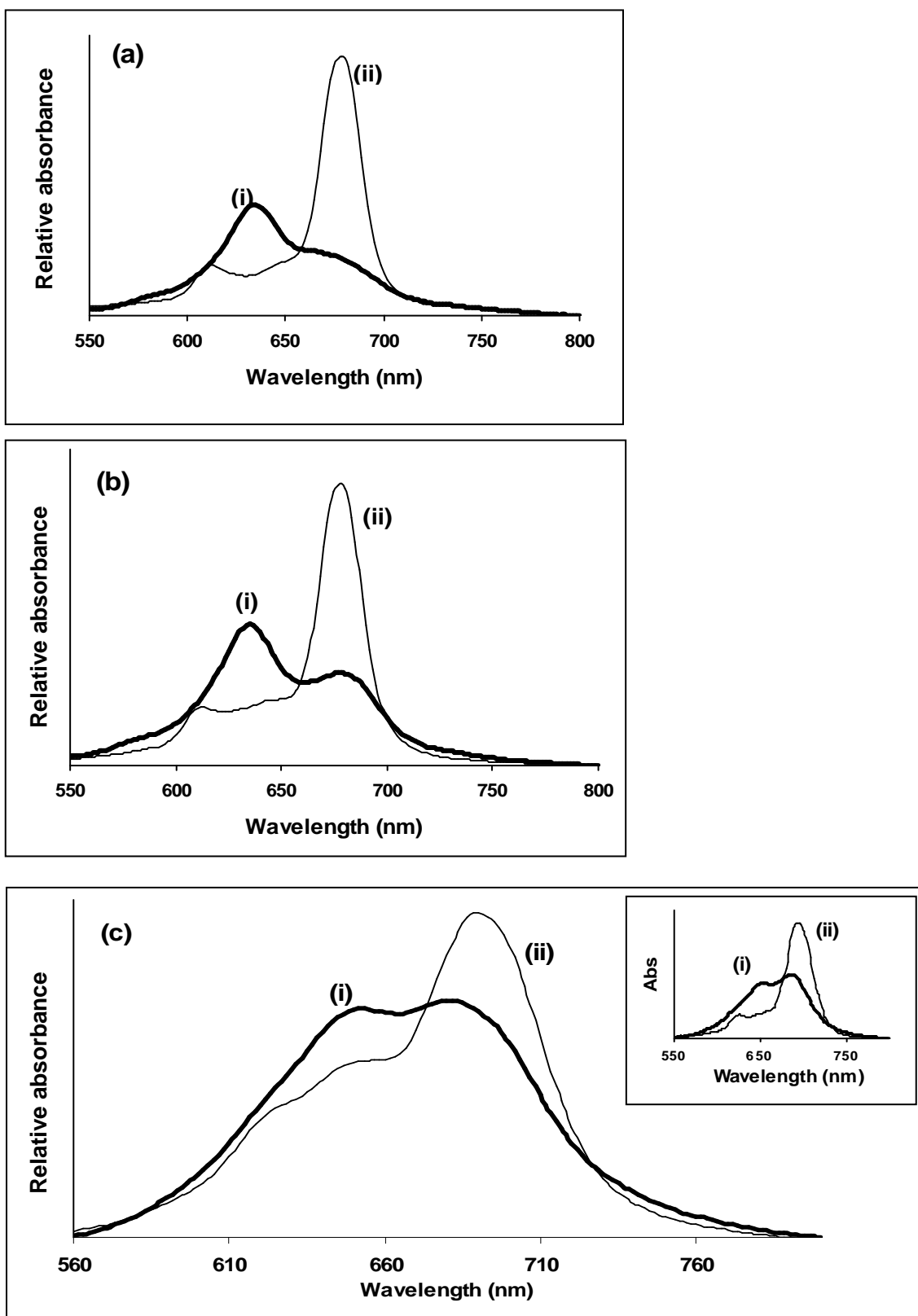


Figure 3.3. Spectral changes observed on addition of Triton X-100 to solutions of (a) $\text{ZnPcS}_{\text{mix}}$, (b) ZnPcS_4 , and (c) $\text{ZnPc}(\text{COOH})_8$ (Inset: complete disaggregation of $\text{ZnPc}(\text{COOH})_8$ using DMSO). (i) Buffer only, and (ii) Buffer and Triton X -100. pH of buffer = 8.2.

The Q-band absorbance maxima, as well as the degree of aggregation (% aggr) of the MPcs in water, are listed in Table 3.1. The NiPcS and ZnPcS complexes in Table 3.1 are both highly aggregated in water (> 70%), while the CoPcS complexes and ZnPc(COOH)₈ are aggregated to a lesser extent (54%, 37% and 42% for CoPcS₄, CoPcS_{mix} and ZnPc(COOH)₈, respectively). The high degree of aggregation for ZnPcS₄ and ZnPcS_{mix} is significant, as it will have a negative influence on their ability to photocatalyse 4-Np.⁷ According to literature both MPcS₄ and MPcS_{mix} are known to exist as aggregates in equilibrium with the monomeric species, with the equilibrium favouring the aggregated species. The degree of aggregation of MPcS_{mix} complexes decreases with an increase in the fraction of more highly sulphonated species in the mixture, therefore the degree of aggregation in water increases with lipophilicity.⁷⁴ The percentage aggregation of ZnPc(COOH)₈ has been reported to be 0% (i.e. it exists as the monomeric species) in pH 10 buffer,⁵⁴⁻⁵⁶ which is inconsistent with the data expressed in Table 3.1, which shows ZnPc(COOH)₈ to be 42% aggregated in pH 8.2 buffer. The formation of aggregates in this study may be due to differences in the composition of buffer solutions used in literature and in this study.

Table 3.1. λ_{max} values and percentage aggregation of water-soluble MPcs in water at pH 7 (pH 8.2 for ZnPc(COOH)₈). Disaggregation achieved using Triton X-100, except for ZnPc(COOH)₈.

Complex	Q-band λ_{max} (monomer) (nm)	Q-band λ_{max} (dimer) (nm)	% aggr
ZnPcS ₄	678	633	72
CoPcS ₄	667	627	54
NiPcS ₄	668	623	77
ZnPcS _{mix}	666	633	82
CoPcS _{mix}	660	625	37
NiPcS _{mix}	665	610	79
ZnPc(COOH) ₈	684 ^a	648	42

^aDisaggregation achieved using DMSO.

The absorption spectra for $\text{FePcS}_{\text{mix}}$ and FePcS_4 are relatively complex, as it is possible for the iron ions (in the +3 oxidation state) of adjacent species to form μ -oxo species.^{29,75} The nature of the species in solution (i.e. $\text{Fe}^{\text{II}}\text{PcS}_{\text{mix}}$ or $\text{Fe}^{\text{III}}\text{PcS}_{\text{mix}}$) was confirmed by chemically reducing a solution of $\text{FePcS}_{\text{mix}}$ in 3:1 $\text{CH}_3\text{CN}:\text{H}_2\text{O}$. Reduction of the complex using NaBH_4 led to the formation of a monomeric species with a Q band at 653nm and loss of the charge-transfer band at 500 nm (Figure 3.4). A shift in the Q band to a shorter wavelength (i.e. from 661 nm to 653 nm as in Figure 3.4) is characteristic of the reduction of $\text{Fe}^{\text{III}}\text{Pc}$ to $\text{Fe}^{\text{II}}\text{Pc}$,^{29,75} therefore the complexes prepared in this study are $\text{Fe}^{\text{III}}\text{Pcs}$. Due to the complexity of the spectra associated with the FePcS complexes, their percentage aggregation was not calculated in Table 3.1.

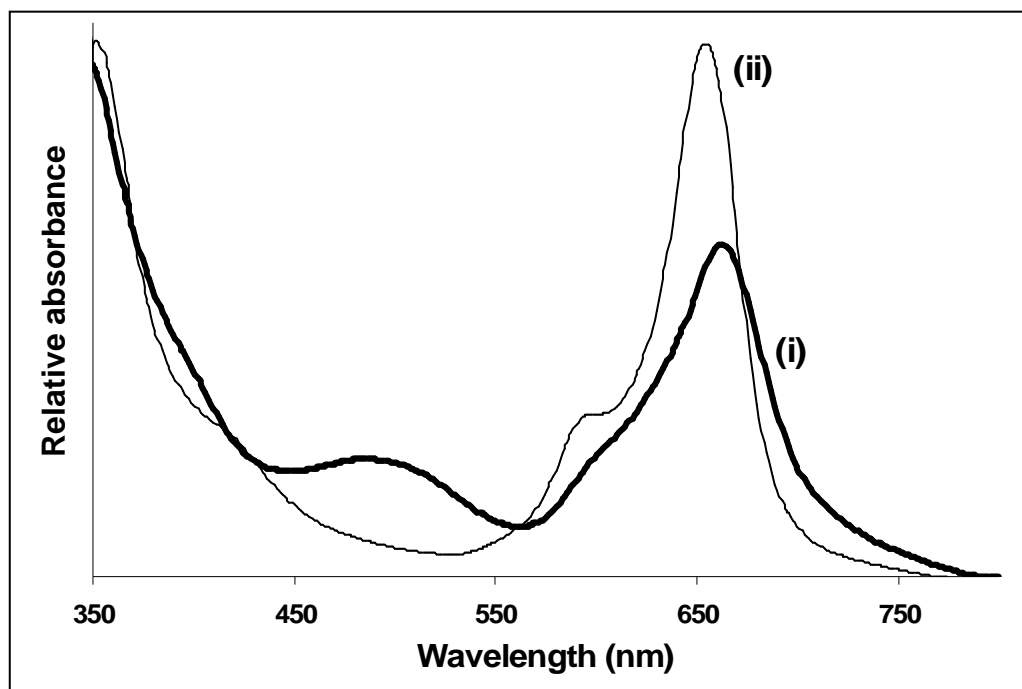


Figure 3.4. Spectral changes of (i) $\text{Fe}^{\text{III}}\text{PcS}_{\text{mix}}$ in 3:1 $\text{CH}_3\text{CN}:\text{H}_2\text{O}$ on addition of NaBH_4 , resulting in (ii) $\text{Fe}^{\text{II}}\text{PcS}_{\text{mix}}$.

3.1.3.2. Water-insoluble MPcs

The absorbance spectra of the water-insoluble MPcs are shown in Figures 3.5 and 3.6. Figure 3.5 shows that AlPc, ZnPc and MgPc are monomeric as judged by the narrow Q-band and the absence of a non-vibronic band at a higher energy relative to the Q-band. The absorption spectrum for ZnPc(NH₂)₄ in Figure 3.6a shows that the species is also relatively disaggregated in DMSO while ZnPc(NO₂)₄ (Figure 3.6b), ZnPcF₁₆ (Figure 3.6d) and ZnPcCl₁₆ (Figure 3.6c) are relatively highly aggregated with peaks due to the aggregated species observed at 643, 638 and 653 nm (Table 3.2), respectively, and those due to the monomeric species were observed at 680, 663 and 727 nm (Table 3.2), respectively. Q-band λ_{max} values were determined directly from Figures 3.5 and 3.6 for all monomeric species (i.e. ZnPc, MgPc, ClAlPc and ZnPc(NH₂)₄). For the aggregated species (i.e. ZnPc(NO₂)₄, ZnPcF₁₆ and ZnPcCl₁₆) sequential dilution of the complex in DMSO resulted in a decrease in the intensity of the dimer peak relative to the monomer peak (Figure 3.7), confirming aggregation of these complexes in DMSO. The difference in Q-band λ_{max} values for the monomeric species of ZnPc(NH₂)₄ and ZnPc(NO₂)₄ can be explained by considering the electron-donating and electron-withdrawing nature of NH₂ and NO₂, respectively. The electron-donating NH₂ group shifts ZnPc(NH₂)₄ to the red region (i.e. lower energy) of the spectrum relative to ZnPc(NO₂)₄ due to destabilisation of the HOMO of ZnPc(NH₂)₄ by the NH₂ group.⁴⁹ The same principle can be applied to the difference in Q-band λ_{max} values for ZnPcF₁₆ and ZnPcCl₁₆. F is more electronegative than Cl, and hence more electron-withdrawing than Cl. As a result of its strong electron-withdrawing ability relative to Cl, F shifts ZnPcF₁₆ to the blue region (i.e. higher energy) of the spectrum relative to ZnPcCl₁₆.⁴⁹

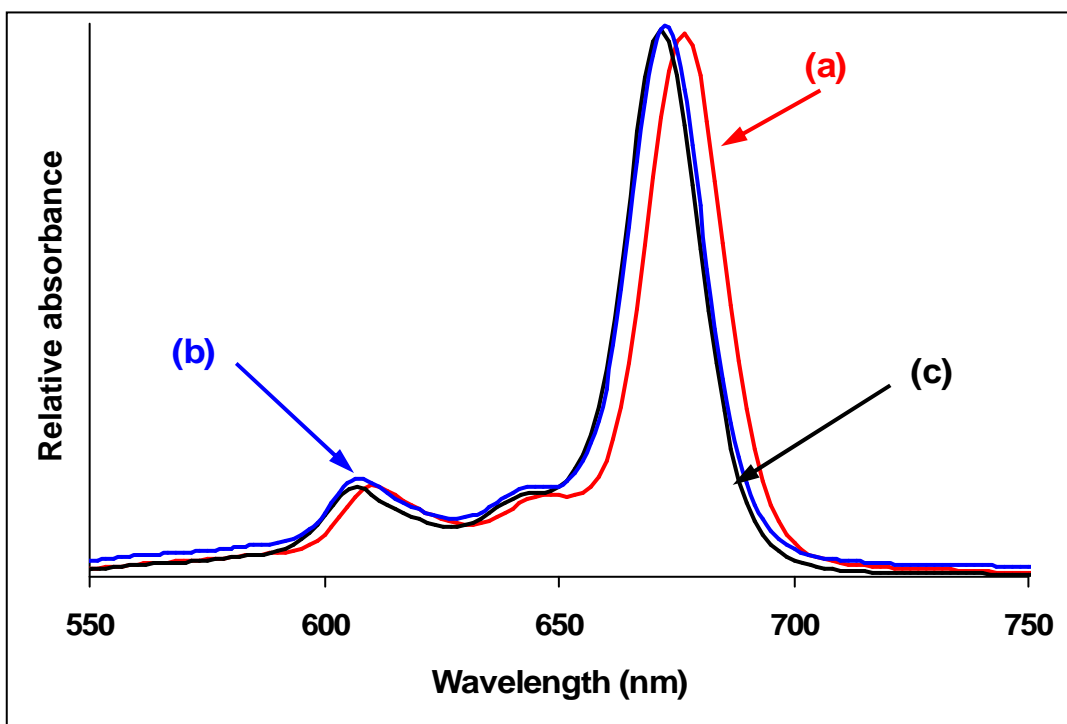


Figure 3.5. Spectra obtained for the unsubstituted Pc complexes in DMSO. (a) ClAlPc ($7.9 \times 10^{-6} \text{ mol dm}^{-3}$), (b) MgPc ($1.9 \times 10^{-5} \text{ mol dm}^{-3}$), and (c) ZnPc ($6.5 \times 10^{-6} \text{ mol dm}^{-3}$).

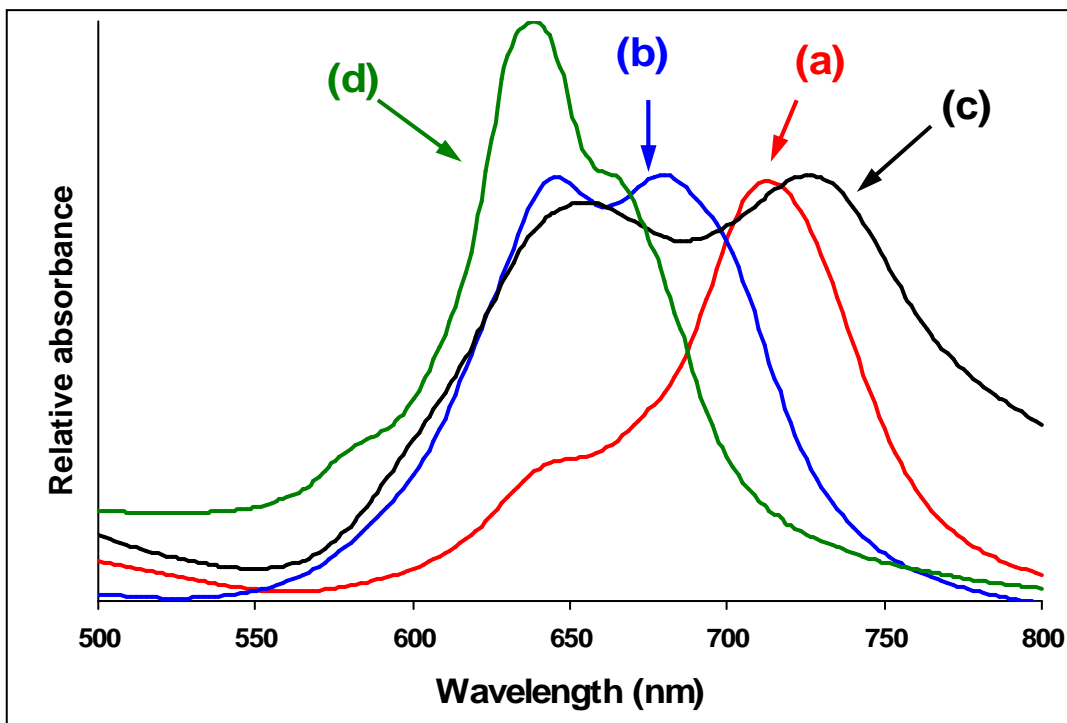


Figure 3.6. Spectra obtained for the substituted zinc Pc complexes in DMSO. (a) $\text{ZnPc}(\text{NH}_2)_4$, (b) $\text{ZnPc}(\text{NO}_2)_4$, (c) ZnPcCl_{16} , and (d) ZnPcF_{16} .

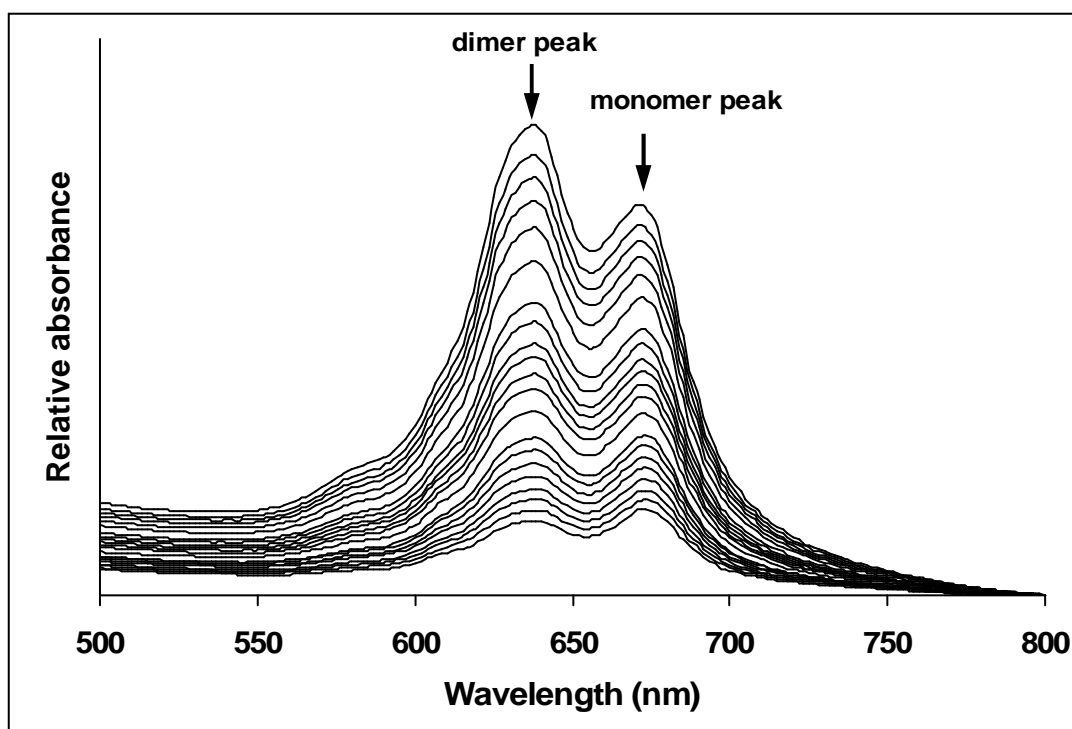


Figure 3.7. Determination of λ_{\max} values for the monomeric and dimeric species of ZnPcF_{16} by sequential dilution in DMSO.

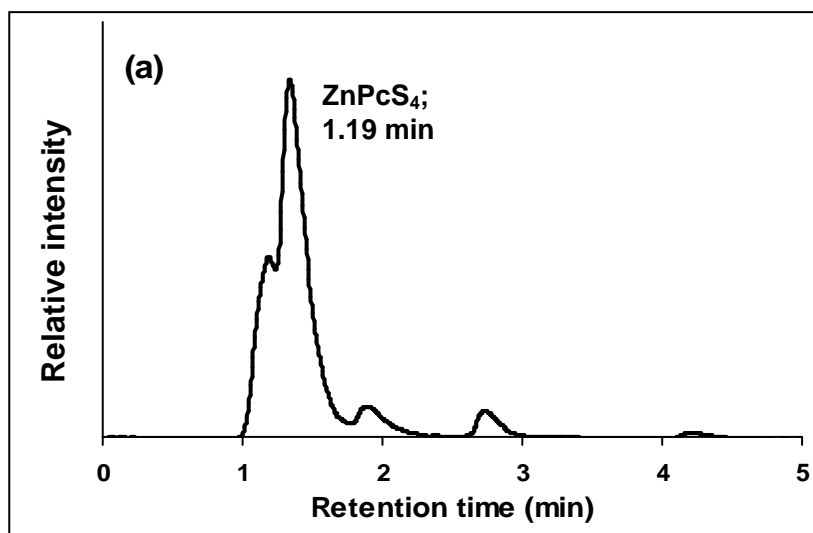
Table 3.2. λ_{\max} values obtained for the water-insoluble MPcs in DMSO.

Phthalocyanine	Q-band λ_{\max} (monomer)	Q-band λ_{\max} (dimer)
	(nm)	(nm)
MgPc	673	—
ZnPc	672	—
ClAlPc	677	—
$\text{ZnPc}(\text{NO}_2)_4$	680	643
$\text{ZnPc}(\text{NH}_2)_4$	713	—
ZnPcF_{16}	663	638
ZnPcCl_{16}	727	653

3.1.4. HPLC Characterisation of MPcS_4 and MPcS_{mix} Complexes

MPcS_{mix} complexes containing a mixture of sulpho (mono-, di-, tri- and tetra-) substituents are important to study (as mixtures) since $\text{AlPcS}_{\text{mix}}$, for example, is already in use as a

photosensitiser for medical purposes, i.e. for PDT.^{76,77} It is known that MPcS_{mix} preparations consisting of the least number of isomeric species show a greater tendency to form aggregates, whereas the more complex preparations consisting of a higher number of differently substituted compounds show less aggregation.⁷⁴ The degree of aggregation increases with lipophilicity,⁷⁴ hence, as stated above, the more sulphonated fractions are less aggregated. The HPLC traces for MPcS_{mix} complexes, using the analytical Prodigy 5 μm ODS (150 x 4.6 mm) column, are shown in Figure 3.8. It is expected that the most highly sulphonated component will be the first to elute from the chromatographic column, and so give the lowest retention time. Therefore the least sulphonated fractions will give the highest retention times.⁶⁵ For the MPcS_{mix} samples, the HPLC signals with the lowest retention times are assigned to the tetrasulphonated fractions, using tetrasulphonated phthalocyanines (MPcS_4) as a reference (Figure 3.8). Thus, $\text{NiPcS}_{\text{mix}}$ and $\text{ZnPcS}_{\text{mix}}$ consisted mostly of the tetrasulphonated Pc, with minute amounts of the less sulphonated derivatives detected. Conversely, $\text{FePcS}_{\text{mix}}$ contained very little of FePcS_4 , and $\text{CoPcS}_{\text{mix}}$ consisted of mainly two components with an almost equal amount of CoPcS_4 in the mixture. The predominance of the ZnPcS_4 isomer in Figure 3.8a is contrary to previous HPLC analyses which showed $\text{ZnPcS}_{\text{mix}}$ to consist of the less sulphonated fractions.^{51,78} This confirms the observation that the composition of the prepared MPcS_{mix} complexes may vary from batch to batch.



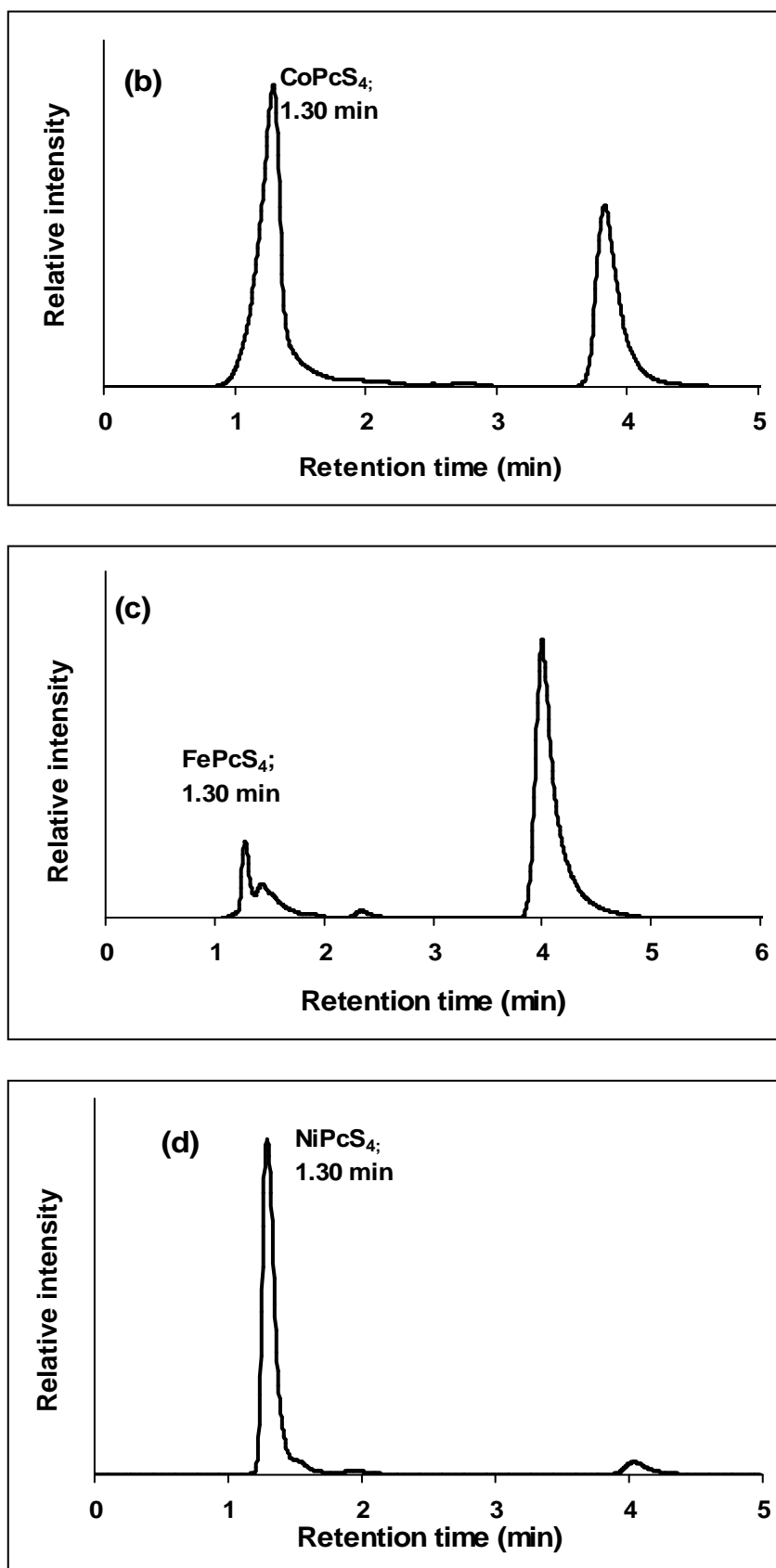


Figure 3.8. HPLC traces of (a) $\text{ZnPcS}_{\text{mix}}$, (b) $\text{CoPcS}_{\text{mix}}$, (c) $\text{FePcS}_{\text{mix}}$, and (d) $\text{NiPcS}_{\text{mix}}$.

3.2. Homogeneous Photocatalysis of 4-Np using Water-soluble Zinc Pc Complexes

Zinc was used as the central metal for this study as it is evident from literature that zinc Pc derivatives are good photocatalysts.^{51,54-56}

3.2.1. Catalyst Loading and $\Phi_{4\text{-Np}}$ Optimisation

Studies for the photocatalysed degradation of 4-Np were carried out at pH = 8.2, as the pKa value for 4-Np is 7.15.⁷⁹ It has been proven that the phenolate/phenoxide ion (ArO^-), which is the predominant species at about 1 pH unit above the pKa of the phenolic complex, is more easily oxidised than the corresponding protonated species (ArOH).^{55,56} Figure 3.9 shows the absorption spectral changes observed on photolysis of 4-Np in the presence of the optimum concentration of $\text{ZnPcS}_{\text{mix}}$ (i.e. 400 mg/L). A peak due to 4-Np was observed at 400 nm and disappeared with time with the formation of peaks due to degradation products at ~280 nm. $\Phi_{4\text{-Np}}$ values were calculated using Eq. (16) by determining the initial rate of disappearance of 4-Np at 400 nm. Data from Figure 3.9 was used to generate a plot of absorbance versus time (Figure 3.10), which was used to determine initial degradation rates. The optimum amount of each ZnPc complex (using $\text{ZnPcS}_{\text{mix}}$ as an example) needed for the photodegradation of 4-Np was determined by plotting $\Phi_{4\text{-Np}}$ versus the concentration of $\text{ZnPcS}_{\text{mix}}$ (Figure 3.11). The curve levelled off after 400 mg/L. Using the optimum concentration of $\text{ZnPcS}_{\text{mix}}$ (i.e. 400 mg/L), the concentration of 4-Np to give the highest $\Phi_{4\text{-Np}}$ value was determined (Figure 3.12). Figure 3.12 shows that the $\Phi_{4\text{-Np}}$ value peaked at $1.5 \times 10^{-4} \text{ mol dm}^{-3}$ for the photodegradation of 4-Np.

Experiments were performed whereby 4-Np was photolysed in the absence of the photosensitiser. No spectral changes (or changes in HPLC traces) were observed, showing that transformation of 4-Np occurred only through photocatalysis in the presence of the photosensitiser.

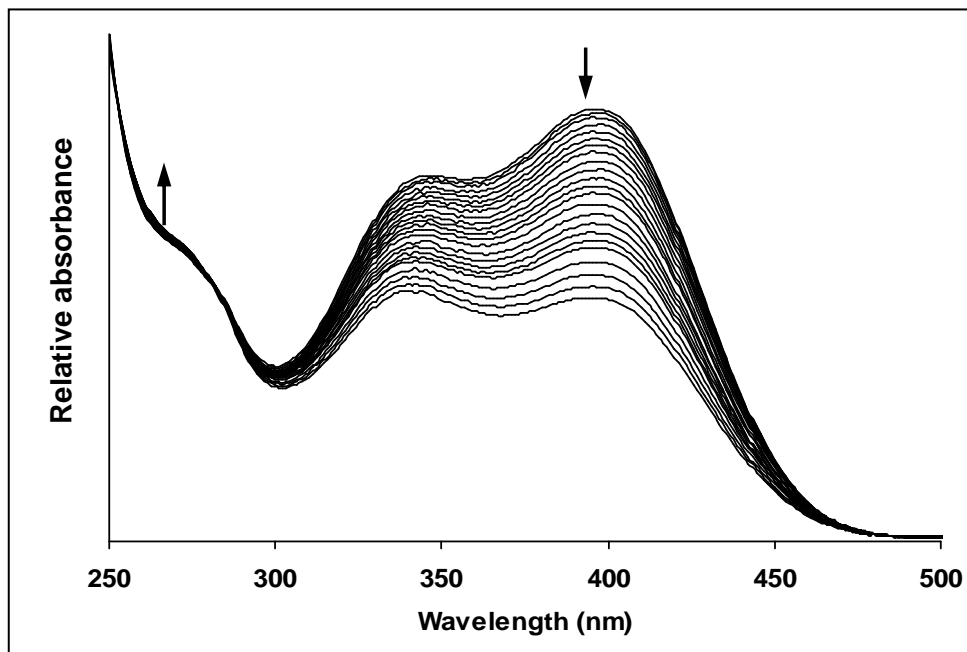


Figure 3.9. Electronic absorption spectral changes observed during the photolysis of 1.0×10^{-4} mol dm⁻³ 4-Np in the presence of 400 mg/L ZnPcS_{mix} in pH 8.2 buffer solution.

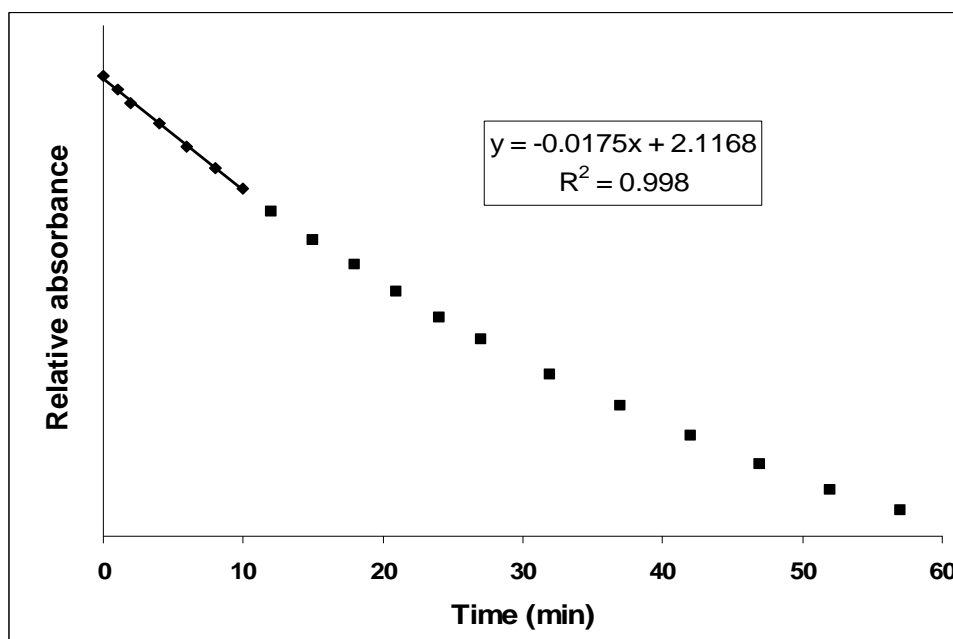


Figure 3.10. Plot of absorbance versus time to determine the initial rate of 4-Np degradation in the presence of ZnPcS_{mix}. ([4-Np] = 1.0×10^{-4} mol dm⁻³, ZnPcS_{mix} = 400 mg/L, pH = 8.2).

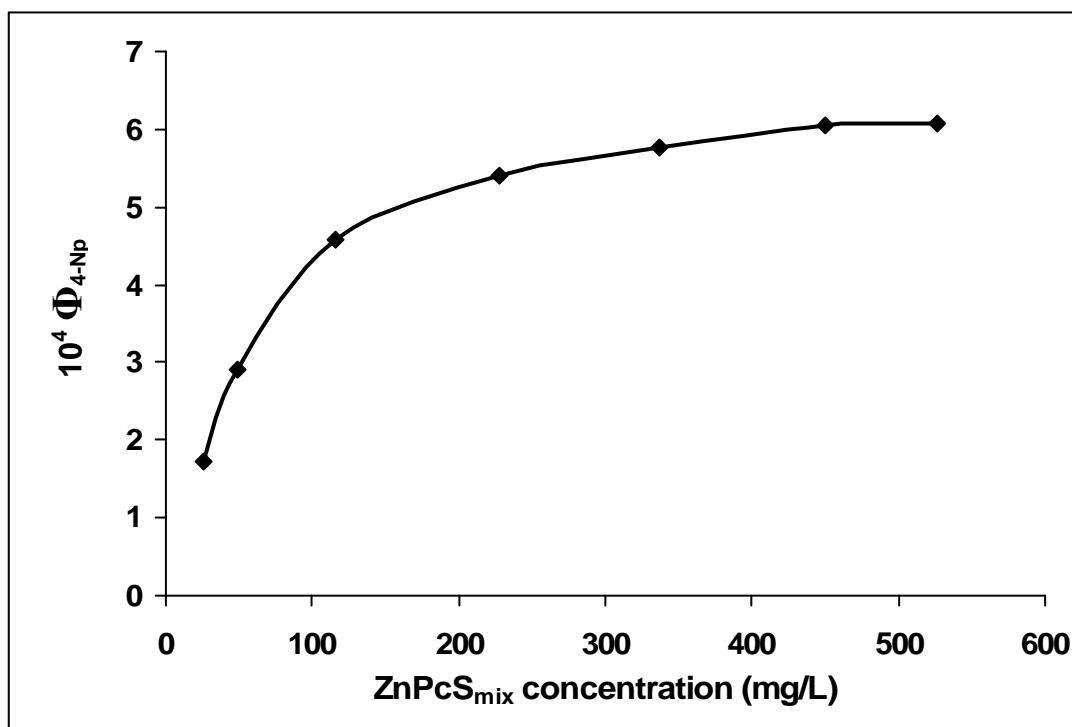


Figure 3.11. Plot of Φ_{4-Np} versus concentration of $ZnPcS_{mix}$ to determine the optimum concentration of $ZnPcS_{mix}$ for the phototransformation of 4-Np ($1.0 \times 10^{-4} \text{ mol dm}^{-3}$), pH = 8.2.

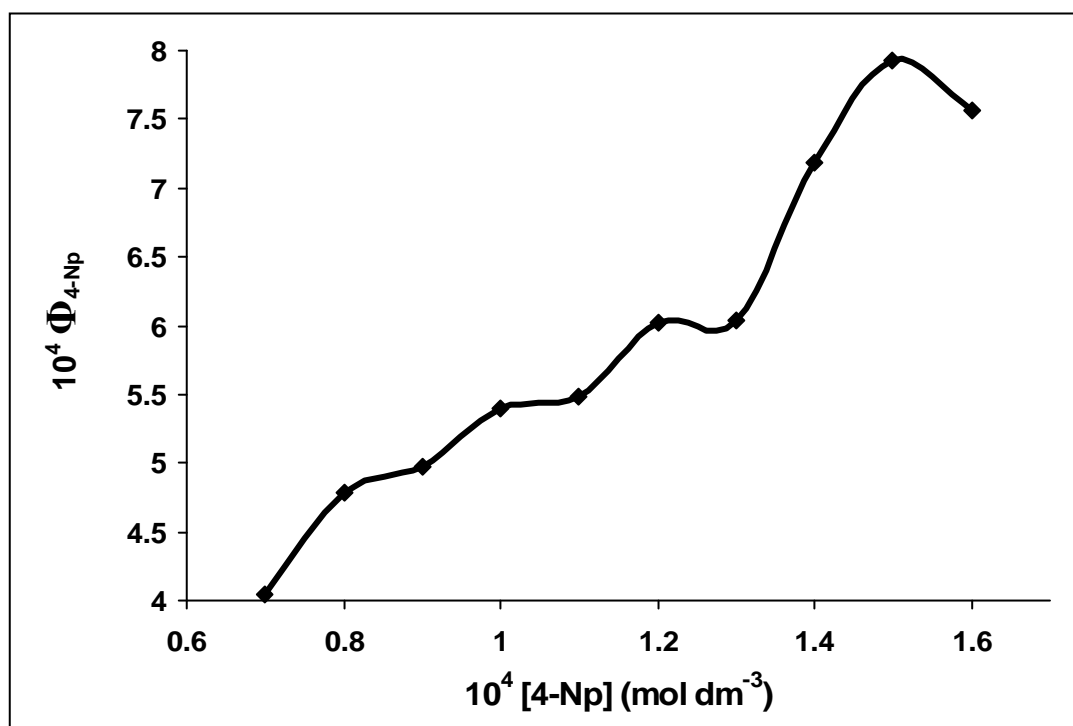


Figure 3.12. Plot of Φ_{4-Np} versus $[4-Np]$ for its phototransformation in the presence of $ZnPcS_{mix}$ (400 mg/L), pH = 8.2.

3.2.2. Comparison of the Photocatalytic Activities of the Zinc Pc Sensitisers

Figure 3.13 shows the decrease in [4-Np] with time during irradiation in the presence of the various photosensitisers at pH 8.2. The disappearance of 4-Np was monitored using UV-vis spectrophotometry. The results show that photooxidation of 4-Np occurred faster when $\text{ZnPc}(\text{COOH})_8$ was used as the sensitizer, as judged by the relatively large slope in Figure 3.13 and Table 3.3. ZnPcS_4 showed the least activity towards the photooxidation of 4-Np. Values of $\Phi_{4\text{-Np}}$ at 400 mg/L for the photosensitizer and $1.0 \times 10^{-4} \text{ mol dm}^{-3}$ for 4-Np were 7.9×10^{-4} , 1.5×10^{-4} and 6.5×10^{-3} for $\text{ZnPcS}_{\text{mix}}$, ZnPcS_4 and $\text{ZnPc}(\text{COOH})_8$, respectively (Table 3.3). Similarly, the values of $\Phi_{4\text{-Np}}$ for 4-Np photosensitized oxidation at 200 mg/L and $1.0 \times 10^{-4} \text{ mol dm}^{-3}$ 4-Np were 7.4×10^{-4} , 1.2×10^{-4} and 1.8×10^{-3} for $\text{ZnPcS}_{\text{mix}}$, ZnPcS_4 and $\text{ZnPc}(\text{COOH})_8$, respectively (Table 3.3). Two main factors determine photosensitizer activity: efficiency of singlet oxygen sensitization and photodegradation of the sensitizer. $\text{ZnPc}(\text{COOH})_8$ has the largest Φ_{Δ} value (Table 3.3), hence it is expected to be the best photocatalyst based on the assumption that the trend in Φ_{Δ} values in pH 10 buffer will be the same as the trend in pH 8.2 buffer. In terms of aggregation (aggr), this complex was aggregated at the concentrations employed in this work, even though it is known to be less aggregated than ZnPcS_4 and $\text{ZnPcS}_{\text{mix}}$.⁵⁵ $\text{ZnPcS}_{\text{mix}}$ has a slightly lower Φ_{Δ} value compared to $\text{ZnPc}(\text{COOH})_8$, and hence a lower photocatalytic activity is expected. The τ_T values of photocatalysts (Table 3.3) also influence catalytic activity. Even though the τ_T values listed in Table 3.3 were determined in DMSO they give a relative indication of the activities of the MPcs. The larger the τ_T value, the higher the probability of encounters of Pc with $^3\text{O}_2$ to form $^1\text{O}_2$. However, τ_T values are relatively similar, and as a result the Φ_{Δ} values provide a more accurate indication of photocatalytic activity.

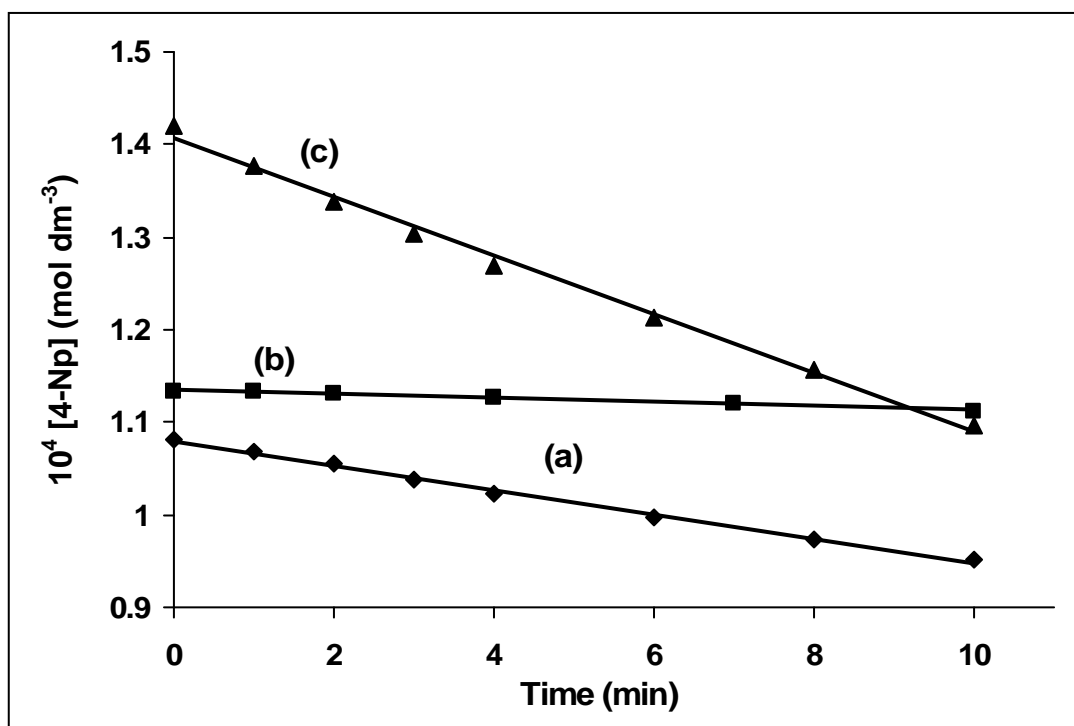


Figure 3.13. Plot of [4-Np] versus time for (a) $ZnPcS_{mix}$, (b) $ZnPcS_4$, and (c) $ZnPc(COOH)_8$.

MPc = 200 mg/L, pH = 8.2.

Table 3.3. Photosensitisation data for 4-Np transformation in the presence of the water-soluble photosensitisers (400 mg/L or 200 mg/L) under visible light irradiation (10 min). (pH = 8.2, [4-Np] = 1.0×10^{-4} mol dm⁻³).

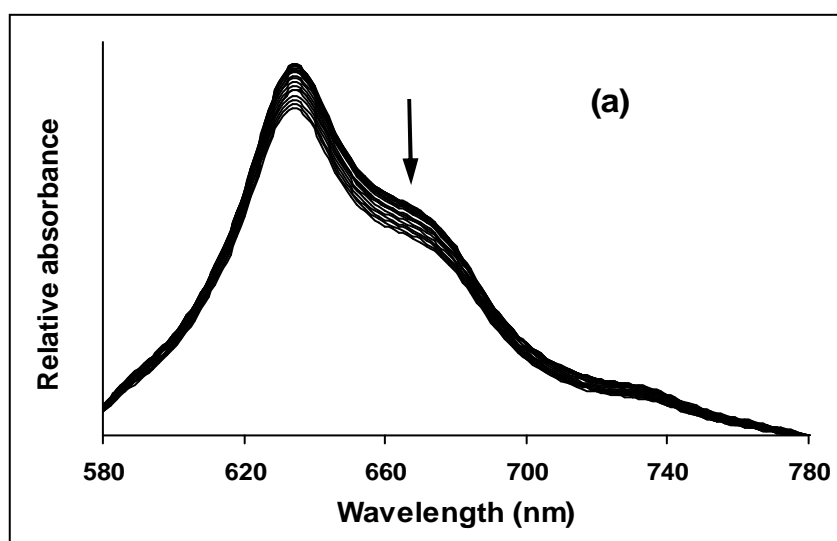
Complex	Φ_{4-Np} (400 mg/L MPc)	Φ_{4-Np} (200 mg/L MPc)	Φ_{Δ}^a	τ_T (μs)	$10^6 k$ (M min ⁻¹) ^d	% deg (10 min)	% aggr
$ZnPcS_{mix}$	7.9×10^{-4}	7.4×10^{-4}	0.48	530 ^b	1.3	15%	82%
$ZnPcS_4$	1.5×10^{-4}	1.2×10^{-4}	< 0.01	470 ^b	0.22	2%	72%
$ZnPc(COOH)_8$	6.5×10^{-3}	1.8×10^{-3}	0.52	480 ^c	3.2	23%	42%

^aFrom reference [54] in pH 10 buffer, ^bFrom reference [31] in DMSO, ^cFrom reference [80] in DMSO,

^dObtained from the slopes of the curves in Figure 3.13.

The fate of the photocatalyst is important. A stable photocatalyst which also results in a high rate of 4-Np degradation would be preferred. Figure 3.14 shows the spectroscopic changes observed for $ZnPcS_{mix}$, $ZnPcS_4$ and $ZnPc(COOH)_8$ during photocatalytic transformation of 4-Np.

ZnPcS_{mix} showed good stability during the catalysis (Figure 3.14a). ZnPcS₄ (Figure 3.14b) showed minimal degradation (only ~2%, Table 3.3). However, due to its small singlet oxygen quantum yield, ZnPcS₄ was not an efficient photocatalyst. ZnPc(COOH)₈ (Figure 3.14c) showed significant degradation during the photolysis process in this work, which is in agreement with the degree of degradation that has been observed during the photooxidation of 4-chlorophenol (4-Cp).⁵⁵ However, this complex gave the best photocatalytic activity for 4-Np compared to the other two. This is contrary to the photocatalysis of 4-Cp,⁵⁵ where ZnPc(COOH)₈ gave poor catalytic activity compared to ZnPcS_{mix}, which was attributed to its high degree of degradation due to attack by the singlet oxygen they generate. Figure 3.14 shows that during degradation of ZnPc(COOH)₈, the monomer peak at 684 nm decreases faster than the dimer peak at 648 nm. It is expected that the monomeric species is responsible for the photocatalysis of 4-Np. On comparing the data for the phototransformation of 4-Np with that reported for the phototransformation of chlorophenols (i.e. 4-Cp, trichlorophenol and pentachlorophenol) in the presence of ZnPcS_{mix} (Table 3.4), it is evident that 4-Np is more resistant to photocatalysis due to stability brought about by resonance stabilisation of the phenolate ion.⁵



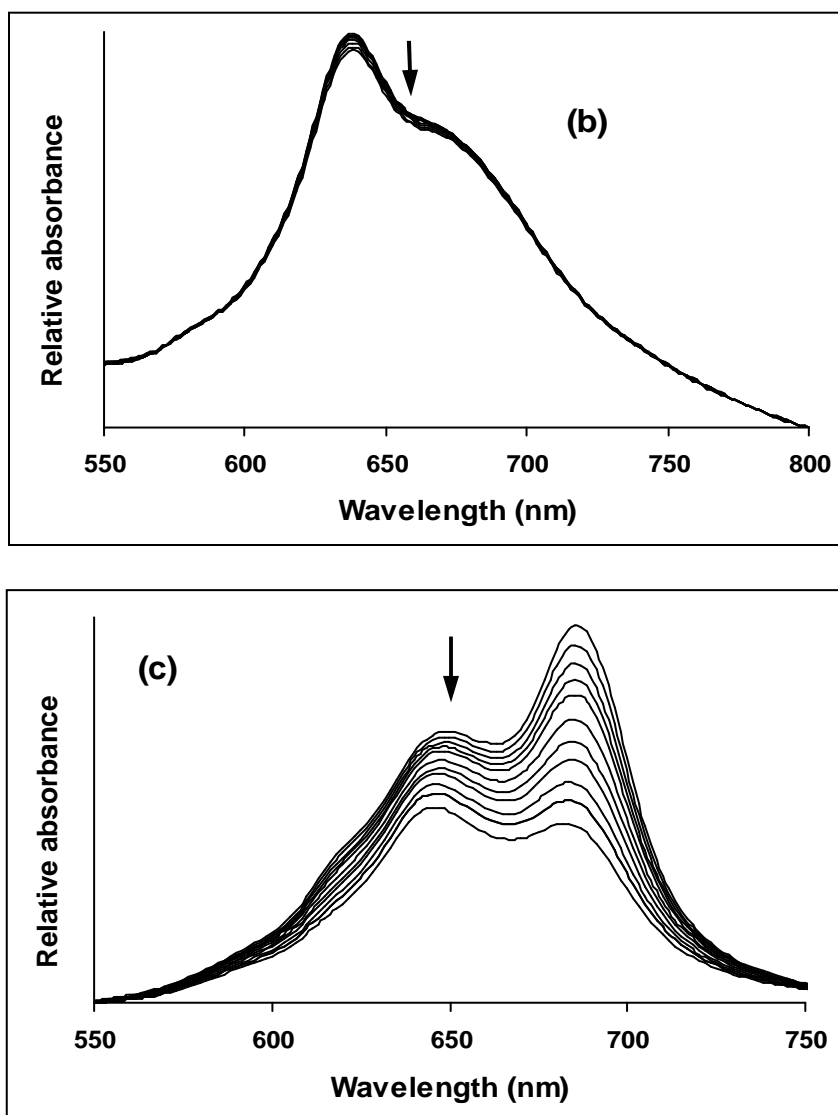


Figure 3.14. Spectral changes observed for (a) $\text{ZnPcS}_{\text{mix}}$, (b) ZnPcS_4 , and (c) $\text{ZnPc}(\text{COOH})_8$ during the photocatalytic oxidation of $1.0 \times 10^{-4} \text{ mol dm}^{-3}$ 4-Np, pH = 8.2.

Table 3.4. Comparison of photosensitisation data obtained for the transformation of chlorophenols and the transformation of 4-Np in the presence of $\text{ZnPcS}_{\text{mix}}$.

Substrate	$\Phi_{\text{substrate}}$	% degradation ^a	Ref
4-Np	7.9×10^{-4}	7.2%	—
4-Cp	1.4×10^{-2}	35%	55
trichlorophenol	1.1×10^{-3}	21%	56
pentachlorophenol	3.9×10^{-3}	32%	56

^aAfter 270s of irradiation. Note that the % degradation in Table 3.3 was at a longer time (i.e. 10 min).

3.2.3. Determination of Rate Constants of $\text{ZnPcS}_{\text{mix}}$ and $\text{ZnPc}(\text{COOH})_8$

Due to the low rate of 4-Np photodegradation in the presence of ZnPcS_4 , due to its low Φ_{Δ} value (< 0.01) (Table 3.3), this complex was not employed for the determination of rate constants. Figure 3.15 shows the linear plot of $1/\Phi_{4\text{-Np}}$ versus $1/[4\text{-Np}]$, using $\text{ZnPcS}_{\text{mix}}$ and $\text{ZnPc}(\text{COOH})_8$ as photosensitisers. Both plots are obtained at the optimum concentration of $\text{ZnPcS}_{\text{mix}}$ (400 mg/L) and $\text{ZnPc}(\text{COOH})_8$ (200 mg/L). The slope, from Eq. (21), is equal to $k_d/\Phi_{\Delta}k_r$, where $k_d = 3.22 \times 10^5 \text{ s}^{-1}$ (Eq. (22)) and $\Phi_{\Delta} = 0.48$ in pH 10, therefore $k_r = 0.67 \times 10^6 \text{ mol}^{-1} \text{ dm}^3 \text{ s}^{-1}$ (Table 3.5) for $\text{ZnPcS}_{\text{mix}}$. The intercept $((k_q + k_r)/\Phi_{\Delta}k_r)$ in Figure 3.15a = 896.5. Using the values of Φ_{Δ} and k_r (0.48 and $0.67 \times 10^6 \text{ mol}^{-1} \text{ dm}^3 \text{ s}^{-1}$, respectively), $(k_q + k_r)$ was calculated to be $2.9 \times 10^8 \text{ mol}^{-1} \text{ dm}^3 \text{ s}^{-1}$ for $\text{ZnPcS}_{\text{mix}}$. For $\text{ZnPc}(\text{COOH})_8$, the values of $(k_q + k_r)$ and k_r are $2.8 \times 10^8 \text{ mol}^{-1} \text{ dm}^3 \text{ s}^{-1}$ and $7.7 \times 10^6 \text{ mol}^{-1} \text{ dm}^3 \text{ s}^{-1}$, respectively. The values of $(k_q + k_r)$ for both $\text{ZnPcS}_{\text{mix}}$ and $\text{ZnPc}(\text{COOH})_8$ are 400 and 40 times greater than k_r (the rate constant for photo-oxidation alone), respectively, which indicates that most of the singlet oxygen that is generated is scavenged by a quenching process. 4-Np therefore quenches singlet oxygen faster than it reacts with it. This situation has been observed for many phenols.¹² The k_r and $(k_q + k_r)$ values for the phototransformation of 4-Cp in the presence of $\text{ZnPcS}_{\text{mix}}$ have been reported to be $2.8 \times 10^8 \text{ mol}^{-1} \text{ dm}^3 \text{ s}^{-1}$ and $12.5 \times 10^8 \text{ mol}^{-1} \text{ dm}^3 \text{ s}^{-1}$, respectively (Table 3.5).⁵⁵ Thus 4-Cp also quenches singlet oxygen faster than it reacts with singlet oxygen, as $(k_q + k_r)$ is 5 times greater than k_r . However, on comparing the k_r values obtained for 4-Cp and 4-Np it is evident that 4-Cp reacts with singlet oxygen to a greater extent than 4-Np. The high stability of 4-Np, due to electron delocalisation within the complex,⁵ accounts for its resistance to photodegradation by singlet oxygen.

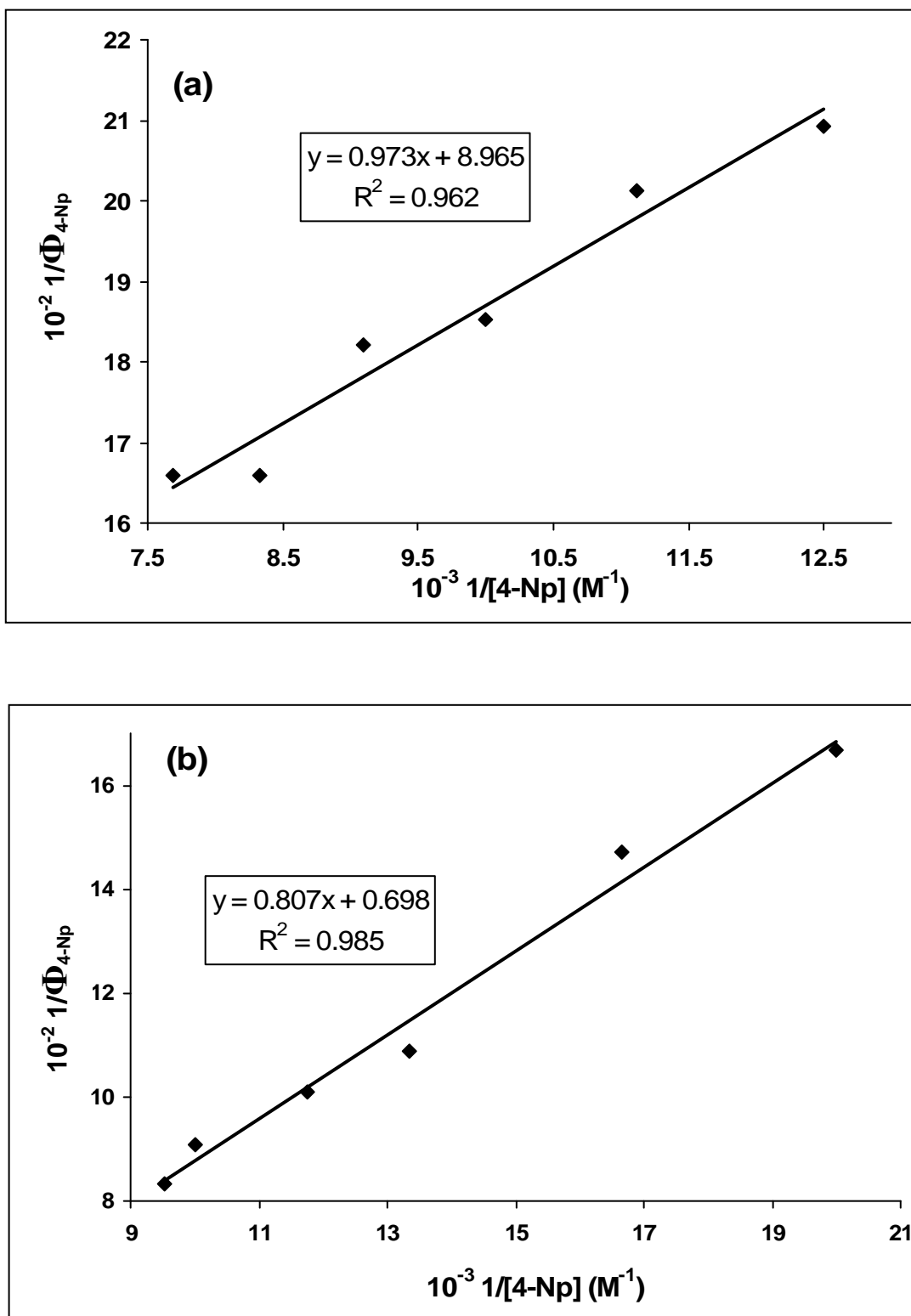


Figure 3.15. Plot of $1/\Phi_{4-Np}$ versus $1/[4-Np]$ for the phototransformation of 4-Np in the presence of (a) ZnPcS_{mix} (400 mg/L), and (b) ZnPc(COOH)₈ (200 mg/L), pH = 8.2.

Table 3.5. Comparison of k_r and $(k_q + k_r)$ values obtained for selected photosensitisers.

Substrate	Complex	pH	Φ_{Δ}^a	$10^{-6} k_r$ (mol ⁻¹ dm ³ s ⁻¹)	$10^{-8} (k_q + k_r)$ (mol ⁻¹ dm ³ s ⁻¹)
4-Np	ZnPcS _{mix}	8.2	0.48	0.67	2.9
	ZnPc(COOH) ₈	8.2	0.52	7.7	2.8
4-Cp	ZnPcS _{mix}	10 ^b	0.48	280 ^b	12.5 ^b

^aFrom reference [54], ^bFrom reference [55]

3.2.4. Mechanism for the Photodegradation of 4-Np using Homogeneous Photosensitisers

The involvement of singlet oxygen in the photocatalysis mechanism was confirmed by performing photocatalysis experiments in air and in the presence of NaN₃, as NaN₃ is an oxygen scavenger.⁵⁴⁻⁵⁶ Figure 3.16 shows faster kinetics for 4-Np in air and slower kinetics on addition of NaN₃, hence confirming the involvement of oxygen. The products for the photodegradation of 4-Np were determined either by LC/MS (see Figure 3.17 for the mass spectrum obtained for 4-nitrocatechol), or by comparing retention times of standards, i.e. 4-nitrocatechol and hydroquinone. The mass spectrum (Figure 3.17) shows the molecular ion peak for 4-nitrocatechol at 156.63 amu. The presence of hydroquinone was confirmed by spiking samples for injection into the reverse-phase HPLC, as hydroquinone could not be detected using MS, as it did not ionise under the conditions employed.

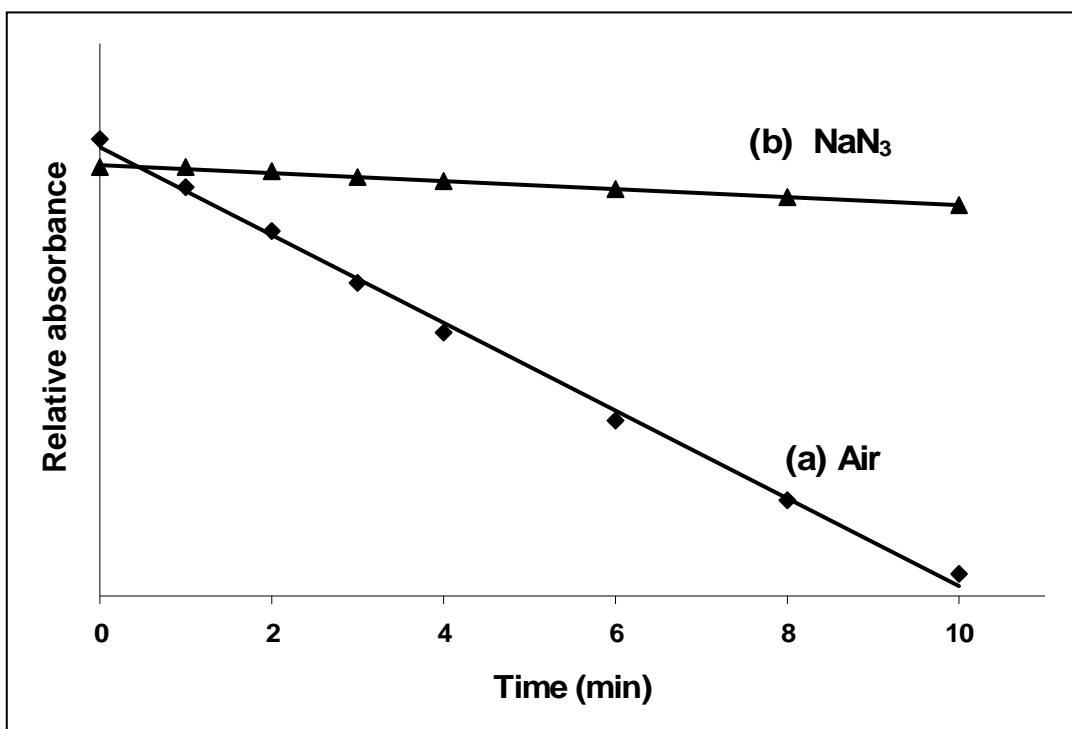


Figure 3.16. Effect of addition of NaN₃ (an oxygen scavenger) on the rate of 4-Np degradation in the presence of ZnPcS_{mix}. (a) no NaN₃, (b) NaN₃ added. ([4-Np] = 1.0×10^{-4} mol dm⁻³, ZnPcS_{mix} = 400 mg/L, pH = 8.2).

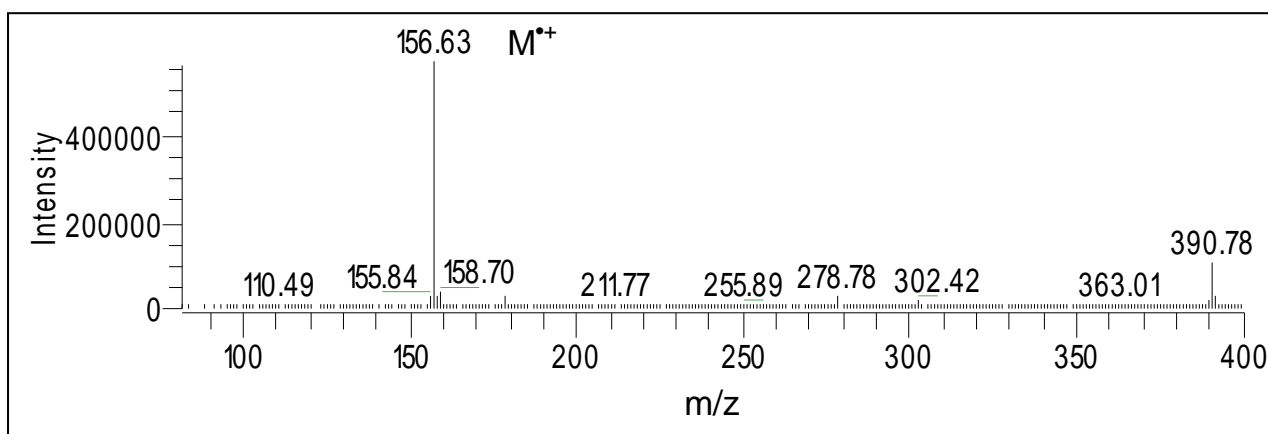
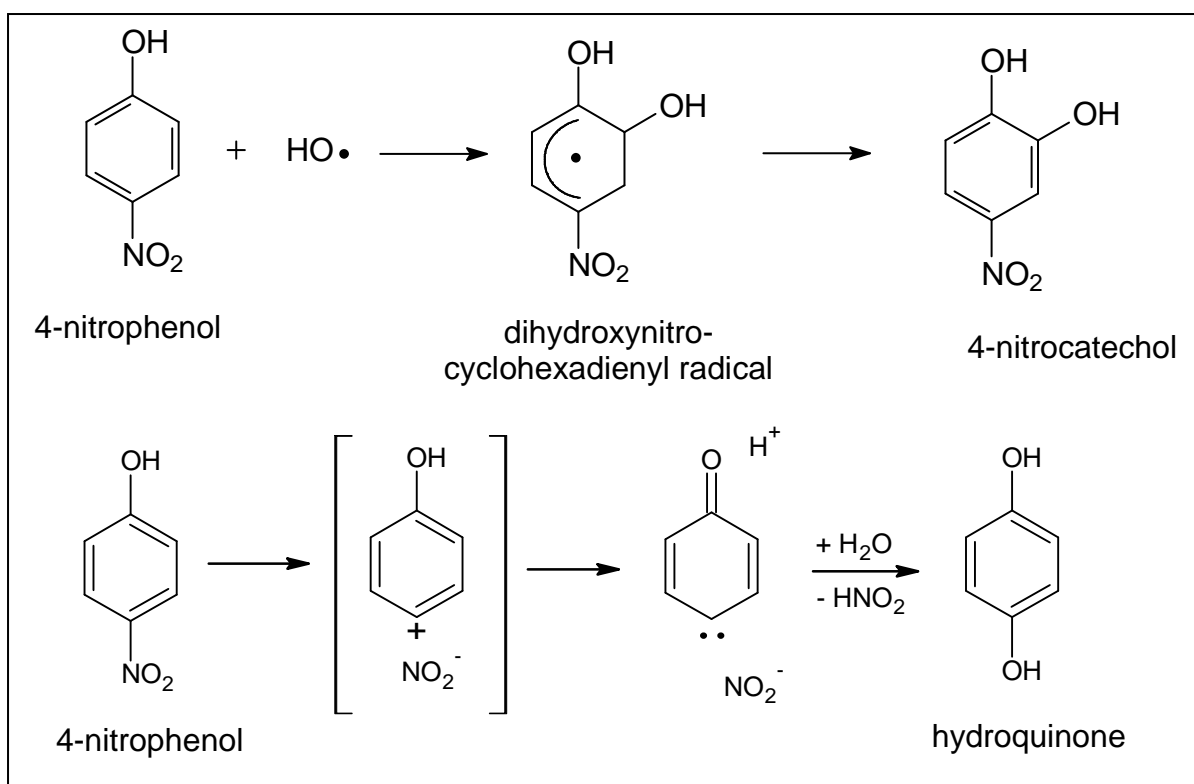


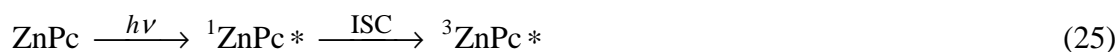
Figure 3.17. Mass spectrum obtained for 4-nitrocatechol ($m/z = 155$ amu) fraction using ESI-MS (retention time = 1.75 min).

Mechanisms that have been proposed in literature for the formation of 4-nitrocatechol and hydroquinone are shown in Scheme 3.7.¹² These reactions occur via the Type I mechanism described in Scheme 1.7, Section 1.4. The formation of 4-nitrocatechol from 4-nitrophenol occurs via a dihydroxynitrocyclohexadienyl radical species, which forms as a result of addition of a hydroxyl group *ortho* to the phenol functional group. The formation of hydroquinone results from loss of the *para* nitro group of 4-Np and reduction of the resulting intermediate to form hydroquinone.



Scheme 3.7. Proposed mechanisms for the phototransformation of 4-Np via the Type I reaction mechanism.

However it was proven, using the oxygen scavenger sodium azide (Figure 3.16), that the degradation of 4-Np occurs via a Type II mechanism, which includes the involvement of singlet oxygen (Scheme 3.8).



Scheme 3.8. Transformation of 4-Np by singlet oxygen mechanism.

The disadvantages associated with the study involving the photodegradation of 4-Np in the presence of homogeneous zinc Pc catalysts include:

- 1) The difficulty of isolating the catalyst for reuse and separating the degradation products from the unreacted substrate.
- 2) The relatively rapid degradation of the most effective catalysts in this study, namely $\text{ZnPcS}_{\text{mix}}$ and $\text{ZnPc}(\text{COOH})_8$, during the photodegradation of 4-Np.
- 3) Formation of degradation products that are less toxic than 4-Np, but are still hazardous to the environment and human health (ORL-RAT LD_{50} values for 4-nitrocatechol and hydroquinone are 260 mg kg^{-1} and 320 mg kg^{-1} , respectively, whereas that for 4-Np is 202 mg kg^{-1}).⁹

3.3. Heterogeneous Photocatalysis of 4-Np Using Suspended MPc Complexes

In this section the MPc complexes were suspended in an aqueous, buffered solution containing 4-Np. Photocatalysis was carried out in the setup shown in Figure 2.2 for 100 min, after which the solution was filtered for analysis of the degradation process and determination of degradation products using HPLC. The MPcs employed in this study are ZnPc, ClAlPc and MgPc derivatives which contain diamagnetic metals which are known to enhance photocatalytic behaviour.^{31,50,51}

3.3.1. Identification of Degradation Products

Figure 3.18 shows the HPLC traces for 4-Np degradation following photolysis for 100 min in the presence of suspended $\text{ZnPc}(\text{NH}_2)_4$ (as an example), followed by filtering of the solution. Inset shows the HPLC trace for 4-Np before photolysis. The products were identified by LC/MS and by spiking the solution with standards. The final products were 4-nitrocatechol (4-NC) and fumaric acid (FA), with the latter being the major product. Benzoquinone (BQ) and hydroquinone (HQ) were observed as intermediate products as they were formed initially and their peaks decreased with time as the peaks due to FA and 4-NC increased. Mass spectral peaks obtained for the final products are provided in Figure 3.19, showing molecular ion peaks for FA and 4-NC at 117.1 and 153.8 amu, respectively. The degradation products were separated using a semi-preparative column attached to a reverse-phase HPLC before injecting the separated fractions directly into the mass spectrometer.

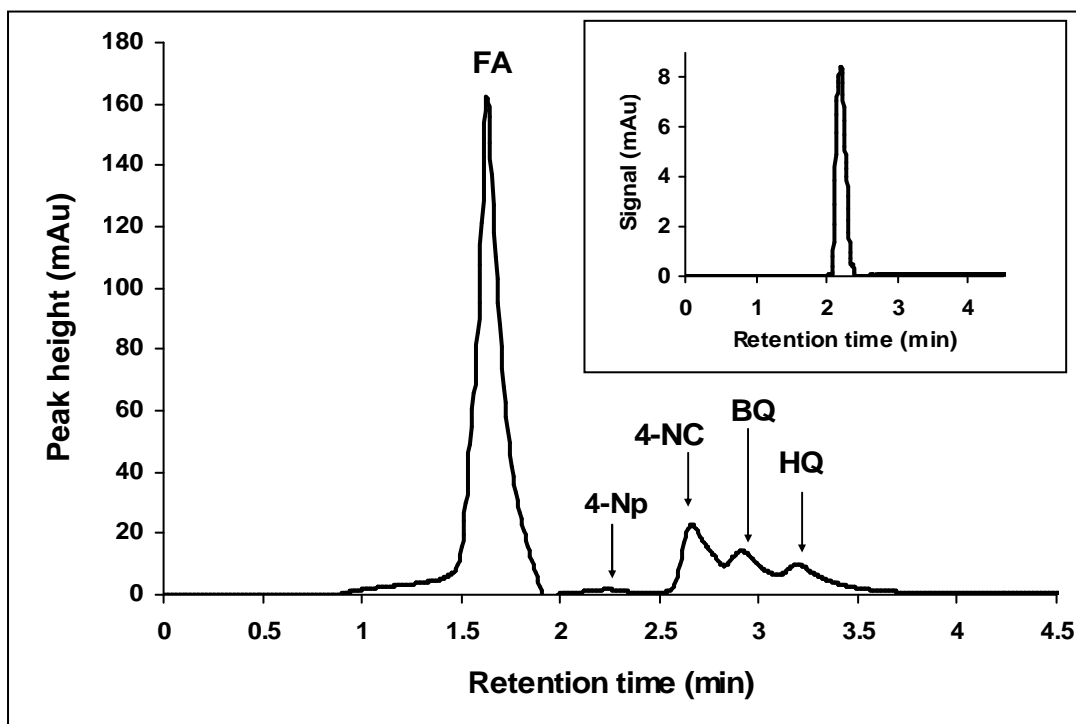


Figure 3.18. HPLC traces of the reaction mixture after photocatalysis of 4-Np for 100 min using $\text{ZnPc}(\text{NH}_2)_4$, $[\text{4-Np}] = 1.0 \times 10^{-5} \text{ mol dm}^{-3}$, pH = 9. Inset: HPLC trace of 4-Np before photolysis.

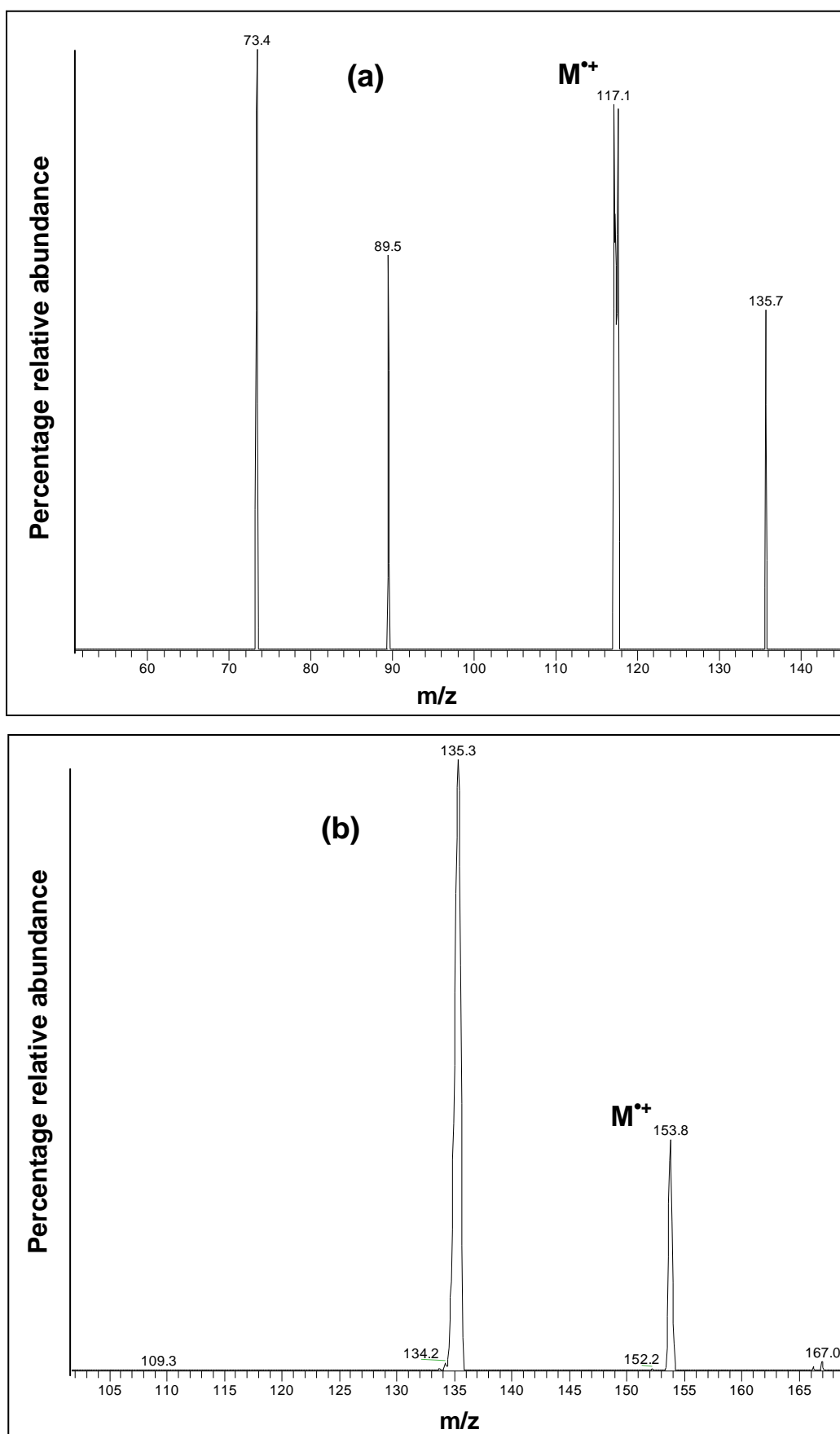
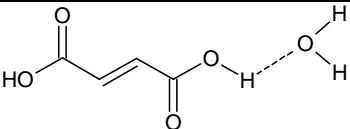
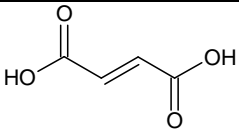
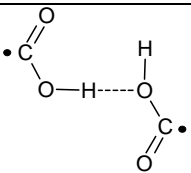
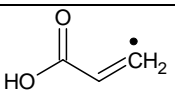
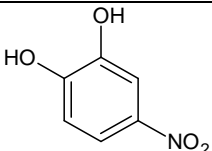
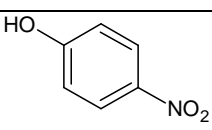


Figure 3.19. Fragmentation patterns obtained for (a) FA ($m/z = 116$ amu) and (b) 4-NC ($m/z = 155$ amu) using ESI-MS (direct injection) ($[4\text{-Np}] = 1 \times 10^{-5} \text{ mol dm}^{-3}$, $\text{pH} = 9$).

The complexes that correspond to the peaks obtained in the mass spectra in Figure 3.19 are provided in Table 3.6. The peak obtained for FA at $m/z = 89.5$ amu would correspond to loss of one of the carbonyl groups (C=O) of FA, however this is not possible as it would also result in loss of the hydroxyl group, therefore it is proposed that the peak at $m/z = 89.5$ amu is due to hydrogen bonding between two carboxyl radicals which were cleaved from FA to form the complex at $m/z = 73.4$ amu. The peaks obtained for 4-NC correspond to 4-NC at 153.8 amu and 4-Np at 135.3 amu. The peak at 135.3 amu may be due to the formation of *p*-nitrophenol or *m*-nitrophenol, however the major complex that would form is the *para* isomer as it is more stable than the *meta* isomer due to steric and resonance effects.⁵

Table 3.6. Mass fragments obtained for fumaric acid and 4-nitrocatechol using ESI-MS.

Degradation product	m/z	Fragment structure
Fumaric acid	135.7	
	117.1	
	89.5	
	73.4	
4-Nitrocatechol	153.8	
	135.3	

The oxidation of 4-Np was performed by maintaining 4-Np at a constant concentration ($1.0 \times 10^{-5} \text{ mol dm}^{-3}$) and varying loadings of the catalyst (ZnPc in this instance). After 100 min of irradiation with visible light, the solution was filtered and analysed using the HPLC system described. A linear increase in the formation of the major degradation product (i.e. fumaric acid) was observed on plotting the average peak height of the degradation product versus the concentration of ZnPc (Figure 3.20). The straight-line plot obtained in Figure 3.20 passes close to the origin, indicating that the catalyst is required for the photocatalysis of 4-Np. A plot of log (peak height) vs. log ZnPc loading results in a linear relationship, with a slope value close to one, indicating that the degradation of 4-Np is first-order with respect to ZnPc (Figure 3.21).⁸¹

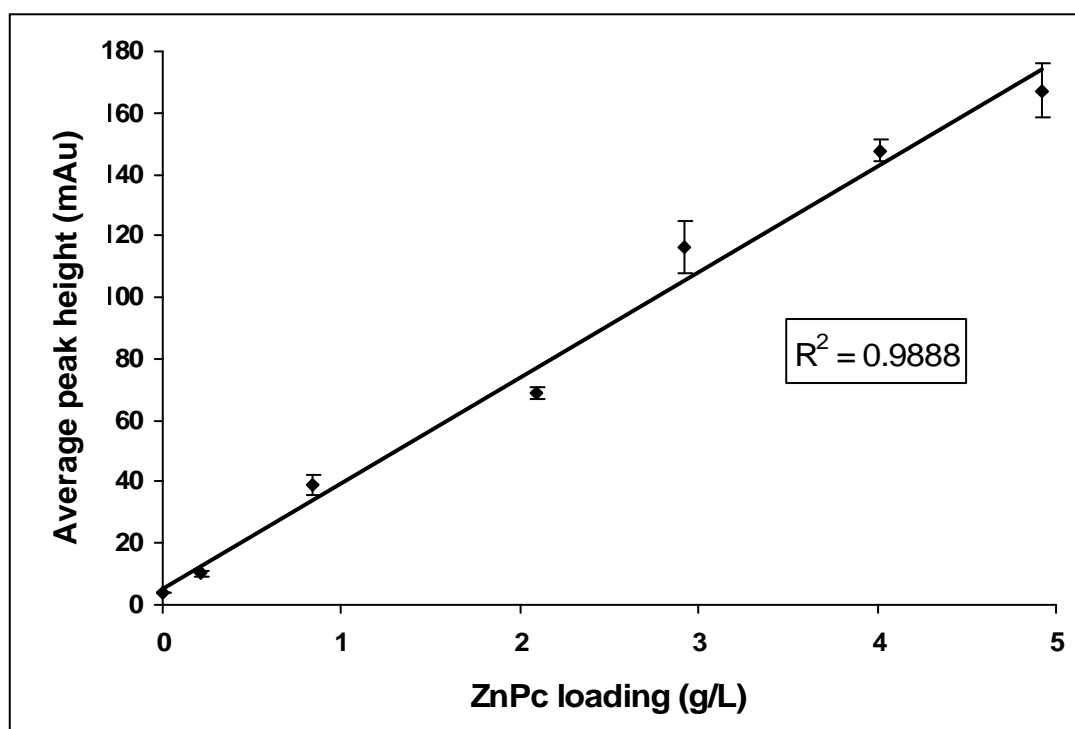


Figure 3.20. Average peak height versus loading of ZnPc to determine the effect of ZnPc on the phototransformation of 4-Np to FA. $[4\text{-Np}] = 1.0 \times 10^{-5} \text{ mol dm}^{-3}$, pH = 9.

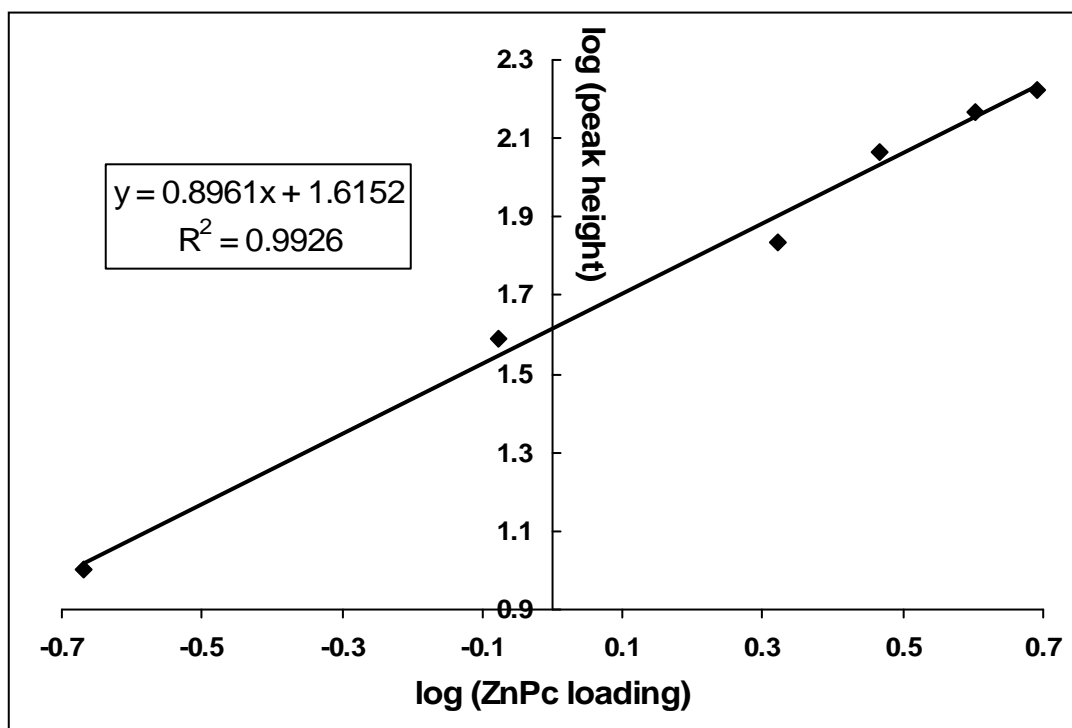


Figure 3.21. Plot of log (peak height) versus log (ZnPc loading) to determine the reaction order with respect to ZnPc.

3.3.2. Comparative Degradation of 4-Np

Triplet lifetimes (τ_T) were determined for the MPc complexes in DMSO, as τ_T values are an indication of the likelihood of energy transfer to $^3\text{O}_2$ to form $^1\text{O}_2$, where complexes with longer τ_T values have a higher probability of energy transfer from the triplet state.³¹ Aggregation is not desired in MPc complexes since it results in reduced τ_T values. The triplet lifetime values obtained for the water-insoluble MPcs are listed in Table 3.7. Unfortunately Φ_Δ literature values listed in Table 3.7 are in different media, however τ_T values were measured in the same media for a more comprehensive comparison of the relative energy transfer efficiencies of the heterogeneous photocatalysts. Even though the triplet lifetime values were determined in solution (DMSO), and the MPc complexes are in the solid state for the photocatalysis of 4-Np, they provide an indication of the relative lifetimes of the complexes. Triplet lifetimes were

determined using the method described in Section 2.2. The triplet decay curve of ZnPc is provided as an example of the data obtained using ORIGIN Pro 6.0 (Figure 3.22).

The trend in triplet lifetime values for the selected phthalocyanine complexes is as follows: ClAlPc > MgPc > ZnPc > ZnPcF₁₆ = ZnPc(NH₂)₄ > ZnPc(NO₂)₄ > ZnPcCl₁₆. The high triplet lifetimes obtained for the unsubstituted MPcs can be attributed to their monomeric character in DMSO (Figure 3.5), as previously discussed. The substituted phthalocyanines, excluding ZnPc(NH₂)₄, are highly aggregated in DMSO (Figure 3.6). The relatively low triplet lifetime value obtained for ZnPcF₁₆, compared to that obtained for ZnPc, can be accounted for by considering the “heavy-atom” effect of fluorines, which is expected to increase triplet quantum yields, but lower triplet lifetime values.³⁰ The “heavy-atom” effect of ZnPcCl₁₆ leads to its inability to remain in the excited triplet state for a measurable amount of time.

Table 3.7. Triplet lifetime (τ_T) and singlet oxygen quantum yield (Φ_Δ) values obtained for the selected water-insoluble MPc complexes in DMSO, unless otherwise stated (references in square brackets).

Photocatalyst	Q-band λ_{\max} (nm)	τ_T (μ s)	Φ_Δ^a
MgPc	673	400 \pm 4.3	0.40 ^b [41]
ZnPc	672	320 \pm 5.6	0.67 [31,82]
ClAlPc	677	470 \pm 3.5	0.29 [31]
ZnPc(NO ₂) ₄	680	60 \pm 2.7	0.11 [82]
ZnPc(NH ₂) ₄	713	150 \pm 2.9	0.11 [82]
ZnPcF ₁₆	663	150 \pm 8.1	0.13 ^c [31]
ZnPcCl ₁₆	727	Not detected	–

^aSinglet oxygen quantum yield (Φ_Δ) represents the amount of singlet oxygen generated per quanta of light absorbed, ^bSolvent = pyridine, ^cSolvent = acetone.

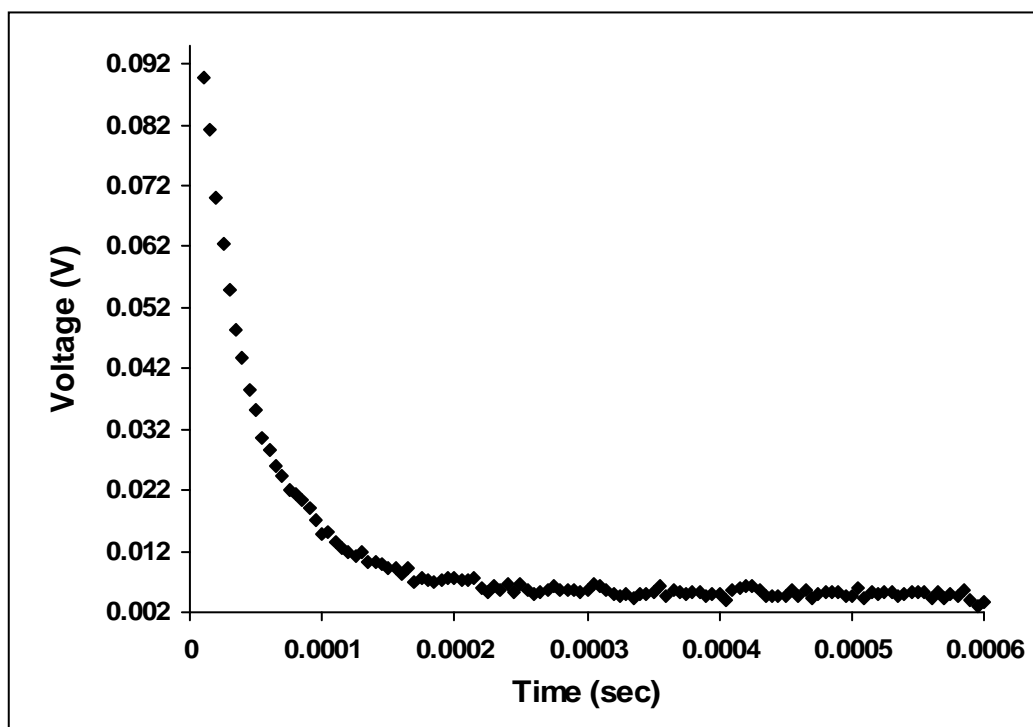


Figure 3.22. First order triplet decay curve obtained for ZnPc in DMSO using ORIGIN Pro 6.0.

The degree to which each phthalocyanine complex photocatalyses 4-Np was determined by comparing the HPLC trace obtained for $1.0 \times 10^{-5} \text{ mol dm}^{-3}$ 4-Np solution before and after photolysis in the presence of individual photocatalysts. Irradiation of the solution with visible light proceeded for 100 min. The results obtained for the percentage degradation of 4-Np are shown in Figure 3.23. The trend in the photodegradation of 4-Np by the selected phthalocyanine complexes is as follows: ClAlPc ($89 \pm 8.4 \%$) > ZnPcF₁₆ ($75 \pm 4.8 \%$) > ZnPc(NH₂)₄ ($54 \pm 2.2 \%$) > ZnPc ($53 \pm 6.3 \%$) > ZnPc(NO₂)₄ ($45 \pm 3.3 \%$) > MgPc ($25 \pm 4.5 \%$) > ZnPcCl₁₆ ($23 \pm 0.62 \%$).

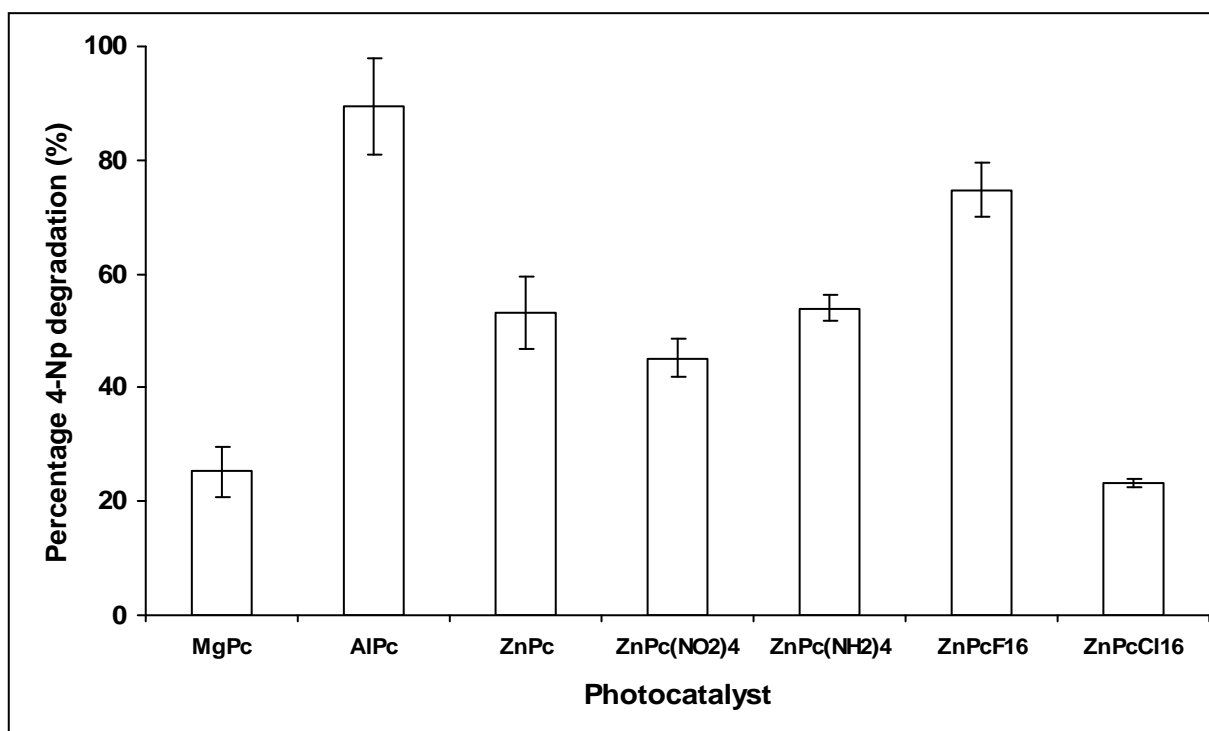


Figure 3.23. Percentage degradation of 4-Np by selected Pc complexes ($[4\text{-Np}] = 1.0 \times 10^{-5} \text{ mol dm}^{-3}$, pH = 9, irradiation time = 100 min).

The use of ClAlPc as a heterogeneous photocatalyst resulted in the highest percentage degradation of 4-Np due to a number of characteristic properties of ClAlPc that contribute to its effectiveness as a photocatalyst. ClAlPc is monomeric in DMSO (Figure 3.5), which reduces quenching of the triplet state, leading to efficient transfer of energy from triplet state MPc to triplet oxygen.³⁰ However, the rate of transfer of energy from the MPc triplet state to triplet oxygen will be substantially reduced in water, as its energy is dissipated as heat, therefore the τ_T values will be substantially lower for all Pcs than those presented in Table 3.7.⁴⁷ Aluminium is a diamagnetic metal and therefore contributes to rapid intersystem crossing of the MPc complex,^{30,31,50,51} leading to relatively high triplet (hence singlet oxygen) quantum yields. The axial chlorine substituent also contributes to intersystem crossing by enhancing spin-orbit coupling due to the “heavy-atom” effect⁴³ in ClAlPc. However, based on singlet oxygen quantum yield values (Table 3.7), ZnPc would be expected to perform better as a photocatalyst since it has a larger Φ_Δ value than ClAlPc in the same solvent. Table 3.7 shows that ClAlPc has

the longest lifetime which could be contributing to its effectiveness as a catalyst, as the number of diffusional encounters between the triplet states of the MPc and ground state molecular oxygen increases with triplet state lifetime.

The degree of degradation of 4-Np obtained for ZnPcF_{16} is relatively high compared to the other complexes in Figure 3.23 (excluding ClAlPc). Therefore the high degree of degradation of 4-Np using ZnPcF_{16} can be attributed to its triplet lifetime and to its high stability due to the presence of electron-withdrawing substituents.^{49,83} ZnPcCl_{16} , like ZnPcF_{16} , is stable, but has an insignificant triplet lifetime hence is less effective compared to ZnPcF_{16} . The ability of $\text{ZnPc}(\text{NH}_2)_4$ to degrade 4-Np to a large extent is unexpected, as amino groups are known to quench singlet oxygen.⁸² However Figure 3.23 shows substantial photodegradation ability of $\text{ZnPc}(\text{NH}_2)_4$ which is comparable to ZnPc . This suggests that the singlet oxygen mechanism (Type II) may not be the only mechanism involved in the photocatalysed transformation of 4-NP in the presence of the selected MPc complexes under heterogeneous conditions. It is thus possible that the Type I mechanism is also involved. In order to determine the degree to which singlet oxygen is involved in the degradation of 4-Np, photocatalytic degradation of 4-Np in the presence of a singlet oxygen scavenger, namely DABCO was carried out (using $\text{ZnPc}(\text{NH}_2)_4$ as an example). In order to determine the degree of 4-Np degradation in the presence and absence of DABCO the relative amounts of degradation products formed are compared (Figure 3.24). It is evident from Figure 3.24 that the Type II mechanism is not the only means of 4-Np degradation, since there is still considerable degradation of 4-NP in the presence of DABCO.

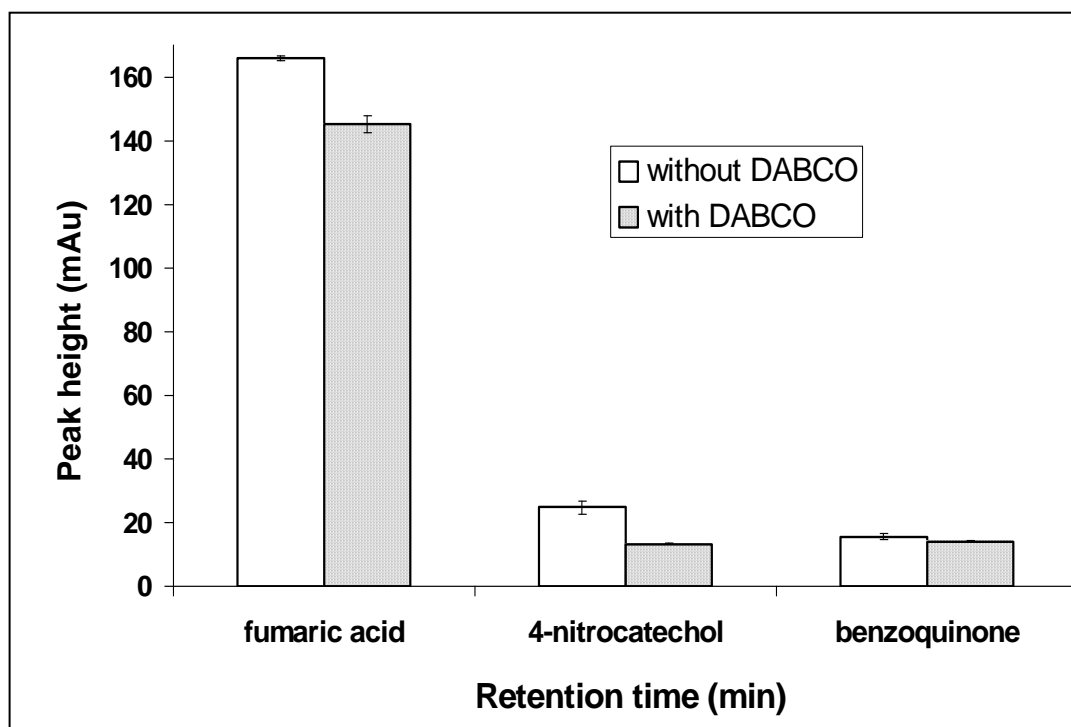


Figure 3.24. Comparison of the degree of formation of degradation products in the presence and absence of a singlet oxygen scavenger (DABCO), using 3.4 g/L $\text{ZnPc}(\text{NH}_2)_4$. ($[\text{4-Np}] = 1.0 \times 10^{-5} \text{ mol dm}^{-3}$, pH = 9, irradiation time = 100 min).

3.3.3. Mechanism for the Photodegradation of 4-Np using Water-insoluble MPcs

In order to confirm singlet oxygen involvement the singlet oxygen scavenger, ADMA, was monitored spectroscopically to confirm that singlet state oxygen ($^1\text{O}_2$, $^1\Delta_g$) forms on visible-light irradiation of the suspended MPc.^{56,84} The sample, which consisted of ClAlPc as the photocatalyst and $6.9 \times 10^{-5} \text{ mol dm}^{-3}$ ADMA, was irradiated with visible light, centrifuged and decanted into the UV/vis cell in order to determine the absorbance of the solution. After determining the absorbance of the sample the clear solution and separated ClAlPc were recombined for further irradiation. Figure 3.25 shows spectral changes that occur on exposure of ADMA to visible light in the presence of ClAlPc. The absorbance of ClAlPc is not observed as the MPc complex is a heterogeneous catalyst. The change in absorbance of ADMA shows that singlet oxygen is formed on photolysis of solid MPc in the presence of ADMA. The singlet

oxygen generated will therefore be involved in the degradation of 4-Np. As mentioned above, radical ions (Type I mechanism) are also involved in the degradation of 4-Np (Figure 3.24).

As previously stated, the final degradation products that were obtained include FA and 4-NC. Reaction intermediates that were detected include BQ and HQ. FA as the final degradation product for 4-Np is significant since the toxicity of FA is considerably lower than that of 4-Np: the ORAL-RAT LD₅₀ value for 4-Np is 202 mg kg⁻¹, while that of FA is 9 300 mg kg⁻¹.⁹

The proposed mechanism for the phototransformation of 4-Np into FA follows a number of steps. The first step is the interaction of 4-Np with a hydroxyl radical generated from the Type I mechanism to form HQ, followed by the oxidation of HQ by oxygen to form BQ. Further oxidation of BQ leads to the formation of FA (Scheme 3.9). The hydroxyl radical in this reaction mechanism is the reaction initiator. The addition of a hydroxyl radical *ortho* to the phenol functional group of 4-Np results in the formation of the dihydroxynitrocyclohexadienyl radical intermediate, which leads to the formation of 4-NC (Scheme 3.10).¹²

The proposed mechanism for the photodegradation of 4-Np in the presence of water-insoluble photosensitisers via the Type II mechanism will be the same as that described in Scheme 3.8.

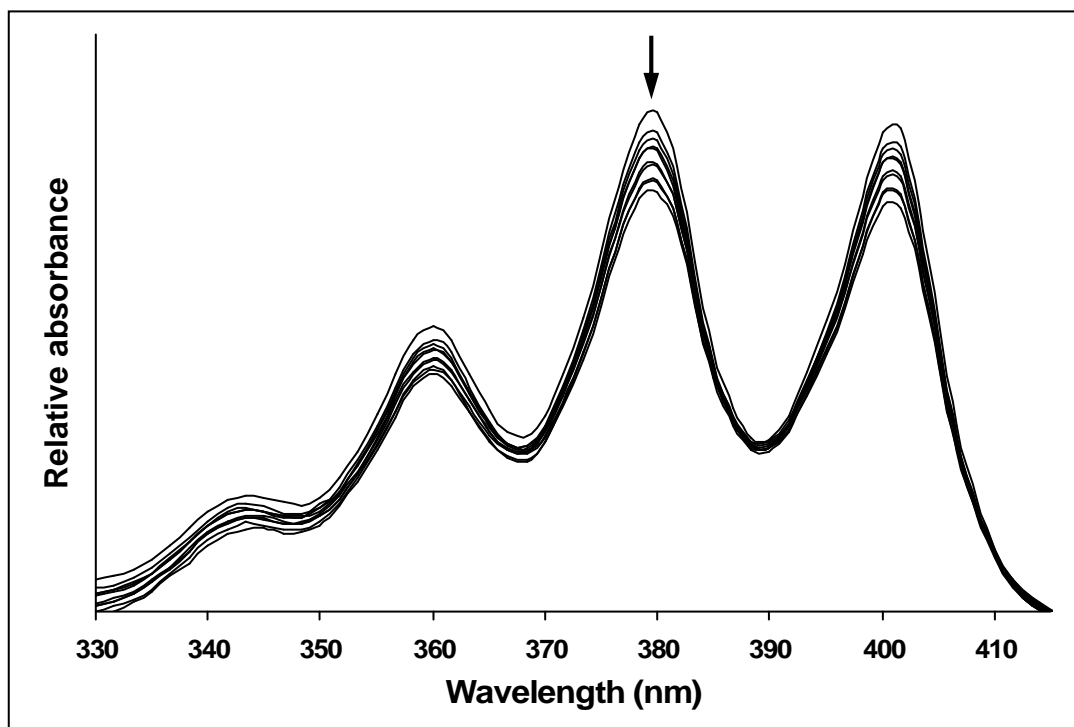
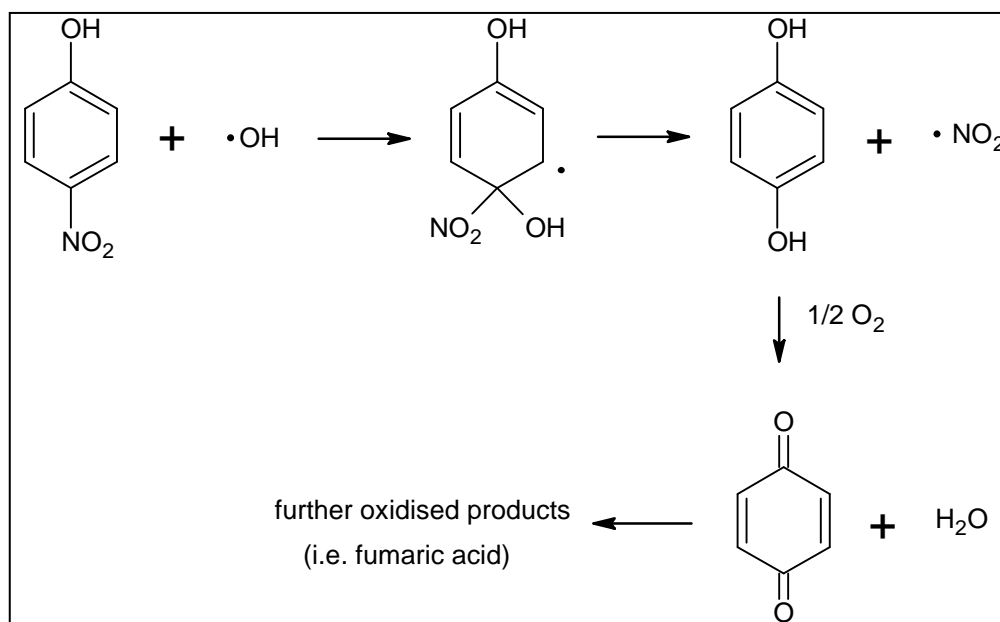
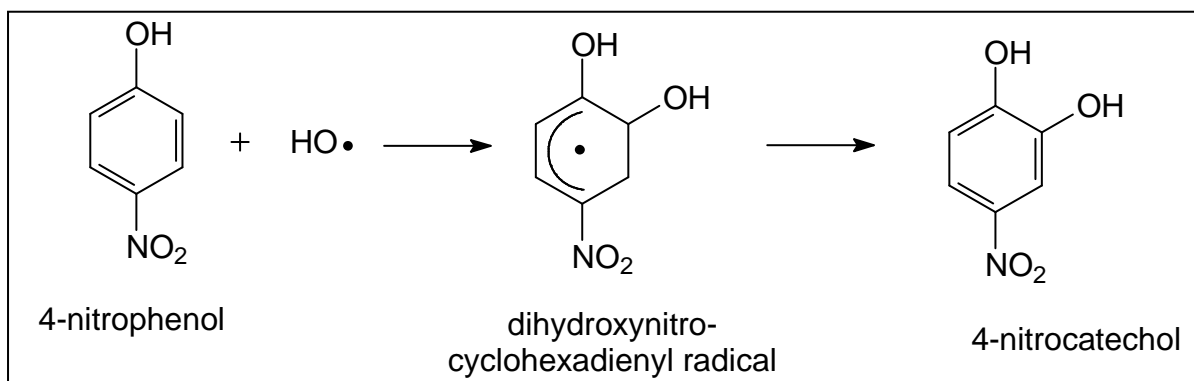


Figure 3.25. Electronic absorption spectral changes of ADMA during its visible light photolysis in the presence of ClAlPc ($[ADMA] = 6.9 \times 10^{-5} \text{ mol dm}^{-3}$).



Scheme 3.9. Proposed mechanism for the phototransformation of 4-Np to BQ and FA in the presence of water-insoluble MPc photocatalysts.¹²



Scheme 3.10. Proposed mechanism for the phototransformation of 4-Np to 4-NC in the presence of water-insoluble MPc photocatalysts.¹²

3.3.4. Practical Application of Water-insoluble MPcs

Due to the successful degradation of 4-Np to a non-aromatic, less toxic species (i.e. fumaric acid), the water-insoluble metallophthalocyanines were considered for the degradation of methyl paraoxon, a non-systemic insecticide.⁸ The most effective MPc employed for the degradation of 4-Np, namely ClAlPc, was selected for the photocatalysis of methyl paraoxon. The photocatalytic reaction proceeded for 100 min using the setup illustrated in Figure 2.2. Complete conversion of methyl paraoxon resulted from its photocatalysis in the presence of ClAlPc (Figure 3.26). Using LC/MS, it was determined that the major degradation product of methyl paraoxon is 4-nitrocatechol, as a molecular ion peak was obtained at $m/z = 157.8$ amu using ESI-MS.

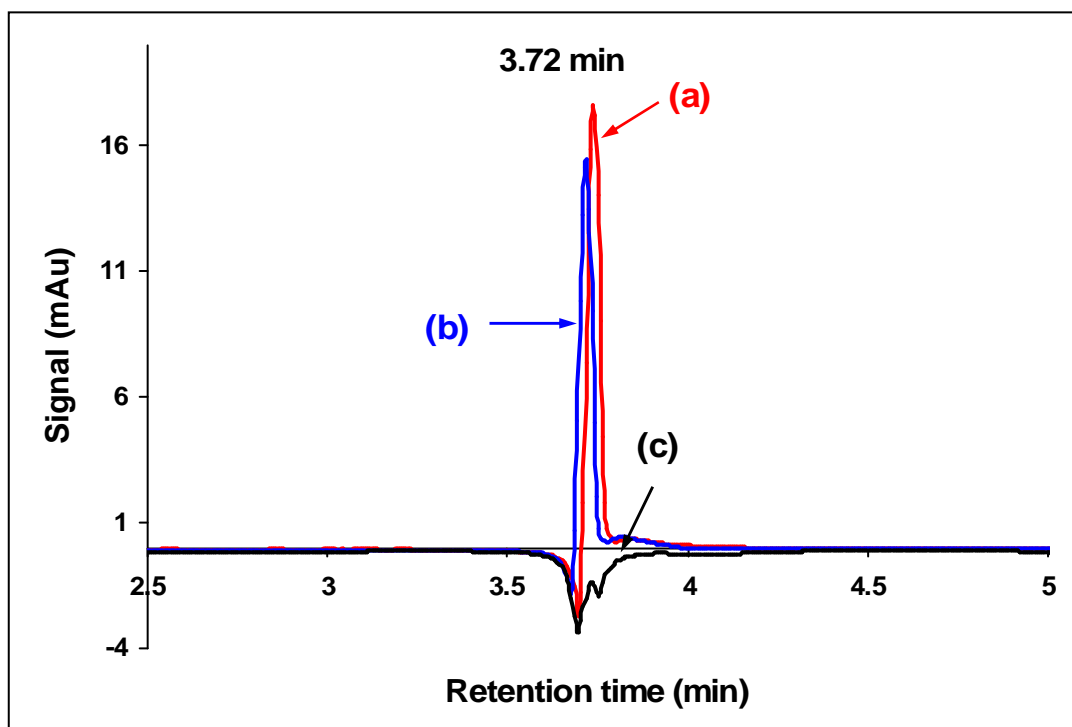


Figure 3.26. HPLC traces of 1.0×10^{-5} mol dm $^{-3}$ methyl paraoxon solution (a) before photocatalysis, (b) after photocatalysis in the absence of ClAlPc, and (c) after photocatalysis in the presence of ClAlPc, pH = 9.

3.4. Adsorption of 4-Np onto Amberlite[®] IRA-900 Modified with MPcs

As was previously mentioned, improved photostability of MPcs with anionic substituents can be achieved by immobilisation of these MPcs onto cationic resins such as Amberlite[®] IRA-900.⁴⁸ It is also possible to employ cationic resins for the isolation of the photocatalyst for reuse after degradation of the substrate. MPcS_{mix} or MPcS₄ complexes can be immobilised onto the aforementioned resin using the method detailed in Section 2.6.

The resin used in this work, i.e. Amberlite[®] IRA-900 ion-exchange resin, is a strongly basic, macroreticular resin of moderately high porosity with benzyltrialkylammonium functionality. The solvent mixture of acetonitrile:water, which was employed as the solvent for immobilising the MPcS complexes, was chosen so as to ensure that sulphonated MPc complexes are in their

monomeric state in solution, since these complexes are notoriously aggregated in aqueous media and organic solvents break the aggregates.²⁹ The concentration of MPc immobilised onto the resin was calculated by measuring the decrease in absorbance of the Q band following immobilisation onto a known amount of resin. Figure 3.27 shows the decrease in absorbance of CoPcS_{mix} (as an example) during its immobilisation onto the resin.

Initially attempts were made to degrade 4-Np in the presence of immobilised ZnPc complexes (i.e. ZnPcS_{mix}, ZnPcS₄, ZnPc(COOH)₈), using visible light. However, on addition of the modified resin to a solution of 4-Np rapid adsorption of 4-Np onto the modified surface occurred (Figure 3.28), due to the interaction between the negatively-charged oxygen on the nitro group of 4-Np and the positively-charged ammonium groups on the Amberlite[®] resin. Due to adsorption of the substrate onto the resin the degradation process cannot be monitored and the degradation products cannot be determined. A similar study involving the degradation of chlorophenols using immobilised sulphonated and carboxylated Pcs on Amberlite[®] IRA-900 was a viable study as there was minimal adsorption of the substrate onto the modified resin.⁵⁴

The immobilisation of a negatively-charged MPc onto an ion-exchange resin was explored further, by testing numerous resins available in the laboratory. There is limited information available for the many resins that were used, and as a result a “trial and error” approach was adopted. The resins were subjected to eliminative tests in an effort to obtain the most effective resin. Resins were first placed in a solution of 1.0×10^{-4} mol dm⁻³ 4-Np. Resins that did not adsorb 4-Np onto their surface were then tested to determine whether they were able to immobilise the photocatalyst (ZnPcS_{mix} in this case). Those that successfully interacted with the photocatalyst were then tested to assess their photostability on exposure to visible light. The results obtained from the series of tests are summarized in Table 3.8.

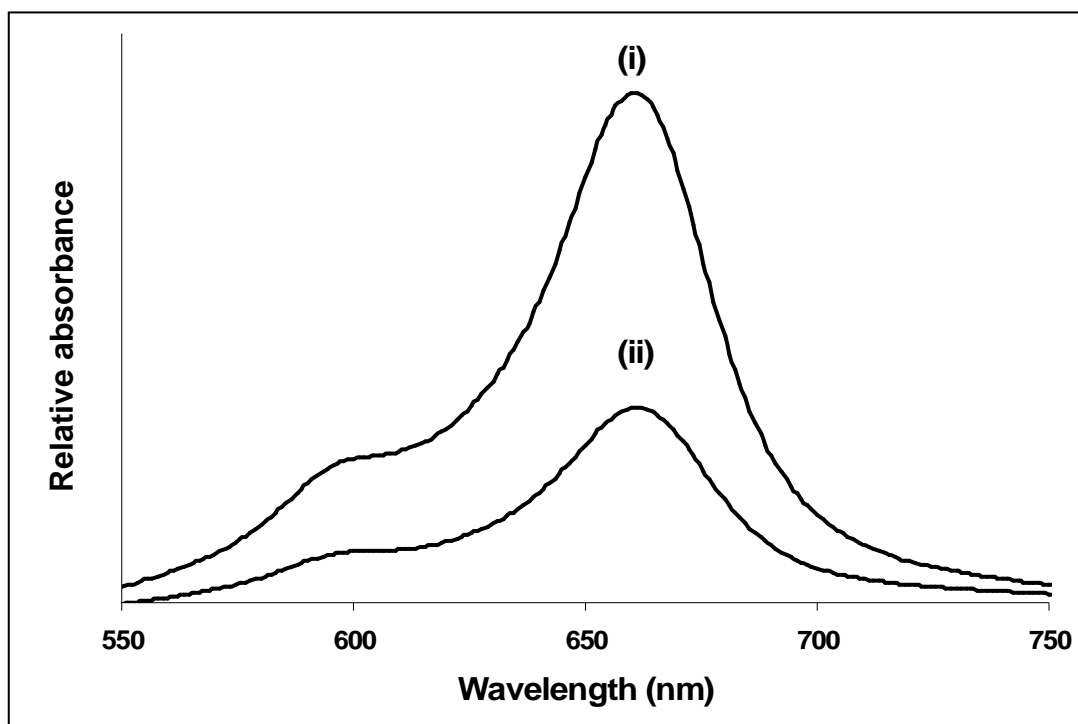


Figure 3.27. Electronic spectral changes with time during the immobilisation of $\text{CoPcS}_{\text{mix}}$ onto Amberlite[®] IRA-900 resin in a mixture of 1:1 $\text{CH}_3\text{CN}:\text{H}_2\text{O}$. Starting concentration of $\text{CoPcS}_{\text{mix}} = 2.5 \times 10^{-5} \text{ mol dm}^{-3}$. Mass of resin = 1.0 g. (i) 0 min, and (ii) 15 min of immobilisation.

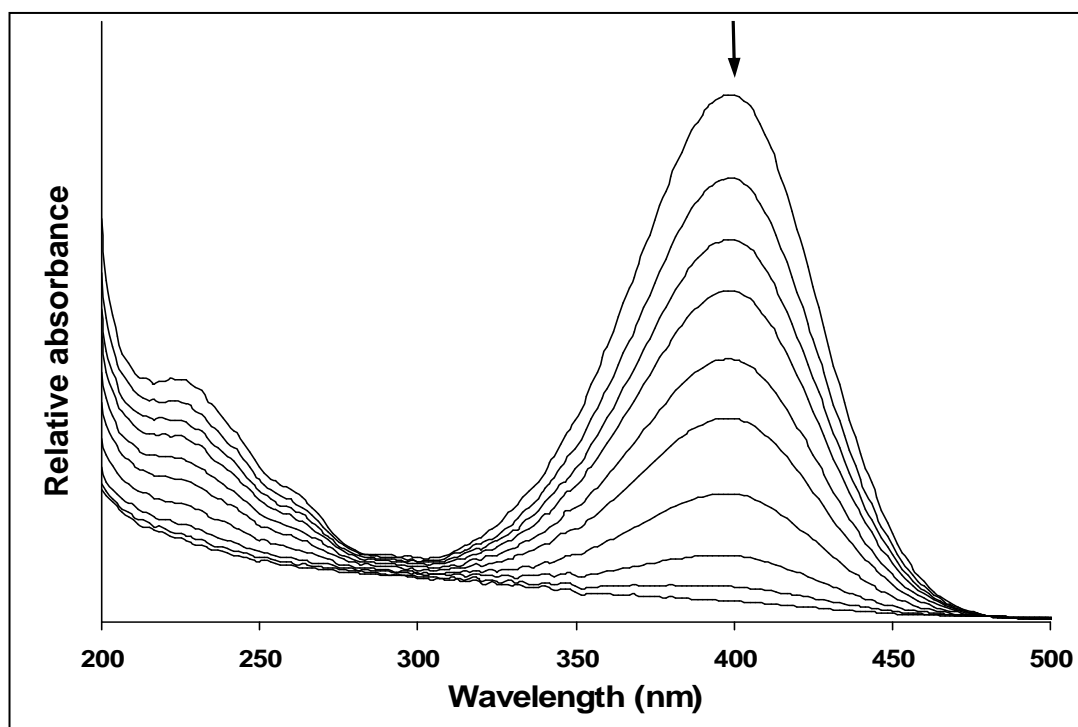


Figure 3.28. Adsorption of 4-Np onto Amberlite[®] IRA-900 modified with $\text{ZnPcS}_{\text{mix}}$. ($[\text{4-Np}] = 1.0 \times 10^{-4} \text{ mol dm}^{-3}$, $\text{pH} = 8.2$).

Table 3.8. Effect of selected resins on the adsorption of 4-Np and immobilisation of ZnPcS_{mix}.

Resin	Adsorbs 4-Np	Immobilises ZnPcS _{mix}
Amberlite MB-3	X	–
Amberlyst 15	X	–
Amberlyst A26	✓	–
Dowex 1-X	✓	–
Amberlite IR-120	X	X
Amberlite IRA-93	✓	–
Amberlite IRA-400	✓	–
Amberlite CG-50	✓	–
Amberlite IR-100-H	X	X
Amberlite XAD-7	X	✓
Amberlite XAD-11	X	✓
Amberlite XE-268	✓	–
Zeo-Karb 225	X	X

Amberlite MB-3 and Amberlyst 15 were not tested for their ability to immobilise ZnPcS_{mix} as these resins are acidic and led to the formation of protonated 4-Np (ArOH), which reacts poorly with singlet oxygen. Two resins, namely Amberlite XAD-7 and Amberlite XAD-11, were successful in immobilising the photocatalyst without adsorbing 4-Np onto their surface, however, the photocatalyst on the surface of each resin was photocatalytically unstable. The degradation of the photocatalyst on exposure to visible light was evident from a change in colour of the surface of the modified resin from blue/green due to the immobilised MPc to the original colour of the bare resin. The degradation of ZnPcS_{mix} was possibly due to weak interactions between the resin and the photocatalyst, when compared with the relatively strong electrostatic interaction that occurs between Amberlite[®] IRA-900 and ZnPcS_{mix} (Figure 1.8).

The rapid adsorption of 4-Np onto the surface of Amberlite[®] IRA-900, which was unsuccessful in improving the stability of the ZnPc complexes for the photodegradation of 4-Np, was exploited in this study in order to determine the effect of modifying the surface of Amberlite[®]

IRA-900 with MPcS_4 and MPcS_{mix} complexes on the rate of adsorption of 4-Np. The metals used for the MPcS_4 and MPcS_{mix} complexes include Fe, Co and Ni. For these studies photocatalysis was not important, but axial ligation could be useful, therefore MPc derivatives chosen include CoPc and FePc which readily coordinate ligands,²⁹ but are photochemically inactive. NiPc was included for comparison even though it does not form axially-ligated complexes.

The diffuse reflectance UV-vis spectra, Figure 3.29, for the six modified Amberlite® IRA-900 adsorbents were obtained in order to verify immobilisation of the MPcs and qualitatively determine the relationship between the monomeric and dimeric species of each MPc on attachment to the resin. The broadness of the Q bands in Figure 3.29 is due to Davydov splitting, a phenomenon that hinders good resolution of the Q band when the MPc is characterised in its solid state.⁸⁵ In general, dimerisation or aggregation is apparent from the presence of a high-energy band near 620 nm (for NiPc and CoPc derivatives) and near 640 nm (for FePc derivatives). The low-energy band at 670 nm or higher is due to the monomeric species.^{29,75} Figure 3.29 (a) shows that FePcS_4 immobilised onto Amberlite® IRA-900 is aggregated as evidenced by a peak at 641 nm, with a small amount present in the monomeric form. $\text{FePcS}_{\text{mix}}$ is adsorbed in its monomeric form, where the broadness of the Q band is due to Davydov splitting. Both the NiPcS and CoPcS complexes in Figure 3.29 (b) and (c), respectively, are immobilised in the monomeric form, with a small degree of aggregation occurring in all cases. The similarities in the reflectance spectra of $\text{NiPcS}_{\text{mix}}$ and NiPcS_4 are not surprising considering the HPLC results discussed in Section 3.1.4, which showed a predominance of the NiPcS_4 isomer for $\text{NiPcS}_{\text{mix}}$. $\text{CoPcS}_{\text{mix}}$ and CoPcS_4 also have similar reflectance spectra even though the HPLC traces showed that the latter is not the only component of the former. The effect of increasing the amount of FePcS_4 loaded onto Amberlite® IRA-900 was determined using diffuse reflectance (Figure 3.30). On increasing the amount of immobilised FePcS_4 there is broadening of the monomer peak accompanied by an increase in its intensity relative to the dimer.

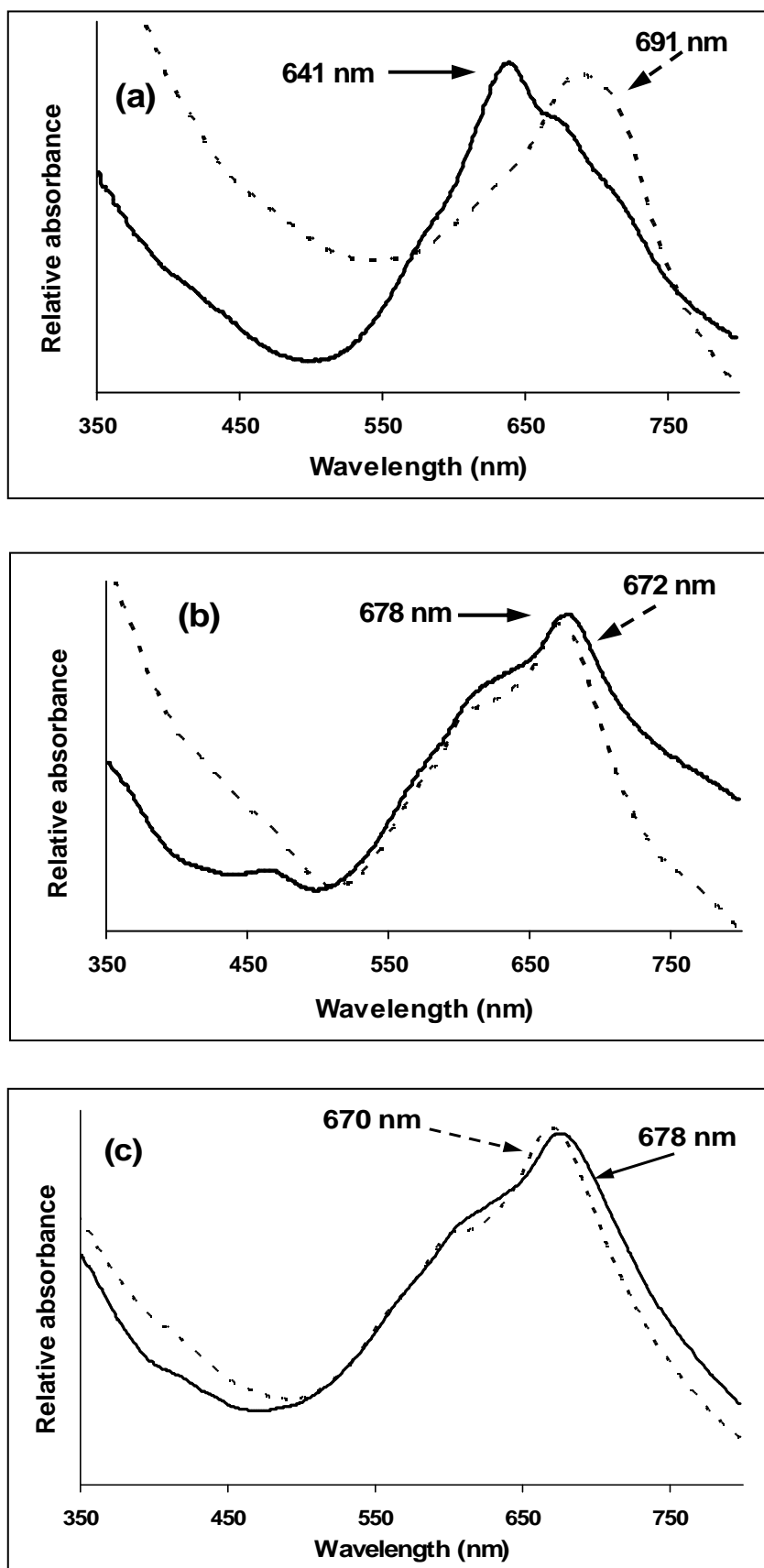


Figure 3.29. Diffuse reflectance spectra of (a) FePcS, (b) NiPcS, and (c) CoPcS complexes after immobilisation onto Amberlite® IRA-900. (— MPcS_4 , ----- MPcS_{mix}).

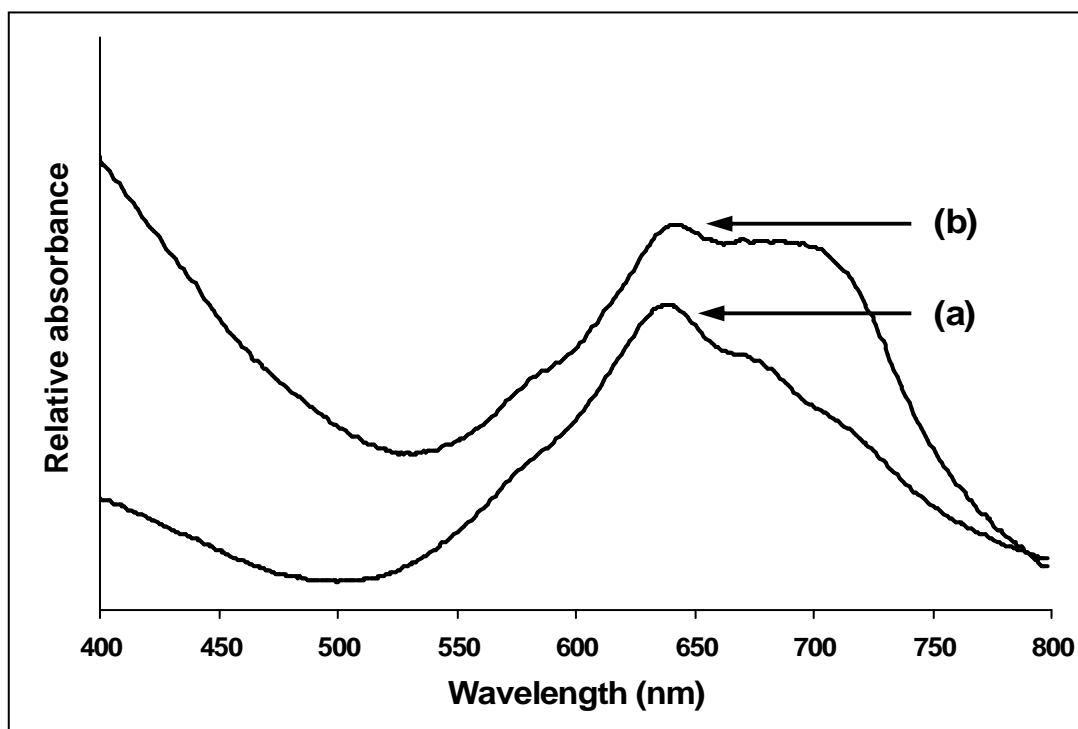


Figure 3.30. Diffuse reflectance spectra of FePcS₄-Amb showing the effect of increasing the amount of immobilised FePcS₄. (a) 1×10^{-5} , and (b) 3×10^{-5} mol FePcS₄/g Amb.

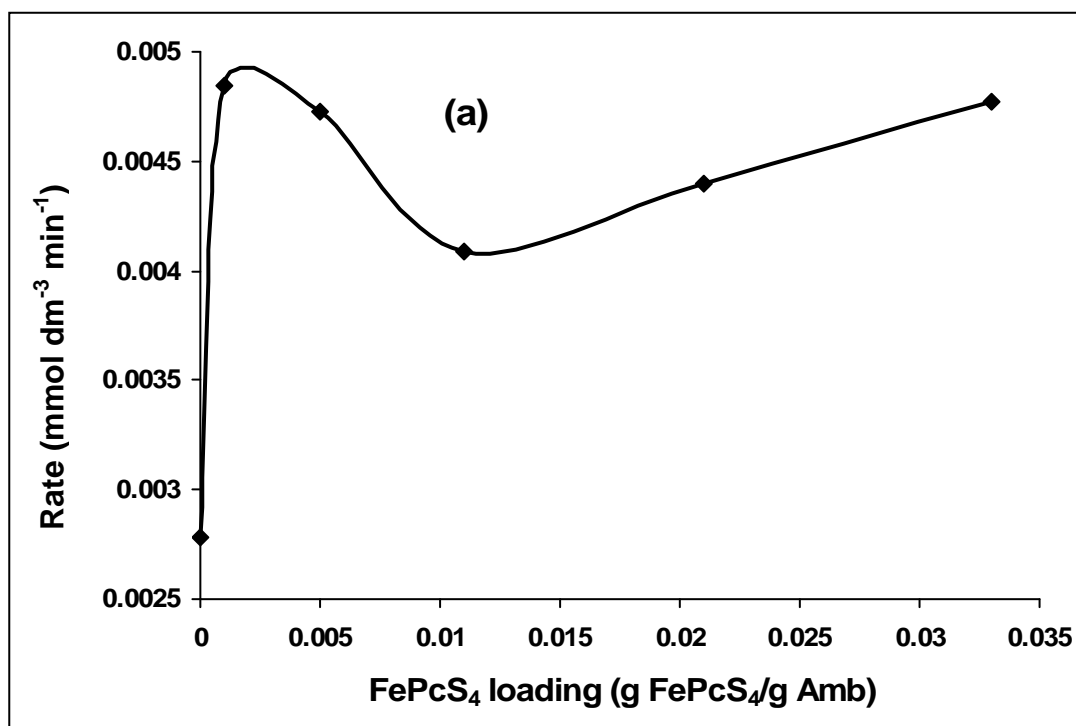
3.4.1. Optimisation of MPc Loading and pH of 4-Np Solution

FePcS₄ was employed as an example for these studies. The spectral changes observed during the adsorption of 4-Np onto FePcS₄-Amb are similar to that shown in Figure 3.28. Similar spectral changes were observed on other MPc-Amb resins and on bare Amberlite[®] IRA-900. The adsorption of 1.0×10^{-4} mol dm⁻³ 4-Np onto bare Amberlite[®] IRA-900 was compared with that obtained when the same concentration of 4-Np was adsorbed onto FePcS₄-Amb adsorbent. The rates were 2.8×10^{-6} and 4.1×10^{-6} mol dm⁻³ min⁻¹, respectively for bare Amberlite[®] IRA-900 and FePcS₄-Amb, showing an almost two-fold increase in 4-Np adsorbed on MPc-modified Amberlite[®] IRA-900.

The optimum loading of the MPc complexes onto Amberlite[®] IRA-900 was established by determining the rate of 4-Np adsorption with various loadings of FePcS₄ (Figure 3.31a). Rate

studies were not carried out on resins modified with loadings greater than 3×10^{-2} g FePcS₄/g Amb, as the immobilisation of FePcS₄ became time-consuming, i.e. 3-4 days above the aforementioned loading. A loading of 1×10^{-3} g FePcS₄/g Amb gave the highest rate of adsorption compared with the other loadings in Figure 3.31a. This loading was then employed for further studies and for all the MPc complexes under investigation. There was a decrease in the rate of 4-Np adsorption going from 1×10^{-3} to 1×10^{-2} g FePcS₄/g Amb, followed by a rise in adsorption rate of 4-Np after the latter loading. The increase in 4-Np adsorption rate beyond 1×10^{-2} g FePcS₄/g Amb may be accounted for by the formation of more than one layer on the resin.

The dependence of the rate of 4-Np adsorption on pH was determined by varying the pH of a 1×10^{-4} mol dm⁻³ solution, Figure 3.31b. The adsorption rate reaches a maximum after pH 9, which correlates with the pH at which 4-Np is highly soluble, and the predominant species in solution is the phenolate ion of 4-Np. This pH was employed for all subsequent studies.



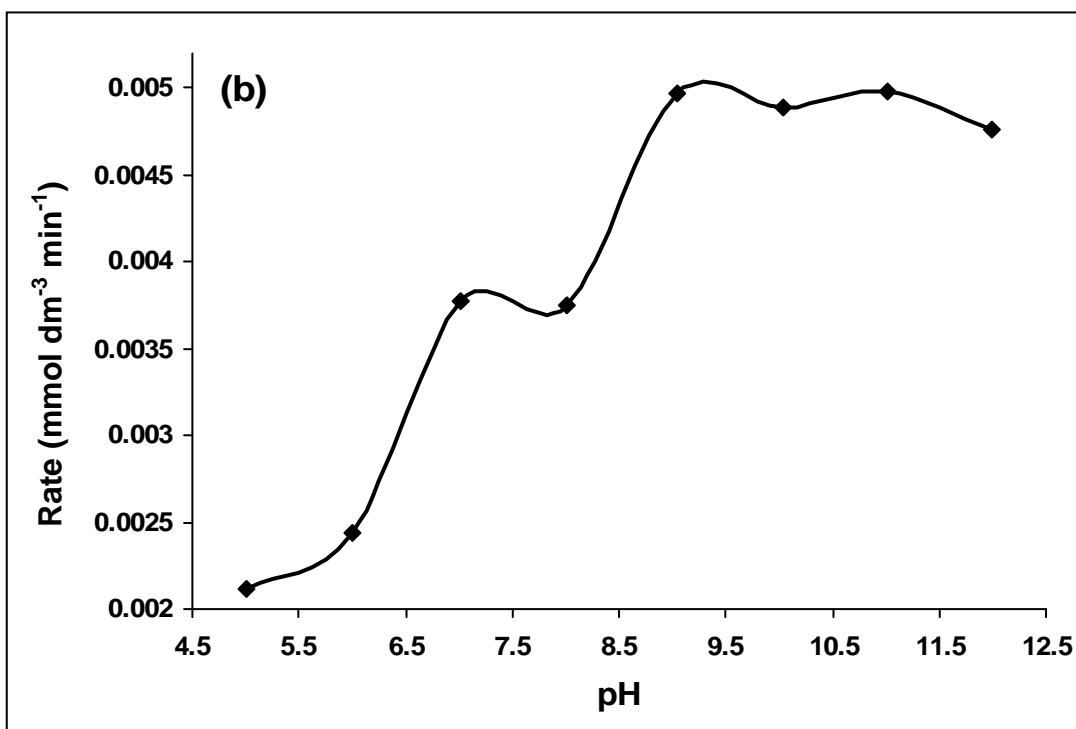


Figure 3.31. (a) Plot of initial adsorption rate versus FePcS₄ loading to determine the optimum amount of FePcS₄ immobilised onto Amberlite[®] IRA-900 for the adsorption of 1.0×10^{-4} mol dm⁻³ 4-Np, pH = 9. (b) Plot of initial adsorption rate versus pH, for the adsorption of 1.0×10^{-4} mol dm⁻³ 4-Np onto 1×10^{-3} g FePcS₄/g Amb.

3.4.2. Comparison of 4-Np Adsorption Rates on MPc-modified Amberlite[®] IRA-900

The rate and amount of 4-Np adsorption was compared for all MPc complexes with a loading of 1×10^{-3} g MPc/g Amb (Figure 3.32). It is evident from Figure 3.32a that the initial rate of 4-Np adsorption is faster for the MPcS₄ complexes than the corresponding MPcS_{mix} complexes. The FePc complexes gave the fastest rate (Figure 3.32a) and highest amount (Figure 3.32b) of adsorbed 4-Np compared with the other MPcs, with the highest rate of adsorption obtained for FePcS₄, and the highest amount of adsorption obtained for FePcS_{mix}. CoPcS_{mix} gave both the lowest amount and rate of 4-Np adsorption.

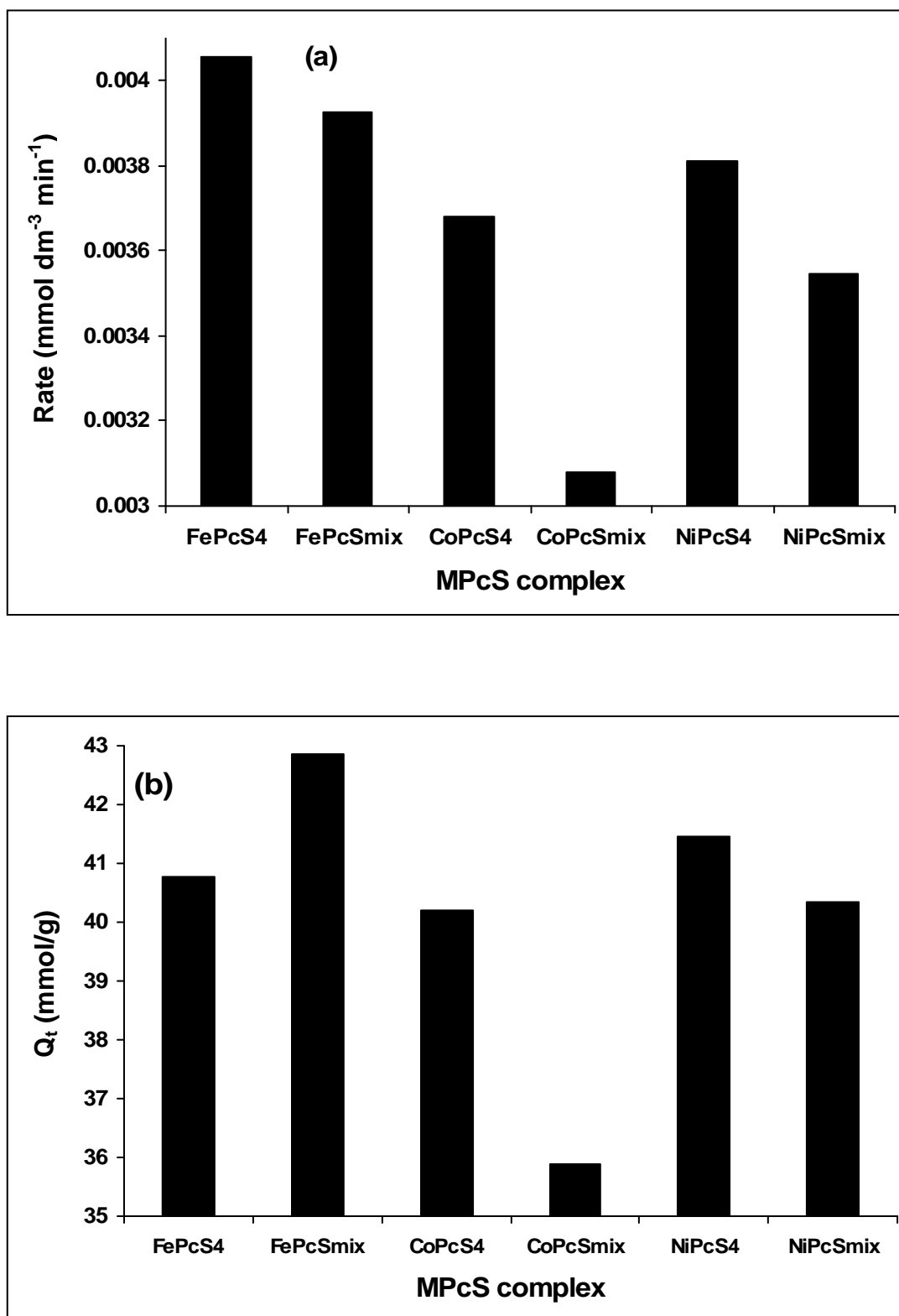


Figure 3.32. Plots of (a) initial rate of 4-Np adsorption and (b) Q_t (time = 30 min) for each MPc complex used to modify Amberlite[®] IRA-900 ($[4\text{-Np}] = 1.0 \times 10^{-4} \text{ mol dm}^{-3}$, pH = 9).

3.4.3. Regeneration of the Modified Resin

These studies were carried out in order to determine whether the resin modified with adsorbed MPc could be used repeatedly for removal of 4-Np. It has been reported that Amberlite XAD-7, a weakly polar polymeric ion-exchange resin, could be regenerated using ethanol as the regenerant for the removal of 4-Np.²⁴ The use of ethanol as a regenerant was unsuccessful in this work. Its ineffectiveness may be due to differences in the interaction of 4-Np with Amberlite XAD-7 compared with modified Amberlite® IRA-900.

The phenolate ion of 4-Np (ArO^-) is relatively stable in solution due to the presence of a *para* nitro group, which results in electron delocalisation⁵ within the complex and the formation of a corresponding quinonoid complex.⁸⁶ The equilibrium that exists between the phenolate ion and the neutral 4-Np species is affected by the pH of the solution. As a result, dilute nitric acid ($1 \times 10^{-3} \text{ mol dm}^{-3}$) was used to regenerate the MPc-modified resin for reuse in 4-Np adsorption. The nitric acid causes a shift in the equilibrium, favouring the formation of the protonated 4-Np species (ArOH), resulting in desorption of 4-Np from the surface of the adsorbent.

The regenerated $\text{FePcS}_4\text{-Amb}$ was reused for further adsorption of $1.0 \times 10^{-4} \text{ mol dm}^{-3}$ 4-Np. The rate of adsorption of 4-Np after regeneration of the resin increased from $4.9 \times 10^{-6} \text{ mol dm}^{-3} \text{ min}^{-1}$ (for original resin) to $6.9 \times 10^{-6} \text{ mol dm}^{-3} \text{ min}^{-1}$ (after the first wash) and $6.1 \times 10^{-6} \text{ mol dm}^{-3} \text{ min}^{-1}$ (after the second wash). Thus, the rate of 4-Np adsorption was increased by a factor of 1.4 and 1.2 after the first and second washing with HNO_3 , respectively, relative to the initial rate of adsorption. The effect of dilute HNO_3 solution on FePcS_4 immobilised on Amberlite® IRA-900 is shown in Figure 3.33. After washing with HNO_3 , FePcS_4 becomes more monomeric, as judged by an increase in the intensity of the low energy band. The presence of a monomeric MPc may account for the increase in 4-Np adsorption, as the metal centre is more readily available to

undergo axial ligation to the negatively-charged phenolate ion, thereby increasing the rate of 4-Np adsorption.

It can be seen from Figure 3.33 that on washing the resin with HNO_3 a new species (with $\lambda_{\text{max}} = 317 \text{ nm}$) with a different spectrum from 4-Np ($\lambda_{\text{max}} = 400 \text{ nm}$) was obtained. In order to determine the nature of the new species, the spectra of 4-Np in acidic and basic media were compared, Figure 3.34a. The spectra matched those observed in Figure 3.33 following washing of 4-Np from MPc-Amb with HNO_3 . Thus the new spectrum with $\lambda_{\text{max}} = 317 \text{ nm}$ is due to the acidic form of 4-Np. The formation of 4-Np increased with immersion time of resin in acid as shown in Figure 3.34b. The absorbance values obtained at 317 nm were used to calculate the percentage 4-Np recovery after 150 minutes of 4-Np desorption (Figure 3.34b, inset). The total amount of 4-Np recovered after using $1 \times 10^{-3} \text{ mol dm}^{-3} \text{ HNO}_3$ for 150 min was 76 %.

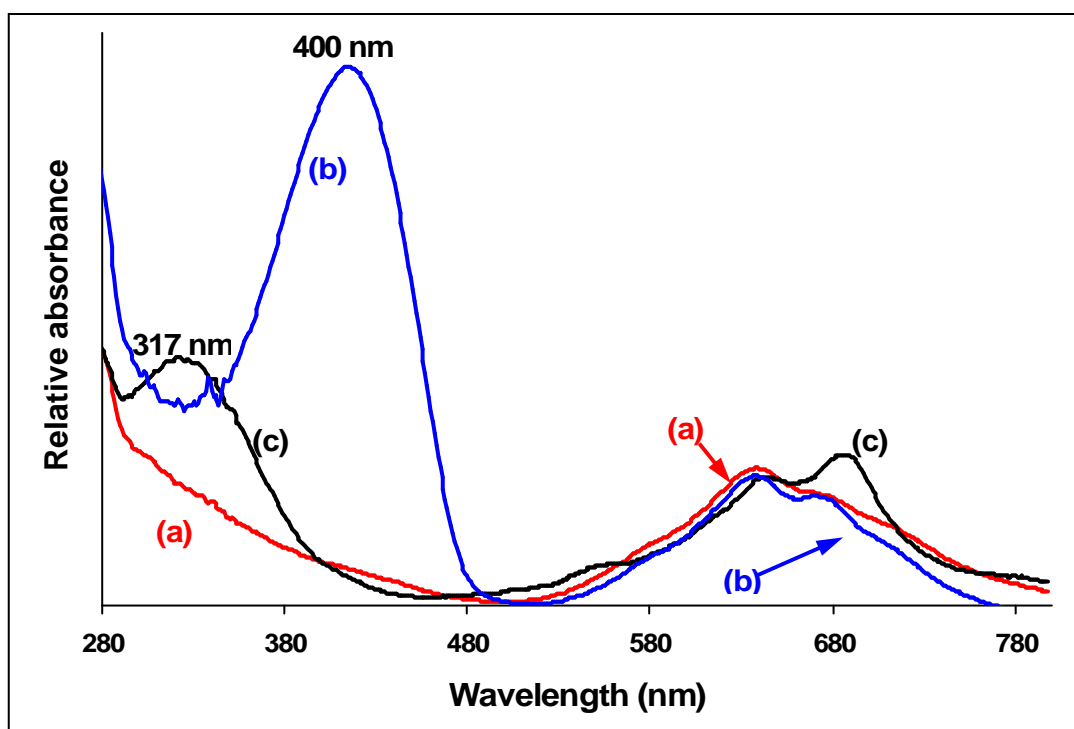


Figure 3.33. Diffuse reflectance spectral changes observed for $\text{FePcS}_4\text{-Amb}$ (a) before adsorption of 4-Np, (b) after adsorption of 4-Np, and (c) following removal of 4-Np from (b) using dilute HNO_3 . $[4\text{-Np}] = 1.0 \times 10^{-4} \text{ mol dm}^{-3}$, $\text{pH} = 9$.

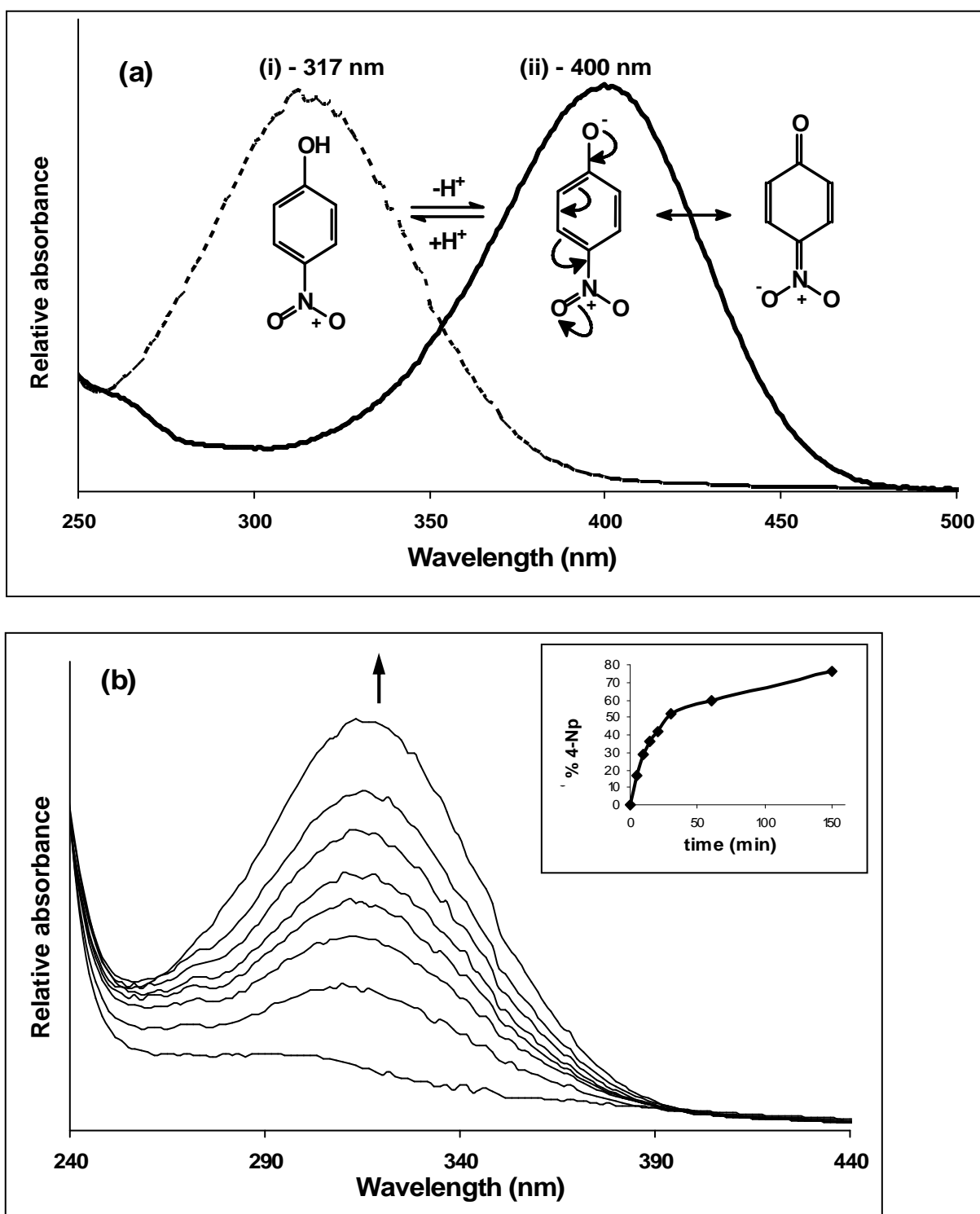
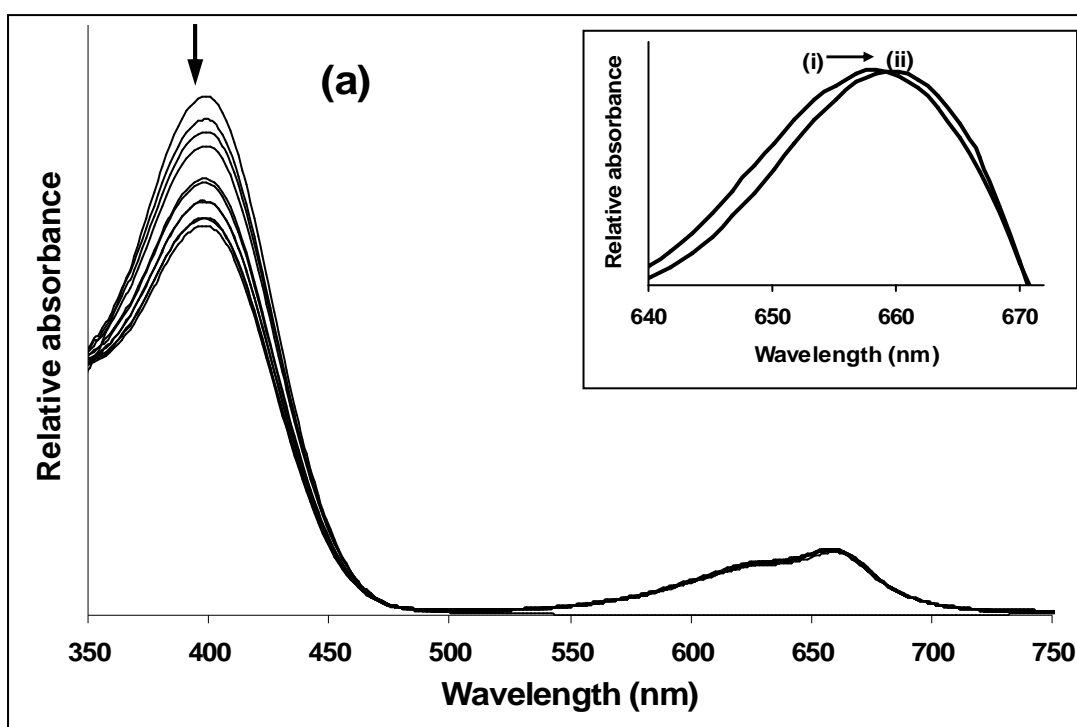


Figure 3.34. Electronic absorption spectra (a) of 4-Np in (i) acidic, and (ii) basic media, and (b) observed with time (total = 150 min) on immersion of $FePcS_4$ -Amb containing 4-Np in HNO_3 . Inset: Percentage 4-Np recovery versus time following immersion of $FePcS_4$ -Amb with adsorbed 4-Np in HNO_3 solution. $[HNO_3] = 1 \times 10^{-3} \text{ mol dm}^{-3}$.

3.4.4. Spectroscopic Study of the Interaction of 4-Np with MPcs

As mentioned previously, possible methods of attachment of 4-Np to the MPc-modified Amberlite[®] IRA-900 resin include π - π interactions with the resin and MPc, and ionic bonds formed between the ammonium groups of Amberlite[®] IRA-900 and the hydroxyl group of 4-Np. Another interaction that is possible is due to axial ligation between the metal centre of the MPc and a phenolate ion, as the metals employed are known to be redox active. The interaction between the MPc metal centre and 4-Np was determined by adding 4-Np to each MPc in aqueous solution and recording the UV-vis spectra with time (Figure 3.35). There was a shift in the wavelength of the Q band for CoPcS₄ and CoPcS_{mix} (Figure 3.35a). Such small changes are associated with axial ligation in MPc complexes.²⁹ An increase in the amount of monomeric species was observed for FePcS₄ and FePcS_{mix} on addition of 4-Np (Figure 3.35b), again suggesting monomerisation due to attachment of axial ligands. There was no change observed for NiPcS₄ and NiPcS_{mix} (figure not shown), merely a degradation of the MPc with time. Therefore, it is hypothesized that the metal centres of both the CoPcS and FePcS species undergo axial ligation to unprotonated 4-Np.



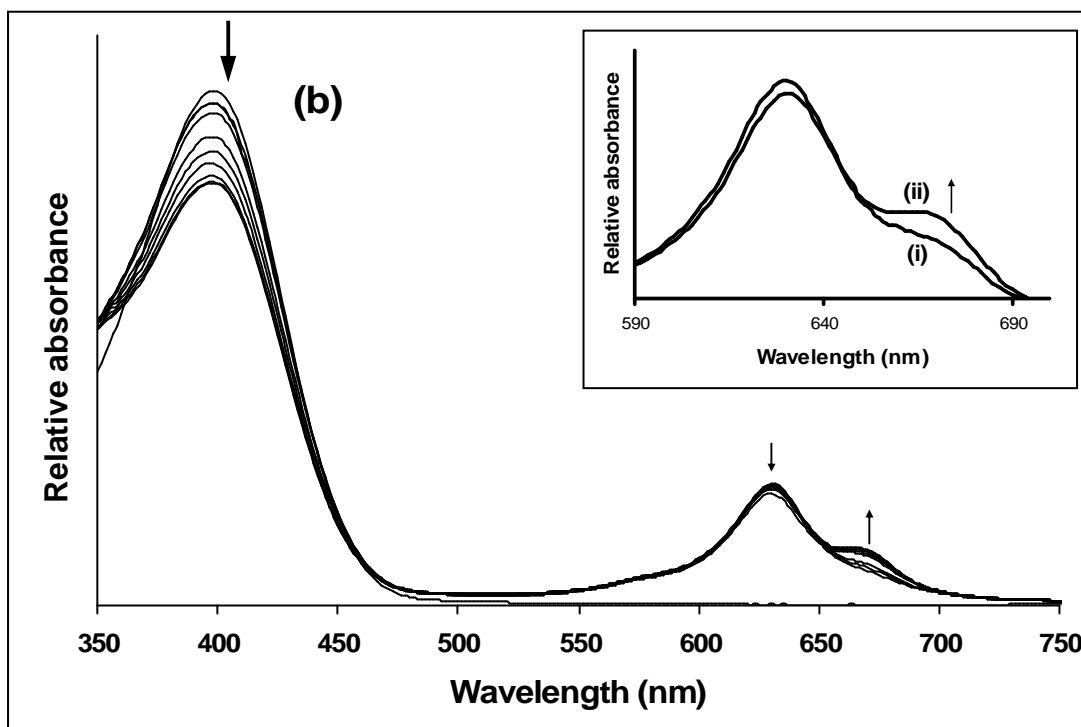


Figure 3.35. Spectral changes of (a) CoPcS₄, and (b) FePcS₄ on addition of $1.0 \times 10^{-4} \text{ mol dm}^{-3}$ 4-Np, pH = 9. (Inset: (i) First, and (ii) last scan obtained for the Q band of (a) CoPcS₄, and (b) FePcS₄ in the presence of 4-Np).

3.4.5. Langmuir-Hinshelwood Kinetic Model (LHKM)

The LHKM model (Eq. (28)) describes the competitive adsorption of substrates, reaction intermediates and phenol oxidant products.^{87,88}

$$\frac{1}{\text{rate}} = \frac{1}{k_r} + \frac{1}{k_r K_{ad} C_{sub}^0} \quad (28)$$

where k_r is the rate constant for the adsorption of 4-Np, C_{sub}^0 is the initial concentration of the substrate (in this case 4-Np). K_{ad} , the adsorption coefficient, represents the equilibrium between the rate of adsorption and desorption of the substrate.⁵¹ Table 3.9 shows the kinetic parameters obtained from the plots of $1/\text{rate}$ versus $1/C_{sub}^0$. A relatively high degree of linearity was

obtained with R^2 values greater than 0.9 for all adsorbents, therefore it can be deduced that the adsorption of 4-Np is dependent on 4-Np concentration. The MPcS complexes adsorbed 4-Np in the following order: (according to the k_r values) $\text{CoPcS}_{\text{mix}} > \text{NiPcS}_4 > \text{NiPcS}_{\text{mix}} > \text{FePcS}_4 > \text{FePcS}_{\text{mix}} > \text{CoPcS}_4$. Adsorption rate (k_r) was lowest for bare Amberlite® IRA-900. The high k_r for the NiPcS complexes shows that axial ligation is not the predominant means of adsorption of 4-Np on MPc-Amb. As expected, adsorption was favoured over desorption, hence K_{ad} was greater than unity in all cases.

Table 3.9. The LHKM parameters obtained for the adsorption of 4-Np onto MPc-Amb adsorbents, $[4\text{-Np}] = 1.0 \times 10^{-4} \text{ mol dm}^{-3}$

Modifier	R^2 value	k_r (min^{-1})	K_{ad} ($\text{mol}^{-1} \text{ L}$)
FePcS ₄	0.9952	7.47×10^{-5}	5.25×10^2
CoPcS ₄	0.9331	5.86×10^{-5}	7.25×10^2
NiPcS ₄	0.9876	1.36×10^{-4}	3.39×10^2
FePcS _{mix}	0.9934	5.88×10^{-5}	7.23×10^2
CoPcS _{mix}	0.9283	7.72×10^{-4}	5.76×10^1
NiPcS _{mix}	0.9362	9.07×10^{-5}	6.24×10^2
Amberlite® IRA-900	0.9249	3.21×10^{-5}	1.06×10^3

4. CONCLUSION

The water-soluble phthalocyanine complexes $\text{ZnPcS}_{\text{mix}}$, ZnPcS_4 and $\text{ZnPc}(\text{COOH})_8$, as well as the water-insoluble complexes (suspended in aqueous solution of 4-Np) MgPc , ClAlPc , ZnPc , $\text{ZnPc}(\text{NO}_2)_4$, $\text{ZnPc}(\text{NH}_2)_4$, ZnPcF_{16} and ZnPcCl_{16} , have been employed for the photocatalytic degradation of 4-Np as homogeneous and heterogeneous photocatalysts, respectively. Of the homogeneous photocatalysts $\text{ZnPcS}_{\text{mix}}$ is most effective with regards to the quantum yield of 4-Np degradation ($\Phi_{4\text{-Np}}$) and the stability of the catalyst. $\text{ZnPc}(\text{COOH})_8$ degrades readily during the catalysis, but has the highest $\Phi_{4\text{-Np}}$ value compared with the other homogeneous photocatalysts. The $\Phi_{4\text{-Np}}$ values were closely related to the singlet oxygen quantum yields (Φ_{Δ}) and aggregation. ClAlPc is the most successful heterogeneous photocatalyst, with $89 \pm 8.4\%$ degradation of 4-Np achieved after 100 min. The lowest percentage degradation was obtained for ZnPcCl_{16} and MgPc . The low degradation yields are due to short triplet lifetimes for both complexes and aggregation and the “heavy-atom” effect in the case of ZnPcCl_{16} . The products of photodegradation of 4-Np were hydroquinone and 4-nitrocatechol for the homogeneous photocatalysts and fumaric acid and 4-nitrocatechol for the heterogeneous photocatalysts. Reaction intermediates detected include hydroquinone and 1,4-benzoquinone for the heterogeneous photocatalysts.

ClAlPc , the most effective photocatalyst for the phototransformation of 4-Np, was successfully employed for the photodegradation of the non-systemic pesticide, methyl paraoxon. Complete degradation of the pesticide was achieved after 100 min of irradiation with visible light.

The chemically modified polymeric adsorbents, MPc-Amb , were employed for the solid phase extraction of 4-Np from aqueous solution. Faster adsorption rates were achieved for the modified MPc-Amb adsorbent compared with bare Amberlite[®] IRA-900, with the fastest rates obtained for

FePcS₄-Amb at pH 9. The resin was regenerated using dilute nitric acid, resulting in 76 % recovery of 4-Np after 150 minutes. MPc-modified Amberlite[®] IRA-900 can be effectively applied as an adsorbent for the removal and recovery of 4-Np from aqueous solution.

5. REFERENCES

1. P. Patnik, in: *Handbook of Environmental Analysis*, CRC Press, Boca Rotan, 1997, p.199-220.
2. US Environmental Protection Agency, *Nitrophenols, Ambient Water Quality Criteria*, USEPA, Washington, DC, 1980.
3. M. Nakagawa, D. G. Crosby, *J. Agr. Food Chem.* **22** (1974) 849-853.
4. T-S. Kim, J-K. Kim, K. Choi, M. K. Stenstrom, K-D. Zoh, *Chemosphere*, **62** (2006) 926-933.
5. F. A. Carey, *Organic Chemistry*, 4th ed., McGraw-Hill, New York, 2000, p. 945.
6. O. A. O'Connor, L. Y. Young, *Environ. Toxicol. Chem.* **8** (1989) 853-862.
7. D. F. Ollis, E. Pellizzetti, N. Serpone, in: *Photocatalysis - Fundamentals and Applications*, ed. N. Serpone and E. Pellizzetti, Wiley, Chichester, 1989, p.603-637.
8. T. R. Fukuto, *Environ. Health Perspec.* **87** (1990) 245-254.
9. Sigma-Aldrich, Material Safety Data Sheet, Version 1.4-1.6, 2006-2007.
10. A. M. Volodin, *Catal. Today*, **58** (2000) 103-114.
11. V. Maurino, C. Minero, E. Pelizzetti, P. Piccinini, N. Serpone, H. Hidaka, *J. Photochem. Photobiol. A: Chem.* **109** (1997) 171-176.
12. A. Di Paola, V. Augugliaro, L. Palmisano, G. Pantaleo, E. Savinov, *J. Photochem. Photobiol. A: Chem.* **155** (2003) 207-214.
13. G. Mele, R. Del Sole, G. Vasapollo, E. García-López, L. Palmisano, M. Schiavello, *J. Catal.* **217** (2003) 334-342.
14. E. Lipczynska-Kochany, *Chemosphere*, **24** (1992) 1369-1380.
15. A. Alif, P. Boule, *J. Photochem. Photobiol. A: Chem.* **59** (1991) 357-367.
16. K-H. Wang, Y-S. Hsieh, L-J. Chen, *J. Hazard. Mater.* **59** (1998) 251-260.
17. M. S. Dieckmann, K. A. Gray, *Wat. Res.* **30** (1996) 1169-1183.
18. M. Zhou, L. Lei, *Chemosphere*, **63** (2006) 1032-1040.
19. X. Zhang, A. Li, Z. Jiang, Q. Zhang, *J. Hazard. Mater.* **B137** (2006) 1115-1122.
20. W. Zhang, J. Chen, B. Pan, Q. Zhang, B. Zhang, F. Wang, *Chin. J. Pol. Sci.* **23** (2005) 441-447.
21. M-W. Jung, K-P. Kim, B-Y. Cho, I. R. Paeng, D. W. Lee, Y. Hun Park, K-J. Paeng, *Bull. Korean Chem. Soc.* **27** (2006) 77-81.

22. M. Carmona, A. De Lucas, J. L. Valverde, B. Velasco, J. F. Rodríguez, *Chem. Eng. J.* **117** (2006) 155-160.
23. Z. W. Ming, C. J. Long, P. B. Cai, Z. Q. Xing, B. Zhang, *J. Hazard. Mater.* **B128** (2006) 123-129.
24. E. H. Crook, R. P. McDonnell, J. T. McNulty, *Ind. Eng. Chem., Prod. Res. Dev.* **14** (1975) 113-118.
25. V. V. Azanova, J. Hradil, *Reac. Func. Pol.* **41** (1999) 163-175.
26. P. Gregory, *J. Porphyrins Phthalocyanines*, **3** (1999) 468-476.
27. T. Torres, *J. Porphyrins Phthalocyanines* **4** (2000) 325-330.
28. T. Nyokong, H. Isago, *J. Porphyrins Phthalocyanines* **8** (2004) 1083-1090.
29. M. J. Stillman, T. Nyokong, in: *Phthalocyanines: Properties and Applications*, Vol. 1, ed. C. C. Leznoff, A. B. P. Lever, VCH, New York, 1989, p.139-247.
30. M. C. DeRosa, R. J. Crutchley, *Coord. Chem. Rev.* **233-234** (2002) 351-371.
31. T. Nyokong, *Coord. Chem. Rev.* **251** (2007) 1707-1722.
32. C. C. Leznoff, in: *Phthalocyanines: Properties and Applications*, ed. C. C. Leznoff, A. B. P. Lever, VCH, New York, 1989, p.1-54.
33. A. Shaabani, *J. Chem. Res. (S)* (1998) 672-673.
34. M. D. Maree, T. Nyokong, *J. Chem. Res. (S)* (2001) 68-69.
35. M. Sommerauer, C. Rager, M. Hanack, *J. Am. Chem. Soc.* **118** (1996) 10085-10093.
36. E. H. Huntress, R. L. Shriner, *Org. Syn. Coll.* **2** (1943) 459.
37. W. J. Kroenke, M. E. Kenney, *Inorg. Chem.* **3** (1964) 696-698.
38. H. F. Shurvell, L. Pinzuti, *Can. J. Chem.* **44** (1966) 125-136.
39. V. Balzani, V. Carassiti, *Photochemistry of Coordination Compounds*, Academic Press, London, 1970, p. 8, 10.
40. J. G. Calvert, J. N. Pitts, *Photochemistry*, John Wiley, New York, 1967, p. 258-259, 285.
41. R. Bonnett, *Chemical Aspects of Photodynamic Therapy*, Gordon and Breach, London, 2000, p. 70-74.
42. R. Gerdes, D. Wöhrle, W. Spiller, G. Schneider, G. Schnurpfeil, G. Schulz-Ekloff, *J. Photochem. Photobiol. A: Chem.* **111** (1997) 65-74.
43. A. Gilbert, J. E. Baggott, *Essentials of Molecular Photochemistry*, Blackwell Scientific, Oxford, 1991, p. 8-9, 32, 100-101.

44. D. F. Shriver, P. W. Atkins, *Inorganic Chemistry*, 3rd ed., Oxford University Press, New York, 1999, p. 228, 438, 439, 450, 452.
45. F. E. Mabbs, D. J. Machin, *Magnetism and Transition Metal Complexes*, Chapman & Hall, London, 1973, p. 28.
46. G. Ferraudi, in: *Phthalocyanines: Properties and Applications*, Vol. 1, ed. C. C. Leznoff, A. B. P. Lever, VCH, New York, 1989, p.291-340.
47. I. J. MacDonald, T. J. Dougherty, *J. Porphyrins Phthalocyanines*, **5** (2001) 105-129.
48. D. Wöhrle, O. Suvorova, R. Gerdes, O. Bartels, L. Lapok, N. Baziakina, S. Makarov, A. Slodek, *J. Porphyrins Phthalocyanines*, **8** (2004) 1020-1041.
49. G. Schnurpfeil, A. K. Sobbi, W. Spiller, H. Kliesch, D. Wöhrle, *J. Porphyrins Phthalocyanines*, **1** (1997) 159-167.
50. X-F. Zhang, H-J. Xu, *J. Chem. Soc. Faraday Trans.* **89** (1993) 3347-3351.
51. A. Ogunsipe, J-Y. Chen, T. Nyokong, *New J. Chem.* **28** (2004) 822-827.
52. J. R. Darwent, P. Douglas, A. Harriman, G. Porter, M-C. Richoux, *Coordin. Chem. Rev.* **44** (1982) 83-126.
53. K. J. Laidler, J. H. Meiser, B. C. Sanctuary, *Physical Chemistry*, 4th ed., Houghton Mifflin, Boston, 2003, p. 553.
54. B. Agboola, K. I. Ozoemena, T. Nyokong, *J. Mol. Catal. A: Chem.* **248** (2006) 84-92.
55. K. Ozoemena, N. Kuznetsova, T. Nyokong, *J. Photochem. Photobiol. A: Chem.* **139** (2001) 217-224.
56. K. Ozoemena, N. Kuznetsova, T. Nyokong, *J. Mol. Catal. A: Chem.* **176** (2001) 29-40.
57. Z. Xiong, Y. Xu, L. Zhu, J. Zhao, *Environ. Sci. Technol.* **39** (2005) 651-657.
58. K. Kasuga, T. Miyazako, T. Sugimori, M. Handa, *Inorg. Chem. Commun.* **6** (2003) 807-809.
59. V. Iliev, A. Mihaylova, L. Bilyarska, *J. Mol. Catal. A: Chem.* **184** (2002) 121-130.
60. H. Tomoda, S. Saito, S. Shiraishi, *Chem. Lett.* **12** (1983) 313-316.
61. I. Seotsanyana-Mokhosi, N. Kuznetsova, T. Nyokong, *J. Photochem. Photobiol. A: Chem.* **140** (2001) 215-222.
62. S. Y. Egorov, V. F. Kamalov, N. I. Koroteev, A. A. Krasnovsky, B. N. Toleutaev, S. V. Zinukov, *Chem. Phys. Lett.* **163** (1989) 421-424.
63. L. D. Rollman, R. T. Iwamoto, *J. Am. Chem. Soc.* **90** (1968) 1455-1463.
64. J. H. Weber, D. H. Busch, *Inorg. Chem.* **4** (1965) 469-471.

-
65. M. Ambroz, A. Beeby, A. J. MacRobert, M. S. C. Simpson, R. K. Svensen, D. Phillips, *J. Photochem. Photobiol. B: Biol.* **9** (1991) 87-95.
66. K. Sakamoto, E. Ohno, *Prog. Org. Coat.* **31** (1997) 139-145.
67. B. N. Achar, G. M. Fohlen, J. A. Parker, J. Keshavayya, *Polyhedron*, **6** (1987) 1463-1467.
68. J. Metz, O. Schneider, M. Hanack, *Inorg. Chem.* **23** (1984) 1065-1071.
69. R. Decréau, M-J. Richard, M. Julliard, *J. Porphyrins Phthalocyanines*, **5** (2001) 390-396.
70. B. Schöllhorn, J. P. Germain, A. Pauly, C. Maleysson, J. P. Blanc, *Thin Solid Films*, **326** (1998) 245-250.
71. M. N. Golovin, P. Seymour, K. Jayaraj, Y. Fu, A. B. P. Lever, *Inorg. Chem.* **29** (1990) 1719-1727.
72. R. Decréau, M. Chanon, M. Julliard, *Inorg. Chim. Acta*, **293** (1999) 80-87.
73. E.N. Abel, J.M. Pratt, R. Whelan, *J.C.S. Dalton* (1976) 509-514.
74. R. Edrei, V. Gottfried, J.E. Van Lier, S. Kimel, *J. Porphyrins Phthalocyanines* **2** (1998) 191-199.
75. N. Grootboom, T. Nyokong, *J. Mol. Catal. A: Chem.* **179** (2002) 113-123.
76. S. M. Bishop, B. J. Khoo, A. J. MacRobert, M. S. C. Simpson, D. Phillips, A. Beeby, *J. Chrom.* **646** (1993) 345-350.
77. W-S Chan, N. Brasseur, C. La Madeleine, R. Ouellet, J .E. van Lier, *Eur. J. Cancer*, **33** (1997) 1855-1859.
78. A. Ogunsipe, T. Nyokong, *J. Photochem. Photobiol. A: Chem.* **173** (2005) 211-220.
79. M. M. Fickling, A. Fischer, B. R. Mann, J. Packer, J. Vaughan, *J. Am. Chem. Soc.* **81** (1959) 4226-4230.
80. M. Idowu, A. Ogunsipe, T. Nyokong, *Spectrochim. Acta A: Mol. Biomol. Spectros.* (2007), *In Press, Corrected Proof*.
81. R. S. Shukla, A. Robert, B. Meunier, *J. Mol. Catal. A: Chem.* **113** (1996) 45-49.
82. P. Tau, A. O. Ogunsipe, S. Maree, M. D. Maree, T. Nyokong, *J. Porphyrins Phthalocyanines*, **7** (2003) 439-446.
83. J. M. Birchall, R. N. Haszeldine, J. O. Morley, *J. Chem. Soc. (C)* (1970) 2667-2672.
84. N. A. Kuznetsova, N. S. Gretsova, O. A. Yuzhakova, V. M. Negrimovskii, O. L. Kaliya, E. A. Luk'yanets, *Russ. J. Chem.* **71** (2001) 36-41.
85. S. M. Critchley, M. R. Willis, M. J. Cook, J. McMurdo, Y. Maruyama, *J. Mater. Chem.* **2** (1992) 157-159.

86. D. Barton, W. D. Ollis, *Comprehensive Organic Chemistry, The Synthesis and Reaction of Organic Compounds*, Vol. 1, Pergamon Press, New York, 1970, p. 710.
87. H. Al-Ekabi, N. Serpone, *J. Phys. Chem.* **92** (1988) 5726-5731.
88. D. D. Dionysiou, A. P. Khodadoust, A. M. Kern, M. T. Suidan, I. Baudin, J-M. Laine, *Appl. Catal. B: Environ.* **24** (2000) 139-155.